ENERGY-EFFICIENT DEHUMIDIFICATION OF CONTROLLED PLANT ENVIRONMENTS VIA THE APPLICATION OF FERTILIZER-BASED LIQUID DESICCANTS

by

SANDEEP ARYAL

A dissertation submitted in partial fulfillment of the
requirements for the degree of

DOCTOR OF PHILOSOPHY IN MECHANICAL ENGINEERING

2025

Oakland University
Rochester, Michigan

Doctoral Advisory Committee:

Jonathan Maisonneuve, Ph.D., Chair
Sarah Beetham, Ph.D.
Ngong Kodiah Beyeh, Ph.D.
Laila Guessous, Ph.D.
Mark Lefsrud, Ph.D.

To my family

ACKNOWLEDGMENTS

I would like to start by dedicating this dissertation to the memory of my late father Madhav Prasad Aryal. His efforts and values have been a constant source of strength and inspiration in my life, even in his absence.

I am deeply grateful to my mother Sadhana Kumari Sharma for her love and sacrifices towards me. Her belief in me has been the basis of my achievements and gave me the strength to continue through challenges. To my wife Ashima, thank you for your firm support, patience and understanding. Your presence and love have been my greatest source of comfort during this journey.

I also owe a sincere debt of gratitude to my advisor Dr. Jonathan Maisonneuve, for his exceptional supervision, mentorship and insight. His support and constructive feedback have been helpful throughout my Ph.D. life. I would also like to thank the members of my dissertation committee, whose expertise, suggestions and evaluations have greatly helped me.

Lastly, I extend my sincere gratefulness to my lab mates, all the officials and individuals who directly or indirectly assisted me during my Ph.D. life. Your contributions have helped me a lot to achieve my goals and to move forward. To everyone who trusted in me and supported me along the way, I will forever be grateful. Thank you so much.

Sandeep Aryal

ABSTRACT

ENERGY-EFFICIENT DEHUMIDIFICATION OF CONTROLLED PLANT ENVIRONMENTS VIA THE APPLICATION OF FERTILIZER-BASED LIQUID DESICCANTS

by

Sandeep Aryal

Adviser: Jonathan Maisonneuve, Ph.D.

To address food security challenges due to population growth, controlled plant environments have become popular because they ensure crop production throughout the year in contrast to open field farming. However, one of the major hurdles in such environments is humidity buildup which has a detrimental impact on crop quality and productivity. Conventional dehumidification strategies such as ventilation, refrigerant-based systems, liquid or solid desiccants, etc. are deployed to tackle this but are often energy intensive and costly. To address this issue, this dissertation proposes the use of fertilizer solutions as a novel and energy efficient method to dehumidify indoor plant environments.

This dissertation establishes the thermodynamic limits and energy saving potential of fertilizer-based liquid desiccant. It then implements transport modeling to provide a more realistic assessment of energy use, followed by comprehensive experimental studies. Finally, it demonstrates the real-time dehumidification of humid air inside the functional plant chamber. From thermodynamic analysis it is found that the fertilizer desiccants consume half the energy required for conventional liquid desiccants systems by

eliminating desiccant regeneration. This study also shows energy savings for different crops taking into account the dehumidification load (evapotranspiration) and the fertilizer requirement for each crop. Based on thermodynamic analysis, energy savings for common crops range from 0.2 to 0.7 kWh/plant/day.

Building on this, transport modeling examines the influence of fertilizer concentration, temperature and fluid circulation rates on the specific energy of dehumidification of fertilizer-based desiccant systems. The results show that minimum specific work input is minimized to 0.16-0.24 kWh/kg at vapor flux level of 1.2-1.6 g/m^2/h by adjusting desiccant temperatures. Following this, the comprehensive experimental study was conducted on a lab-scale test bench to measure the system's energy use for different fertilizers, concentrations, and temperatures. The experiments confirm competitive energy use as low as 0.29 kWh/kg and pinpoint the importance of managing fertilizer temperature to optimize the system's energy efficiency.

Finally, the real-time application of a fertilizer-based desiccant dehumidification system was demonstrated in a closed plant chamber with hydroponic arugula. The fertilizer desiccant effectively maintained different humidity setpoints inside the chamber over the complete growth cycle of the plants.

TABLE OF CONTENTS

TABLE OF CONTENTS—Continued

TABLE OF CONTENTS—Continued

TABLE OF CONTENTS—Continued

LIST OF TABLES

LIST OF FIGURES

NOMENCLATURE

A_o	constant
a	membrane surface area (m^2)
B	vapor permeability ($g.m^2/s/Pa$)
B_o	constant
C_o	constant
c	concentration (g/l)
cop	coefficient of performance
cp	specific heat (J/kg.K)
D	diffusivity (m^2/s)
d	diameter (m)
E	energy (J)
G	Gibbs energy (J)
H	heat transfer coefficient ($W/m^2.K$)
h	enthalpy (J/kg)
i	number of ions
J	water vapor flux ($g/m^2/s$)
K	mass transfer coefficient ($g.m^2/s/Pa$)
k	thermal conductivity (W/m.K)
L	membrane thickness (m)
M	molar mass (kg/mol)
m	mass (kg)

Δm	mass of water vapor removed from air (kg)
$\Delta m'$	dehumidification capacity (kg/plant/day)
Δm^*	dehumidification load (kg/plant/day)
Pr	Prandtl number
p	pressure (Pa)
Q	heat transfer (J) or thermal load (J)
q	specific energy use of dehumidification (kWh/kg)
R	gas constant (J/mol.K)
RH	relative humidity
Re	Reynolds number
E	energy (J)
R_{th}	thermal resistivity ($K/W/m^2$)
r	recovery ratio
Sc	Schmidt number
T	temperature (K)
t	time (s)
V	volume (m^3)
VPD	vapor pressure deficit (kPa)
V_m	molar volume (m^3/mol)
W	work (J)
w	mass fraction (g/kg) or specific work input (kWh/kg)

x	mole fraction

Subscripts

1	initial state
2	final state
b	bulk fluid
d	desiccant
F	feed air
H2O	water
m	membrane interface
o	standard conditions
sat	saturation

Greek symbols

π	osmotic pressure (Pa)
ε	effectiveness

CHAPTER ONE

INTRODUCTION

1.1 Motivation

The world is facing the significant challenge of rapidly increasing human population. By 2050, the world's population is expected to reach almost 10 billion [1]. With the world's population increasing fast, the growing demand for important resources such as land, energy, food, and water is a concern. Of these, the demand for more food is among the most pressing concerns for human survival and well-being. Global food demand is projected to increase by 56 % in 2050 compared to the levels in 2025 [2]. Also, due to climate change, a major portion of the Earth's surface is becoming extremely dry or very cold making crop production problematic. Currently, drylands make up about 40 % of the Earth's land area and are home to about 30 % of the world's population [3,4]. In those areas scarcity of food is an issue due to water shortage, extreme temperatures and degraded soil fertility [5,6]. To confront this challenge, sustainable and efficient methods of growing food to meet the need for a rising population is vital. Agricultural, technological and resource management advances will be at the forefront of managing food security without hampering the environment.

1.2 Indoor Farming and Controlled Plant Environments

One promising strategy to accelerate food and crop production is to use an indoor agricultural or farming system which is unaffected by external climatic conditions or factors. Traditional agriculture involves cultivating crops in open fields, exposing them to

external climatic conditions, and growing them until they are ready to be harvested. In contrast, indoor and greenhouse farming techniques such as hydroponics, aeroponics, greenhouses, etc., are farming techniques that cultivate crops in an enclosed space where local climate such as light, temperature, CO_2, and humidity is controlled [7]. These techniques are also well known as controlled environment agriculture [8]. The advantages of indoor farming are several such as cultivation of crops throughout the year, lower use of resources, and no reliance on external climatic factors, reduced risk of crop failure, and improved efficiency of water, fertilizer and energy inputs [9-12]. Additionally, it also uses less pesticides and fertilizers compared to open field cultivation, making it a more sustainable and productive method of farming [13]. Apart from these there are other advantages of indoor farming such as crop production in buildings and rooftops, providing important sources of nutrition in space missions and production of high-value pharmaceuticals and medicinal plants, where strict quality control is required [14- 17].

With the growing popularity and advantages of indoor farming systems over open field farming, the indoor farming industry has experienced significant growth. The indoor farming industry around the globe was valued at $40 billion in 2022 and is likely to grow at a rate of over 10 % annually, reaching around $96 billion by 2032 [18]. In 2023 the U.S. had around 52,000 indoor farms with a total market value of $4 billion, and this number is forecasted to grow at a rate of 11.9 % annually, reaching to $8.8 billion by 2030 [18]. However, the expansion of open field farming has slowed down in recent decades, with an average rate of 1.93 % between 2015 and 2025 [19]. These trends suggest that the indoor farming industry is undergoing significant worldwide market expansion to meet the increasing food demands. Despite the market expansion of indoor

farming, it often faces hurdles that need to be addressed. One such issue is humidity control which is discussed in section 1.3.

1.3 Indoor Climate and Humidity Control

Controlled environment agriculture is transforming agriculture today to increase the world's food supply with the help of advanced technology to improve environmental factors such as light, temperature and humidity [20]. While these systems offer numerous benefits, they have a drawback due to the buildup of humidity by evapotranspiration, which can adversely affect the crops. In the absence of proper humidity regulation, important plant processes like transpiration, photosynthesis, and nutrient uptake are impacted [21,22]. Also, high humidity leads to mold issues, plant diseases, slow growth and yields [23], while low humidity leads to wilting and browning of crops, susceptibility to pests like spiders and bugs and flowering and fruiting issues [24]. Proper regulation and control of humidity are therefore important for healthy crops to reach their ideal productivity.

The importance of regulating proper humidity levels in indoor farms or greenhouses is well understood [22-24]. But keeping the correct moisture levels can use a lot of energy, be complex and costly. Various dehumidification technologies are commonly employed, which have their own advantages and limitations. Mechanical ventilation, dewpoint condensing heat exchangers, desiccant wheels, and liquid desiccants are some of the ways commonly used for humidity control [25].

Mechanical ventilation is the simplest dehumidification technology that uses fans to drive out humid air from the crop environment and bring in fresh outdoor air. In dewpoint

heat exchangers, a cold refrigerant flows inside the heat exchanger tubes, cooling their surface below the dewpoint temperature. This causes moisture from warm, humid air to condense on the tubes and lowers the air's humidity. A desiccant wheel reduces air moisture by rotating through humid air where moisture is absorbed by a desiccant material on a wheel. The desiccant material usually in the desiccant wheel are silica gel, zeolite or activated alumina. The desiccant material is regenerated again by blowing hot air through it to eject the absorbed moisture. Liquid desiccants remove moisture by pulling water vapor from moist air as it passes over the liquid. The low vapor pressure of a liquid desiccant compared to hot-humid air causes the transport of water vapor from air towards the desiccant. Afterwards, the liquid desiccant is regenerated again by heating it to drive out moisture dissolved in it. A heat pump removes moisture by actively cooling the air using a refrigeration cycle, lowering its temperature below the dewpoint to cause condensation. Heat pumps are more efficient compared to dewpoint heat exchangers. These dehumidification technologies are shown in Figure 1.1. A common limitation of these technologies is their energy inefficiency, cost and complexity. To better understand trade-offs of some dehumidification technologies, their advantages and disadvantages are listed in Table 1.1.

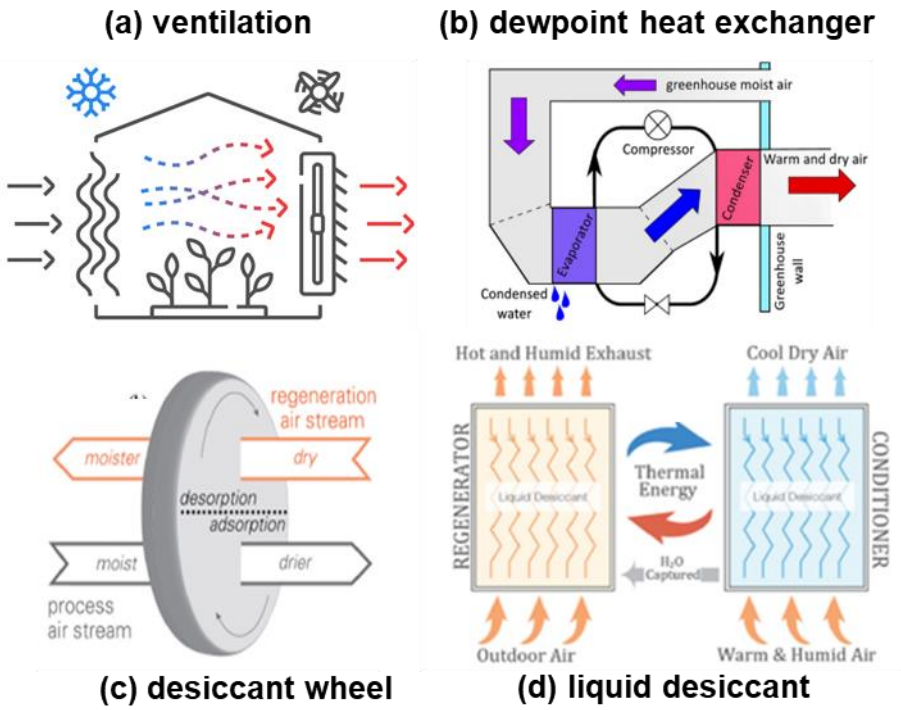

Figure 1.1 Different dehumidification technologies deployed in indoor farming: (a) ventilation, (b) dewpoint heat exchanger, (c) desiccant wheel, and (d) liquid desiccant [25].

Table 1.1 Advantages and disadvantages of dehumidification technologies employed in indoor farming [26]

Technology	Advantages	Disadvantages
Ventilation	Good indoor air quality and low risk of mold growth	Significant energy losses, dependent on external climatic conditions
Dewpoint heat exchangers	Recovers latent and sensible heat	Higher initial costs, fouling and efficiency loss
Desiccant wheel	Can operate when humidity and temperature is low, precise control	Regeneration energy required, Increase operational cost
Traditional liquid desiccant	Precision, high efficiency	Regeneration energy required, need maintenance to avoid crystallization
Heat pump	Energy efficient	Higher initial cost and less effective in extreme conditions

From an energy standpoint, all of the discussed dehumidification methods consume from 0.35 to 2.6 kWh of electrical energy per kg of water vapor removed, which is relatively high compared to energy standards and most efficient dehumidifiers from US Energy Star program [27-29]. These high energy requirements burden indoor farming operations, from both economic and environmental sides. Such issues press the need for innovative and low-energy alternatives for dehumidification. This challenge drives the search for new, sustainable technologies capable of reducing the energy footprint while properly regulating humidity in controlled plant environments.

1.4 Fertilizer-Based Liquid Desiccant for Dehumidification

To overcome the problem of excess energy requirement and enhance sustainability, a novel proof-of-concept was introduced previously at our lab: using fertilizer as a liquid desiccant [30] instead of conventional dehumidification methods. In this concept, unlike traditional liquid desiccant such as lithium chloride (LiCl), lithium bromide (LiBr), magnesium chloride ($MgCl_2$) or calcium chloride ($CaCl_2$), the fertilizer solution is used to remove moisture from moist air from greenhouse environment. For the proof-of-concept, investigators built a lab-scale bench setup where a concentrated fertilizer solution was pumped through a hollow fiber membrane's shell side and humid air was flowed to the lumen side. The water vapor pressure gradient between the liquid desiccant and the humid air causes water vapor to diffuse from air through the membrane towards the fertilizer desiccant. As the fertilizer solution absorbed moisture from air, it became diluted, and the air was dehumidified. The schematic of this proof-of-concept is shown in Figure 1.2.

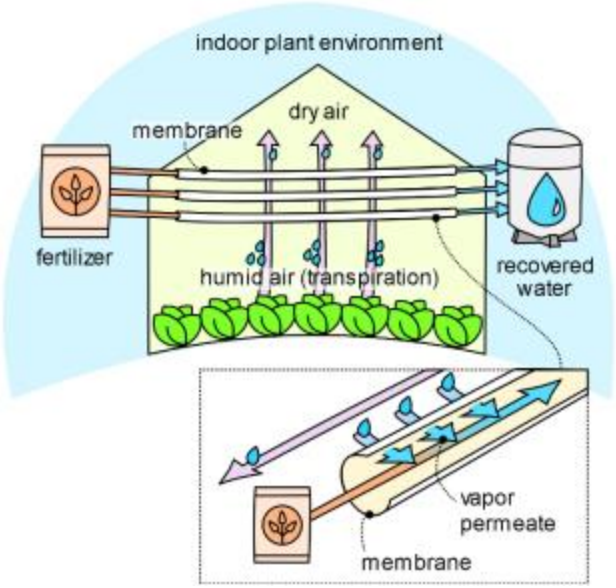

Figure 1.2 Fertilizer desiccant dehumidification system where water vapor from moist air passes through a selective polymer membrane because of vapor pressure gradient between air and the fertilizer solution [30].

Experimental findings from this investigation indicated that fertilizer solution was able to achieve water vapor removal fluxes as high as 1.9 $g/m^2/h$ (under low-temperature conditions) and relative humidity levels could be reduced from 70 % to 40 %. This study also has showed that some fertilizer solutions have vapor pressure values comparable to conventional desiccants like $MgCl_2$, making them possible alternatives for moisture removal from humid environments [30]. Figure 1.3 depicts a comparison of equilibrium humidity and vapor pressure for different fertilizer solutions to support their potential for effective dehumidification.

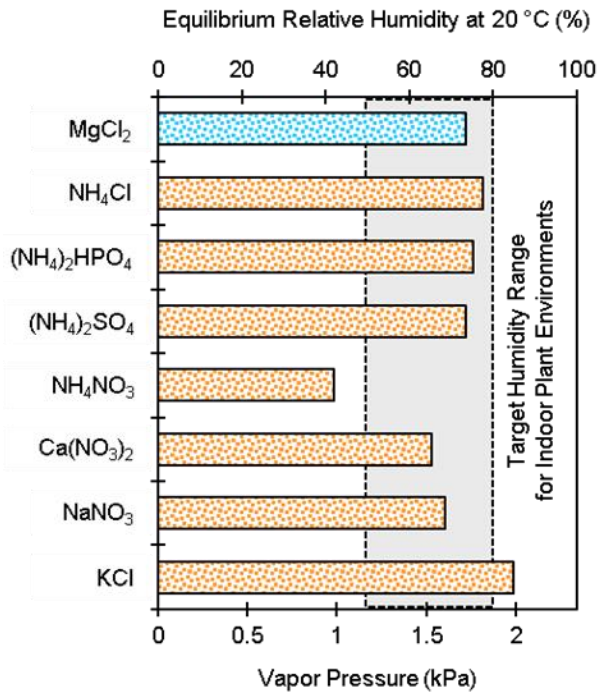

Figure 1.3 Comparison of vapor pressure and equilibrium humidity of common fertilizer solutions at their solubility limits with magnesium chloride, under standard temperature and pressure [30].

From Figure 1.3 and results from the proof-of-concept study, it is evident that the dehumidification potential of fertilizers can be harnessed. The key advantage of fertilizer-based desiccants is that it eliminates regeneration, significantly reducing energy consumption for dehumidification. Unlike conventional liquid desiccants, where energy-intensive heating and cooling are employed to recover their moisture absorption capacity (shown in Figure 1.4), fertilizer desiccants will not only help humidity control in indoor farming, but will also recover water and after sufficient fertilizer dilution, can be given back to plants to meet fertigation[1] needs without need for regeneration.

[1] Fertigation: It is the application of fertilizers or nutrients into a farming system through irrigation.

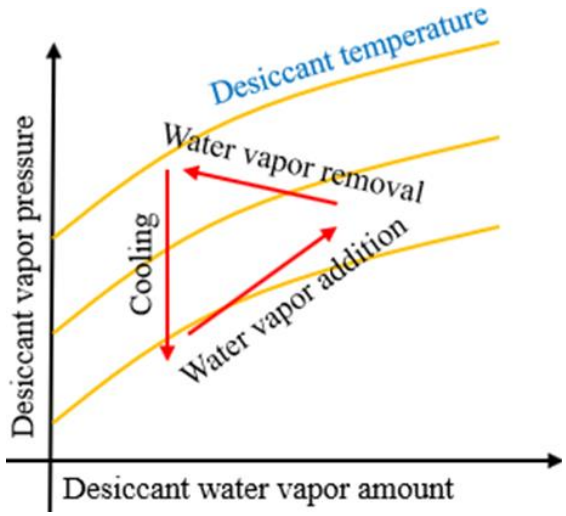

Figure 1.4 Processes involved in the liquid desiccant dehumidification. The process involves water vapor absorption, heating the desiccant to remove water vapor and cooling the desiccant to restore its dehumidification capacity [31].

To the best of my knowledge, no existing studies [25,27-30] have systematically examined fertilizer-based liquid desiccant system from a thermodynamic, modeling, or real-world application standpoint. This lack of foundational research on fertilizer desiccants has limited progress in developing such system as viable alternatives to conventional dehumidification methods. Although previous study in our lab [30] demonstrated that fertilizers can work as desiccant, it was preliminary exploration that did not include thermodynamic modeling, energy modeling, experimental validation, or practical implementation in crop environments. These critical gaps form the basis for this dissertation, which aims to advance the field through detailed analysis, simulation, experimentation, and real-time application. The research is organized around four aims, introduced in Section 1.5 and explored in Chapters Two through Four.

1.5 Outline

This dissertation is organized into four main specific aims as chapters which are discussed briefly as follows:

Chapter Two establishes thermodynamic limits and evaluates energy saving potential of fertilizer-based liquid desiccant system dehumidification in controlled plant environments. The motivation results from the high energy needs of conventional liquid desiccant systems, which require regeneration to maintain their dehumidification efficacy. In contrast, fertilizer solutions do not need to be regenerated as after sufficient dilution, they can be routed to plants for fertigation. The main question addressed in this chapter is whether the fertilizer requirements of crops are sufficient to handle some portion of dehumidification load coming from evapotranspiration. To address this, thermodynamic analysis is applied, first with the derivation of the minimum Gibbs energy of moisture removal under typical greenhouse conditions. The thermal load is then estimated for both conventional and fertilizer-based liquid desiccants. Using mass and energy balances, the fertilizer amount input to crops is linked to its potential dehumidification capacity and compared with the crop's evapotranspiration rate. The analysis further evaluates the weighed thermal load based on moisture removal requirements for individual crops. In the end, energy and work savings are estimated for common greenhouse crops and energy savings are generalized in terms of dehumidification load, fertilizer amount and final fertilizer concentration.

Chapter Three presents the numerical transport modeling and parametric analysis of fertilizer-based desiccant dehumidification. This study shows the specific energy use of dehumidification in relation to desiccant temperature for varying air and desiccant flow rates and concentration of desiccant. These changing parameters have an impact on water vapor removal rates and thus affect energy consumption for dehumidification. A theoretical heat and mass transfer model is established for energy analysis and was later

validated using experiments that showed reasonably satisfactory agreement with the model. The study identifies the temperature of desiccant as key to determining the specific thermal load of dehumidification of the system.

Chapter Four presents a comprehensive experimental investigation of fertilizer-based desiccant dehumidification's specific energy use. The investigation considers system performance for a range of fertilizer desiccant conditions, including different temperatures and concentrations of fertilizers in a lab scale bench for constant air side conditions. It investigates the specific energy use of multi-ion fertilizer blends and compares all the results with those of conventional and state of the art dehumidification technologies.

Chapter Five shows the design and development of a prototype fertilizer-based dehumidification system integrated with a plant chamber. A lab-scale plant chamber, along with a hydroponic system, is built in order to monitor real time humidity. Two membrane modules connected in parallel configuration are employed to reduce and control moisture levels in a plant chamber, showing real-time performance. As humidity increases in the plant chamber due to evapotranspiration, this chapter shows the real time operation of the dehumidification system to regulate the humidity at different setpoints. This chapter also details the monitoring of humidity control in the plant chamber throughout the entire plant growth cycle, from germination to mature stage.

Chapter Six concludes this dissertation by highlighting contributions of works presented in Chapters Two through Five. It outlines possible future investigations to improve fertilizer-based liquid desiccants and addresses shortfalls identified in this study. Finally, this dissertation demonstrates how fertilizer-based liquid desiccants can be

incorporated for dual purpose—simultaneously controlling humidity and delivering nutrients through fertigation.

CHAPTER TWO

THERMODYNAMIC ANALYSIS: ENERGY SAVING AND LIMITS OF USING FERTILIZER-BASED LIQUID DESICCANTS TO DEHUMIDIFY INDOOR PLANT ENVIRONMENTS

2.1 Introduction

As discussed in Chapter One, careful control of humidity is essential in controlled plant environments. Traditionally, humidity is managed with fresh air ventilation, i.e., exhausting humid air and replacing it with drier fresh air [32]. However, for controlled plant environments in extreme environments, fresh air requires energy intensive reconditioning and can introduce unwanted contaminants into the controlled space [33,34]. Efficient separation technologies are therefore needed to support the functions of closed plant environments. In an effort to develop energy efficient dehumidification systems, it is helpful to first consider the Gibbs energy of separation ΔG for water vapor and air. This is defined in equation (2.1a and 2.1b) in terms of mole fraction of water vapor in dry air and relative humidity of air. Different forms of this expression are developed in the literature [35], but for convenience we provide a detailed derivation in Supplementary Note 2.5.1.

$$\frac{\Delta G}{\Delta m} = \frac{R\,T}{M_{H2O}}\left[\left(1 - \frac{1}{r\,x_{H2O}}\right)\ln(1 - r\,x_{H2O}) + \left(\frac{1}{r} - 1\right)\ln(1 - r) - \ln(x_{H2O})\right] \qquad 2.1a$$

$$\frac{\Delta G}{\Delta m} = \frac{R\,T}{M_{H2O}}\left[\left(1 - \frac{1}{r}\,\frac{p_{atm}}{rh\,p_{sat}}\right)\ln\left(1 - r\,\frac{RH\,p_{sat}}{p_{atm}}\right) + \left(\frac{1}{r} - 1\right)\ln(1 - r) - \ln\left(\frac{RH\,p_{sat}}{p_{atm}}\right)\right] \qquad 2.1b$$

Where Δm is the mass of water vapor removed, R is the universal gas constant, T is absolute temperature, M is molar mass, r is the recovery ratio, x_{H2O} is the mole fraction of water vapor in dry air, RH is relative humidity, p_{sat} is saturation pressure, and p_{atm} is atmospheric pressure.

Figure 2.1 shows the minimum energy required per unit mass of vapor removed from air with a variety of relative humidities at 30 °C. Results are plotted against recovery ratio, but in most dehumidification applications for greenhouses, only small amounts of water vapor are removed at a time, so that r→0. In such a case, we see that between 0.013-0.016 kWh/kg is thermodynamically required for separation.

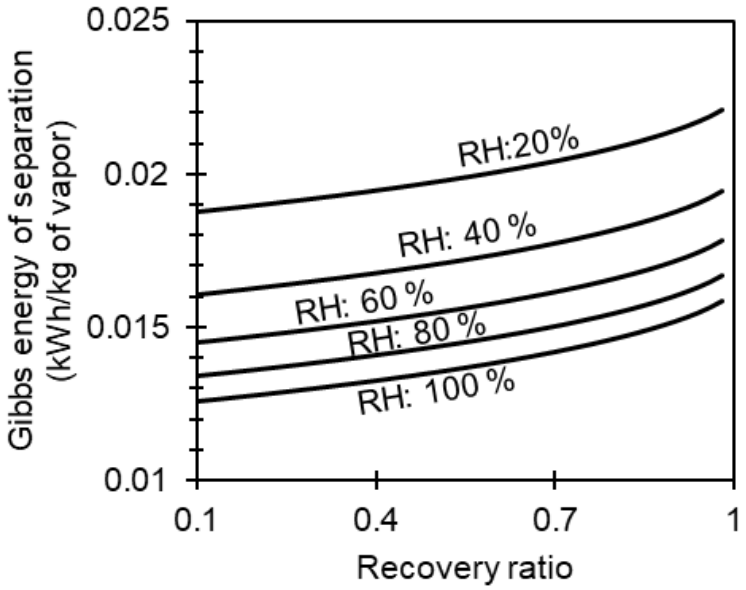

Figure 2.1 Gibbs energy of separation per unit mass of water vapor recovered from a binary gas mixture of water and air. Recovery ratio is the mass of water vapor removed relative to the total mass of water vapor contained in the air. Results are shown for various relative humidities at a temperature of 30 °C.

In practice, much more energy than this is used for dehumidification. For example, even technologies that are certified by the U.S. Energy Star program consume between 0.30 and 0.47 kWh/kg [35,36]. Table 2.1 provides an overview of some of the most

common dehumidification systems and their energy use. Most retail dehumidification products are refrigeration-based. They remove water vapor by condensation that occurs as air is circulated over a coil that is cooled by a refrigerant. As shown, such systems typically consume from 0.52-2 kWh/kg, usually in the form of work (i.e., electricity) to power the refrigeration cycle [36]. Alternatively, desiccant wheels have become increasingly common in commercial applications, especially where exhaust air is available. These use a hygroscopic solid or gel material that is packed into a circular frame or "wheel" to remove water vapor from air and then rotate the material into a regeneration air stream. As shown in Table 2.1, between 0.44-0.9 kWh/kg is typically used by such systems, mostly in the form of heat to regenerate the desiccant, but also some work (i.e., electricity) to cool the air after drying (since it can be heated by the dehumidification process) [37]. Recently liquid desiccants have been studied for dehumidification. These use a hygroscopic material just like desiccant wheels do, but in this case the material is in liquid phase. This provides interesting operational flexibility as liquid desiccant temperature, concentration, and circulation can be adjusted for precise humidity control [38-41]. As shown in Table 2.1, between 0.3-0.6 kWh/kg is typically used, including both heat and work to regenerate the liquid desiccant and then return it to its preferred operating temperature [42,43]. Several studies have specifically looked at the application of liquid desiccants to plant environments and shown encouraging results [44,45]. In these studies, a membrane-based liquid desiccant system using magnesium chloride and triple-bore hollow fiber membrane successfully maintained 70-90 % relative humidity for a bench scale greenhouse. This was one of the pioneering research for the indoor farming dehumidification.

Table 2.1 Energy use by common dehumidification systems

Dehumidification Technology	Energy Use (kWh/kg)
U.S. Energy Star [46]	0.30 – 0.47 (work)
Refrigeration-based [36]	0.52-2 (work)
Desiccant wheel [37]	0.44-0.92 (heat + work)
Liquid desiccant [44,45]	0.2-0.55 (heat + work)
Fertilizer-based liquid desiccant [47]	0.16-0.24 (work)

In more recent years, the concept of using plant fertilizer or nutrient solution as a liquid desiccant for greenhouse dehumidification has been proposed as an energy efficient alternative to conventional liquid desiccants [30,47]. The rationale is that while conventional liquid desiccants require energy intensive regeneration to retain their hygroscopic effectiveness, fertilizer solutions can be used as consumable desiccants and can be delivered to plants after being diluted by water vapor removed from the environment, to be replaced by the next batch of fertilizer input to the plant system. The basic concept is illustrated in Figure 2.2. As shown, water vapor that is released by plant evapotranspiration is removed from the indoor environment by a concentrated fertilizer solution with a low vapor pressure. When the solution is sufficiently diluted to levels that are suitable for plants, it is supplied for fertigation. Throughout the batch process, the fertilizer solution can be gradually cooled to maintain its vapor pressure at target levels.

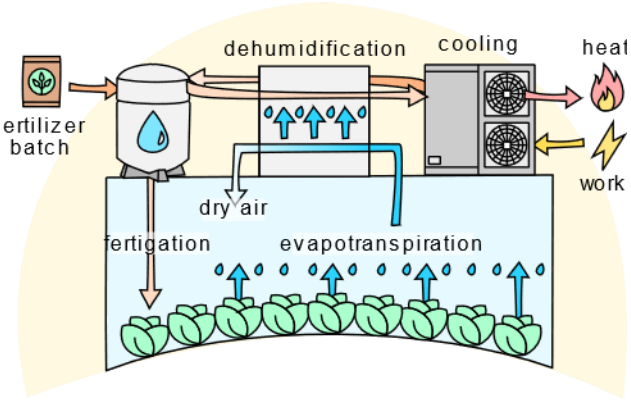

Figure 2.2 Dehumidification system using a consumable fertilizer-based liquid desiccant that can recover water from the humid air of a plant environment and then be returned to the plants as a diluted nutrient input.

So far, the concept has been experimentally validated, and good specific energy use of dehumidification results were reported, ranging from 0.16-0.24 kWh/kg under certain conditions (as shown in Table 2.1) [47]. Therefore, while the idea is promising, one fundamental question has remained unanswered: do plants use enough fertilizer to handle a substantial amount of their dehumidification load? And if so, how much energy could be saved by switching from conventional desiccants to fertilizer-based solution? This study answers these questions by considering the mass and energy balance of the process.

This chapter is organized as follows: first, the thermal load of dehumidification is evaluated for systems that use conventional liquid desiccant and that use fertilizer-based liquid desiccant. Then the amount between the mass of fertilizer input is compared against the mass of water vapor that must be removed from the plant system, to determine the limits to how much of the dehumidification load can be handled by fertilizer. This mass balance is used to define the weighted thermal load, which is then compared with the thermal load of conventional desiccants to determine energy savings. To illustrate, a variety of common plant crops like tomato, lettuce, basic, and bell pepper are used as

case studies. Also, a general set of charts are presented to show energy savings across a broad range of conditions. Finally, the future prospects of fertilizer-based liquid desiccant dehumidification are discussed.

2.2 Theory

2.2.1 Vapor Pressure as a Function of Liquid Desiccant Concentration and Temperature

Dehumidification with a liquid desiccant is driven by the vapor pressure deficit between the ambient air and the desiccant solution. For a controlled plant environment, such as a greenhouse or plant chamber, the vapor pressure of the ambient air will be relatively constant since temperature and humidity are regulated. But for a liquid desiccant solution, changes in vapor pressure can be quite significant as energy and mass are transferred to the solution, causing its temperature to increase and its concentration to decrease. The relationship between vapor pressure p_{H2O}, temperature T, and concentration c of a liquid desiccant, is described by the Kohler equation (2.2), Antoine equation (2.3), and Van't Hoff equation (2.4). The Kohler equation assumes ideal solution behavior, Antoine equation assumes vapor pressure depends only on temperature for pure substance, and the Van't Hoff equation assumes dilute and ideal solutions.

$$p_{H2O} = p_o \exp\left(\frac{V_m}{R\,T}(p - \pi)\right) \tag{2.2}$$

$$p_o = 10^{\left(A_o - B_o \frac{1}{C_o + T}\right)} \tag{2.3}$$

$$\pi = i\,R\,T\,c \tag{2.4}$$

p_o is the vapor pressure of a pure substance as described by the Antoine equation (2.3), where A_o, B_o, and C_o are empirical constants. In the case of water, A_o = 8.07131,

B_o = 1730.61, and C_o = 233.426 when temperature T is in °C and p_o is in mmHg [48]. V_m is the specific molar volume of water. R is the ideal gas constant, p is the gauge pressure, π is the osmotic pressure, which can be approximated by the Van't Hoff equation (2.4) as a function of the number of ions in the solution i. Osmotic pressure is a measure of force applied to solutions to prevent solvents from transporting across a semi-permeable membrane.

To illustrate, Figure 2.3 shows the vapor pressure of a variety of solutions as predicted by equations (2.2)-(2.4). Plots are shown for several common fertilizers such as calcium nitrate, $Ca(NO_3)_2$, potassium chloride KCl, and dipotassium hydrogen phosphate K_2HPO_4, and for conventional liquid desiccant lithium chloride LiCl. As shown from the graph, LiCl is a much stronger desiccant compared to fertilizer solutions, achieving much lower vapor pressure at a given temperature. Nevertheless, a fertilizer solution is capable of achieving the target vapor pressures of typical indoor plant environments, especially when it is cooled. The vapor pressure of pure water is shown for reference. As a desiccant solution is diluted, it is weakened, and vapor pressure approaches the curve for pure water.

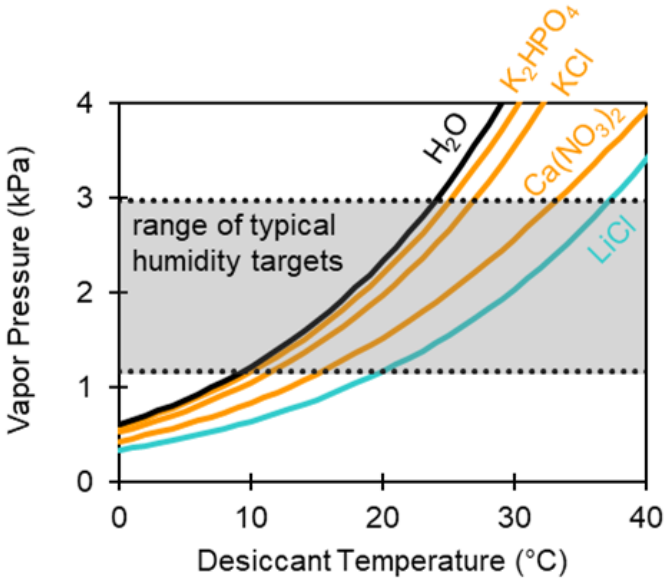

Figure 2.3. Vapor pressure of common fertilizer solutions (calcium nitrate $Ca(NO_3)_2$, potassium chloride KCl, and dipotassium hydrogen phosphate K_2HPO_4) and conventional liquid desiccant (lithium chloride LiCl) as predicted by equations (2.2)-(2.4). Vapor pressure is plotted as a function of desiccant temperature. Plots are shown for solutions at their solubility limit. As solutions are diluted, curves approach the results for pure water. Results are compared to the range of humidity targets that are typical for indoor plant environments.

2.2.2 Energy Balance of Conventional Liquid Desiccant Dehumidification

In a conventional liquid desiccant dehumidification system, a concentrated desiccant solution is brought into contact with humid indoor air, where the vapor pressure deficit of the desiccant draws water vapor out of the air to condense on the liquid desiccant surface. Energy and mass that are transferred to the desiccant solution cause it to weaken as a function of its increasing temperature and decreasing concentration. For this reason, the desiccant solution must be regenerated. This can be done via a number of methods such as reverse osmosis, membrane distillation, and other novel methods [49-53], but most commonly the solution is heated so that its vapor pressure increases above that of ambient air, allowing vapor to be transferred from the solution and rejected from the

system [54,55]. The solution is then cooled to desired operating temperature via a heat exchanger and active chiller. The process is illustrated in Figure 2.4.

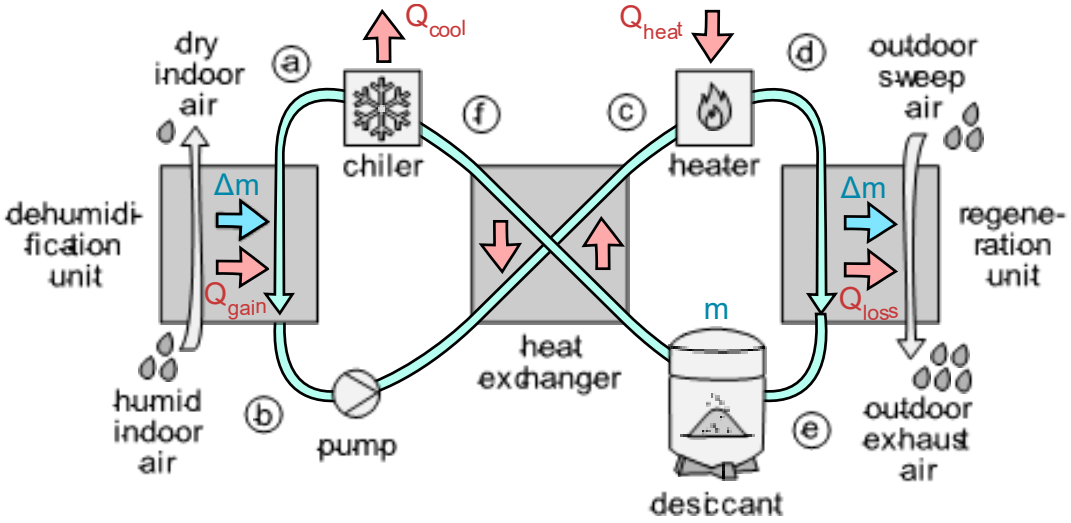

Figure 2.4 Conventional liquid desiccant cycle. (a-b) Air is dehumidified as water vapor and heat are transferred to the desiccant. (b-c) Liquid desiccant is pumped through a heat exchanger and then (c-d) a heater to raise the vapor pressure of the desiccant above exhaust air conditions. (d-e) Liquid desiccant is regenerated as water vapor and heat are dumped to the exhaust air stream. (e-f) Liquid desiccant is circulated through a heat exchanger and then (f-a) a chiller to reduce the vapor pressure to the target operating point.

The energy requirements of the conventional liquid desiccant system can be determined by considering the energy balance of its individual components. Equations (2.5)-(2.10) describe the energy balance across the chiller, dehumidification unit, heater, and regeneration unit. A detailed derivation is provided in Supplementary Note 2.5.2.

$$\Delta\dot{E}_{a-f} = -\dot{Q}_{cooling} = \dot{m}\, h_a - \dot{m}\, h_f \qquad 2.5$$

$$\Delta\dot{E}_{b-a} = \dot{Q}_{gain} + \Delta\dot{m}\, h_{H2O} = (\dot{m} + \Delta\dot{m})\, h_b - \dot{m}\, h_a \qquad 2.6$$

$$\Delta\dot{E}_{c-b} = \dot{Q}_{HX} = (\dot{m} + \Delta\dot{m})\, h_c - (\dot{m} + \Delta\dot{m})\, h_b = \varepsilon\, (\dot{m} + \Delta\dot{m})\, (h_e - h_b) \qquad 2.7$$

$$\Delta\dot{E}_{d-c} = \dot{Q}_{heating} = (\dot{m} + \Delta\dot{m})\, h_d - (\dot{m} + \Delta\dot{m})\, h_c \qquad 2.7$$

$$\Delta\dot{E}_{e-d} = -\dot{Q}_{loss} - \Delta\dot{m}\, h_{H2O} = \dot{m}\, h_e - (\dot{m} + \Delta\dot{m})\, h_d \qquad 2.8$$

$$\Delta\dot{E}_{c-b} = \dot{Q}_{HX} = (\dot{m} + \Delta\dot{m})\, h_c - (\dot{m} + \Delta\dot{m})\, h_b = \varepsilon\, (\dot{m} + \Delta\dot{m})\, (h_e - h_b) \qquad 2.10$$

Where $\dot{E}$ is the rate of energy transfer, $\dot{Q}$ is heat transfer rate, h is specific enthalpy, $\dot{m}$ is the initial mass flow rate of the liquid desiccant, $\Delta\dot{m}$ is the mass flow rate of water vapor removed from the indoor environment, and ε is effectiveness of the heat exchanger.

Using equations (2.5)-(2.10) it is then possible to obtain expressions for the heating load and cooling load, which together are the total energy required for the conventional liquid desiccant cycle. Equations (2.11) and (2.12) show the results for the idle case where ideal heat exchangers have an effectiveness $\varepsilon = 1$ with an assumption of infinite area, and where both the dehumidification unit and regeneration unit are assumed adiabatic, so that $\dot{Q}_{gain} = 0$ and $\dot{Q}_{loss} = 0$. In the equations (2.11) and (2.12), h_d is the enthalpy of liquid desiccant after it exits the heater.

$$\frac{\dot{Q}_{cooling}}{\Delta\dot{m}} = (h_{H2O} - h_d)\left(1 - \frac{\Delta\dot{m}}{\dot{m}}\right) \qquad 2.11$$

$$\frac{\dot{Q}_{heating}}{\Delta\dot{m}} = (h_{H2O} - h_d)\left(1 - \frac{\Delta\dot{m}}{\dot{m}}\right) \qquad 2.12$$

The total thermal load can be written as the combined cooling and heating loads $\dot{Q} = \dot{Q}_{cooling} + \dot{Q}_{heating}$.

$$\frac{\dot{Q}}{\Delta\dot{m}} = 2\,(h_{H2O} - h_d)\left(1 - \frac{\Delta\dot{m}}{\dot{m}}\right) \qquad 2.13$$

Equation (2.13) reveals that the thermal load of conventional liquid desiccant dehumidification is a function of (i) the enthalpy of water vapor, (ii) the enthalpy of liquid desiccant as it enters the regeneration unit, and (iii) the mass ratio of rate of water vapor removed from the indoor environment relative to the initial mass flow rate of liquid desiccant. The first of these is a fluid property, but the other two represent important

design variables. Consider the enthalpy of desiccant entering the regeneration unit. This will be a function of the temperature of the desiccant at this point, which must be set so that the rate of regeneration is equal to the rate of dehumidification (this is required for steady state operation of the cycle). For example, in the case where both the regeneration unit and the dehumidification units have the same mass transfer coefficient, the regeneration temperature must be set so that the difference between the liquid desiccant vapor pressure and the exhaust air, is equal to the difference between the indoor air and the liquid desiccant vapor pressure. Next, consider the mass ratio of vapor removal versus the initial liquid desiccant. This will determine the drop in performance as liquid desiccant moves from inlet to outlet of the dehumidification unit. For example, for more uniform performance, it is desirable for $\Delta\dot{m}/\dot{m}\rightarrow 0$ but this will produce the greatest thermal load from equation (2.13) and also has implications for sizing and cost.

2.2.3 Energy Balance of Fertilizer-Based Liquid Desiccant Dehumidification

The energy requirements of a fertilizer-based liquid desiccant dehumidification system are different from one using conventional desiccant because the solution is not regenerated to maintain constant concentration. Rather, dilution of fertilizer solution is one of the features of the process that allows for integration with the greenhouse system and delivery to the plant crops. The process is illustrated in Figure 2.5. As shown, concentrated fertilizer is brought into contact with humid indoor air, where the vapor pressure deficit of the desiccant draws water vapor out of the air to condense on the liquid desiccant surface. Energy and mass that are transferred to the desiccant solution cause it to weaken as a function of its increasing temperature and decreasing concentration. A

chiller is then used to cool the liquid desiccant to restore the desired vapor pressure deficit to maintain the constant water vapor removal rate from the air.

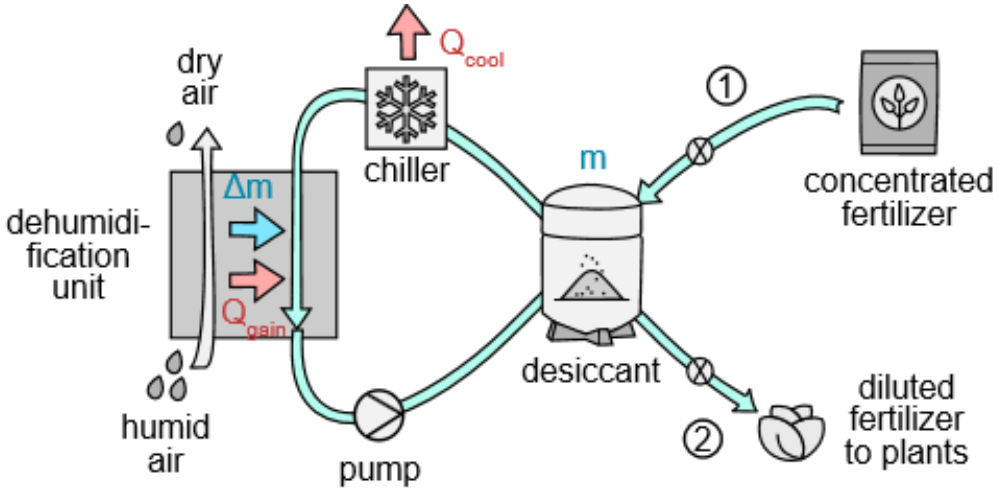

Figure 2.5 Fertilizer-based liquid desiccant dehumidification cycle. (1) An initial quantity of fertilizer is introduced to the system and cooled to achieve some target vapor pressure. Air is dehumidified as water vapor (and heat) are transferred to the desiccant. Liquid desiccant is recirculated through a chiller to reduce the vapor pressure to meet the target operating point. (2) At its final state, after sufficient dilution, the fertilizer solution is delivered to plants and a new batch of concentrated fertilizer is input to the system.

Since the proposed fertilizer-based liquid desiccant system is a batch process (rather than a cycle like for conventional liquid desiccant), its energy requirements are best determined by considering the energy balance of the liquid desiccant from start (super concentrated fertilizer solution near its solubility limit) to finish (diluted fertilizer solution that is ready for plants). Applying the first law of thermodynamics, we can show that the change in energy from initial to final state $\dot{E}_1$ and $\dot{E}_2$ is equal to the balance between heat gain from the warm air to the cool desiccant $\dot{Q}_{gain}$, mass transfer rate of pure water vapor $\Delta\dot{m}$ with its associated enthalpy h_{H2O}, and heat removed by active cooling $\dot{Q}_{cooling}$. The resulting energy balance is described in equation (2.14) with a detailed derivation provided in Supplementary Note 2.5.3.

$$\Delta \dot{E}_{2-1} = h_{H2O}\, \Delta \dot{m} + \dot{Q}_{gain} - \dot{Q}_{cooling} \quad (2.14)$$

Then, treating liquid desiccant solution as incompressible, and neglecting changes in kinetic and potential energy, we can then express the change in energy in terms of the liquid desiccant mass rate ṁ, specific heat cp of fertilizer desiccant, and temperature T to obtain equation (2.15). In this study we assume that the dehumidification unit is adiabatic so that $\dot{Q}_{gain} = 0$, and thereby obtain equation (2.16). While heat gain can be quite significant, it relates to the kinetics of the process and therefore can be neglected for the purpose of establishing thermodynamic limits. The assumption in this ideal analysis is that only water vapor is responsible for energy transfer from air side to the desiccant side in the dehumidification unit.

$$\frac{\dot{Q}_{cooling}}{\Delta \dot{m}} = h_{H2O} + \frac{\dot{Q}_{gain}}{\Delta \dot{m}} - \frac{1}{\Delta \dot{m}} \int_1^2 \dot{m} \cdot c_p dT \quad (2.15)$$

$$\frac{\dot{Q}_{cooling}}{\Delta \dot{m}} = h_{H2O} - \frac{1}{\Delta \dot{m}} \int_1^2 \dot{m} \cdot c_p dT \quad (2.16)$$

The total thermal load of fertilizer-based liquid desiccant dehumidification can then be written simply as the cooling load $\dot{Q}_{fertilizer} = \dot{Q}_{cooling}$, since there is no regeneration of the fertilizer, and therefore no associated heating load like in the case of conventional desiccant.

$$\left(\frac{\dot{Q}}{\Delta \dot{m}}\right)_{fertilizer} = \frac{\dot{Q}_{cooling}}{\Delta \dot{m}} = h_{H2O} - \frac{1}{\Delta \dot{m}} \int_1^2 \dot{m}\, cp\, dT \quad (2.17)$$

Equation (2.17) reveals that the thermal load of fertilizer-based liquid desiccant dehumidification is a function of (i) the enthalpy of water vapor, and (ii) the relationship between liquid desiccant mass, specific heat, and temperature. The first of these is a fluid

property, but the latter depends on the way in which the fertilizer batch process is operated. Specifically, it depends on how the temperature of the fertilizer desiccant is managed as the solution is diluted. To illustrate, Table 2.2 describes three possible operating modes. In the 1st mode of operation, no active cooling is provided such that $\dot{Q}_{cooling} = 0$. As a result, the energy of the desiccant will increase as the batch is diluted, causing temperature to increase, the vapor pressure difference to decrease, and the dehumidification rate to drop.

In the 2nd mode, only enough cooling is provided to keep the desiccant temperature constant, or in other words, the cooling load is equal to the enthalpy of the water vapor transfer. As a result, temperature remains constant and yet vapor pressure difference decreases due to desiccant dilution, and ultimately the dehumidification rate also drops.

In the 3rd mode, enough cooling is provided to keep the vapor pressure difference between the greenhouse air and the desiccant solution constant throughout the batch process. In other words, the cooling load is equal to the enthalpy of the water vapor transfer, plus the drop in energy that is needed to reduce desiccant temperature and maintain a constant pressure difference. As a result, the dehumidification rate remains constant throughout the batch process, even as the fertilizer solution is diluted. The advantage of this constant vapor pressure operation is that the dehumidification can be operated for a long time depending on the need in the indoor farming system without stalling like in the case of other two processes. But achieving constant vapor pressure requires precise control of the temperature during cooling. Deviation from the precise temperature can stall the system early without reaching the dilution requirements proper for the fertigation of the plants.

Table 2.2 Modes 1, 2, and 3 are different strategies for adjusting desiccant temperature throughout the batch process as concentration of the fertilizer desiccant is diluted. The associated cooling load, and the effect that this has on vapor pressure difference (and hence vapor flux) are shown.

	Mode 1: No Cooling	Mode 2: Constant Temp	Mode 3: Constant Vapor Pressure	
Desiccant concentration	↓	↓	↓	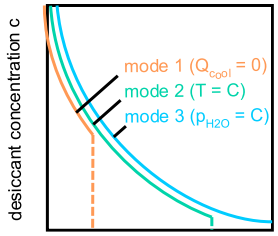
Desiccant temperature	↑	constant	↓	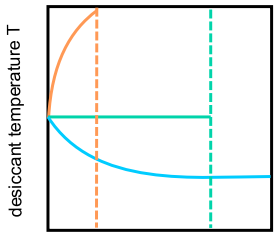
Vapor pressure difference (∝ Vapor flux)	↓	↓	constant	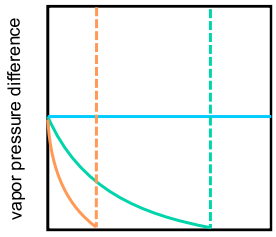
Cooling load $\frac{Q_{cooling}}{\Delta m} = h_{H2O} - \frac{\Delta E_{2-1}}{\Delta m}$	0	h_{H2O}	$h_{H2O} - \frac{1}{\Delta m}\int_1^2 m\, cp\, dT$	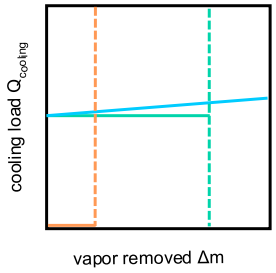

To illustrate further, Figure 2.6 shows a numerical example of fertilizer dehumidification with the three modes of operation from Table 2.2. Calcium nitrate fertilizer with an initial concentration of 1,000 g/l is used as the liquid desiccant and is diluted by a factor of up to 1000× (i.e., to a final concentration of 1 g/l, which is suitable

for plants). The controlled plant environment is assumed to have a constant relative humidity and temperature of 60 % and 30 °C. As shown, in mode 1, the temperature of the desiccant rises rapidly as enthalpy is carried by the vapor to the desiccant solution. As a result, the vapor pressure difference between desiccant and air rapidly collapses to zero and dehumidification stalls, achieving only negligible dilution of the fertilizer. In mode 2, desiccant is cooled, but only enough to maintain a constant temperature. Therefore, as the concentration of the desiccant drops, the vapor pressure difference also drops. If the operating temperature that is maintained is too cold, the vapor pressure difference may even drop to zero, causing the dehumidification process to stall, and achieve only a portion of the fertilizer dilution. In mode 3, desiccant temperature is managed so that a constant vapor pressure difference of 100 Pa is maintained even as fertilizer is diluted. The result will be steady performance, as dehumidification rates remain constant throughout dilution of the fertilizer batch. This represents an important advantage as compared to mode 2, where a significant drop in dehumidification performance is observed throughout the batch. Furthermore, the results for thermal load indicate that there is only a negligible difference in the energy requirements for modes 2 and 3 ($\dot{Q}/\Delta\dot{m}$ ≈0.69 kWh/kg in both cases). Of course, the thermal load for mode 1 is the lowest of all ($\dot{Q}/\Delta\dot{m} = 0$), but as explained previously, the process is not sustained and cannot handle a significant portion of the plant environment's dehumidification load. Given these considerations, we conclude that mode 3 is the best method of operation for the proposed fertilizer system, which involves actively cooling liquid desiccant in order to ensure a constant vapor pressure difference throughout the batch process.

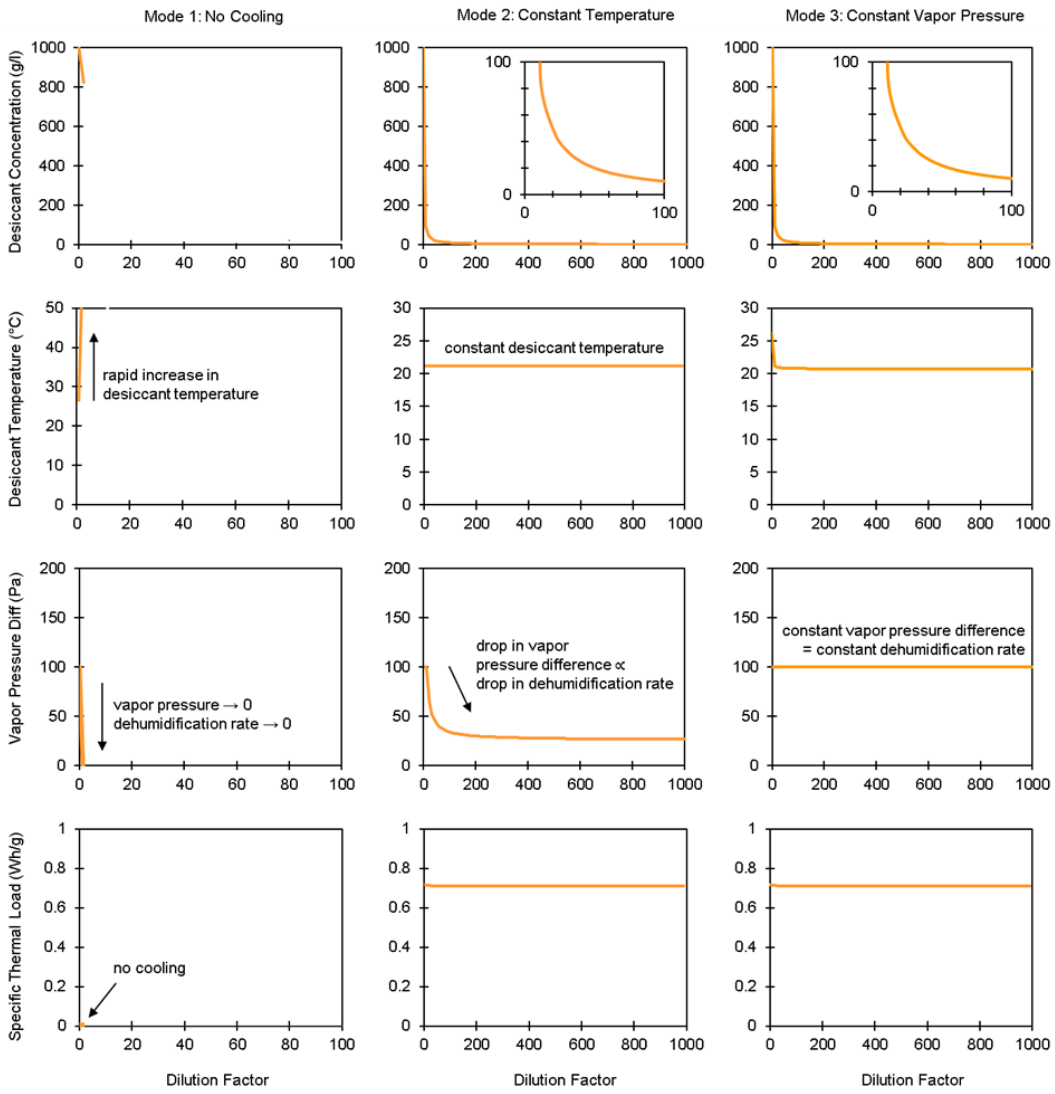

Figure 2.6 Performance of a fertilizer-based liquid desiccant batch process with three modes of operation as defined in Table 2.2. Calcium nitrate fertilizer is used with an initial concentration of 1,000 g/l and then diluted to a final concentration of 1 g/l (i.e., dilution factor of up to 1000×). Initially, the temperature of the desiccant is set so that the initial vapor pressure difference is 100 Pa. After, temperature and vapor pressure are allowed to vary according to the mode of operation.

2.2.4 Comparing Energy Use of Conventional and Fertilizer-Based Liquid Desiccants

To evaluate the performance of conventional and fertilizer-based liquid desiccant dehumidification, we can use equations (2.13) and (2.17) respectively. To illustrate, Figure 2.7 shows the normalized thermal load of both liquid desiccant processes with a controlled plant environment that has constant relative humidity and temperature of 60 %

and 30 °C. For the conventional liquid desiccant, lithium chloride LiCl is selected with a concentration of 420 g/l (~ 50 % solubility). For the fertilizer-based desiccant, calcium nitrate is selected with an initial concentration of 1000 g/l (~ 100 % solubility). Plots are shown for three different inlet vapor pressure deficits (20, 200, and 2000 Pa), which are obtained by changing the desiccant temperature. Plots are also shown as a function of the drop in the vapor pressure deficit from when it enters the dehumidification unit to when it leaves. This is done by changing the mass ratio of vapor permeate relative to the initial quantity of liquid desiccant. As shown, thermal loads only change slightly in response to different inlet vapor pressures and to different inlet to outlet vapor pressure ratios. Also, the thermal loads compare very well showing discrepancy around 3 % with the simple approximations provided by $2 \times h_{H2O}$ for conventional desiccant and $1 \times h_{H2O}$ for fertilizer-based desiccant. Therefore, for convenience, we use these approximations as simple benchmarks against which to compare our proposed fertilizer-based system against conventional liquid desiccant.

$$\left(\frac{\dot{Q}}{\Delta\dot{m}}\right)_{conventional} \approx 2\, h_{H2O} \tag{2.18}$$

$$\left(\frac{\dot{Q}}{\Delta\dot{m}}\right)_{fertilizer} \approx h_{H2O} \tag{2.19}$$

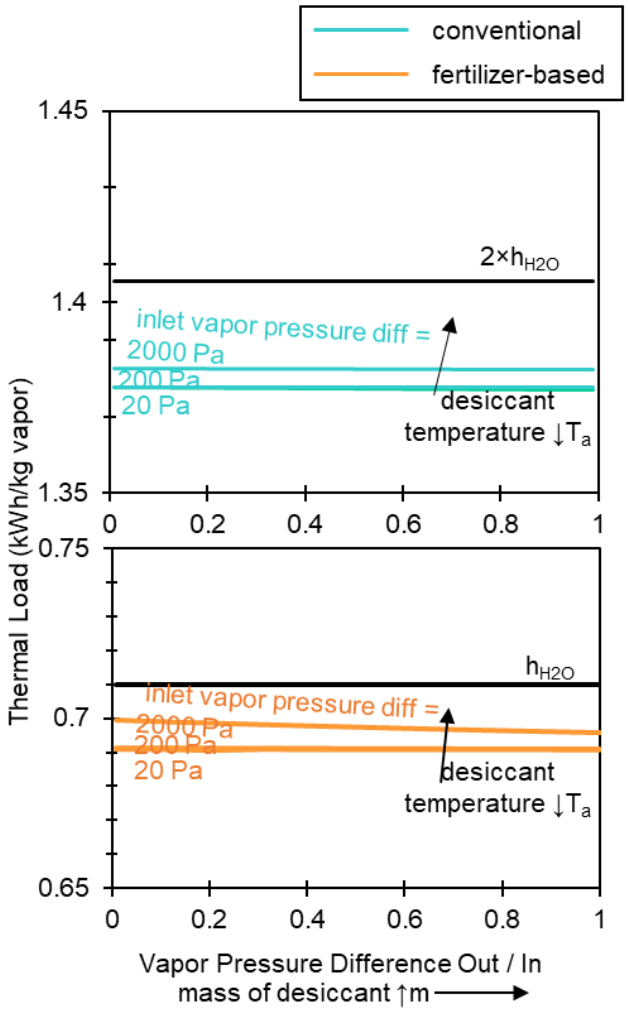

Figure 2.7 Thermal load of both conventional and fertilizer-based liquid desiccant dehumidification. Environmental conditions are 30 °C and 60 % relative humidity. Lithium chloride at 420 g/l is used as conventional desiccant. Calcium nitrate at 1000 g/l is selected as the fertilizer desiccant. Fertilizer desiccant is operated using Mode 3, as defined in Table 2.2.

2.2.5 Dehumidification Limits Imposed by the Amount of Fertilizer

One of the fundamental limits to fertilizer-based liquid desiccant dehumidification is the limited quantity of fertilizer input that is required by a given plant crop. This ultimately limits the dehumidification capacity of the fertilizer-based desiccant. Therefore, while fertilizer-based desiccants will only require about half the thermal

energy of conventional desiccant (as shown above), these savings need to be weighted against the portion of the dehumidification load that they will be able to handle.

To evaluate this, consider first the dehumidification capacity of a given quantity of fertilizer, $\Delta m'$. This can be established as a function of the fertilizer solution's initial and final concentrations in equation (2.20).

$$\Delta m' = \dot{m}_2 - \dot{m}_1 = \left(\frac{1}{w_2} - \frac{1}{w_1}\right) m_d \qquad 2.20$$

Where w_1 is the initial mass fraction of the desiccant solution, which can approach the solubility limit of the fertilizer solute, w_2 is the final mass fraction of the solution, which is the plant crop's preferred concentration, and m_d is the mass of desiccant solute, which is equal to the amount of fertilizer that the plant crop requires.

The key question is then whether the dehumidification capacity of a plant's fertilizer input is sufficient to match its dehumidification load, which we designate with Δm^*. In some cases, the dehumidification capacity of a plant's fertilizer input may satisfy or exceed the load, $\Delta m' \geq \Delta m^*$. But in other cases, the capacity may be less than the load, $\Delta m' < \Delta m^*$. This ratio of dehumidification capacity to load has important implications for the proposed fertilizer-based desiccant process and its potential for energy savings. Once a fertilizer desiccant reaches capacity, it will be necessary for any remaining dehumidification load to be handled by some other dehumidification system. This obviously has important implications for cost, but from an energy standpoint, which is the focus of this thermodynamic analysis, it will limit the energy savings that can be realized from the fertilizer system. Equation (2.21) provides an expression for the weighted thermal load that results when fertilizer desiccant is used to handle some of the

dehumidification load and conventional desiccant is used to handle the balance. It should be noted, that equation (2.21) assumes that the thermal load of fertilizer-based liquid desiccant is approximately $\dot{Q}/\Delta\dot{m}_{\text{fertilizer}} \approx h_{H2O}$, and that the thermal load of conventional liquid desiccant is approximately $\dot{Q}/\Delta\dot{m}_{\text{conventional}} \approx 2h_{H2O}$ (as shown in Section 2.4.4).

$$\left(\frac{\dot{Q}}{\Delta\dot{m}}\right)_{\text{weighted}} = \frac{\Delta m'}{\Delta m^*}\left(\frac{\dot{Q}}{\Delta\dot{m}}\right)_{\text{fertilizer}} + \left(1 - \frac{\Delta m'}{\Delta m^*}\right)\left(\frac{\dot{Q}}{\Delta\dot{m}}\right)_{\text{conventional}} \quad 2.21a$$

$$\left(\frac{\dot{Q}}{\Delta\dot{m}}\right)_{\text{weighted}} \approx \left(2 - \frac{\Delta m'}{\Delta m^*}\right) h_{H2O} \quad 2.21b$$

Finally, based on this weighted thermal load, we can define the energy savings of the proposed fertilizer-based liquid desiccant dehumidification system $\Delta\dot{Q}_{\text{savings}}$ as in equation (2.22). These thermal energy savings can also be translated to work savings, by assuming that a heat pump will handle the load with a certain coefficient of performance cop[2], so that $\Delta\dot{W}_{\text{savings}}=\Delta\dot{Q}_{\text{savings}}/\text{cop}$.

$$\Delta\dot{Q}_{\text{savings}} = \dot{Q}_{\text{conventional}} - \dot{Q}_{\text{weighted}} \quad 2.22a$$

$$\left(\frac{\Delta\dot{Q}}{\Delta\dot{m}}\right)_{\text{savings}} = \frac{\Delta m'}{\Delta m^*}\, h_{H2O} \quad 2.22b$$

2.3 Results

2.3.1 Mass Balance for Common Greenhouse Crops

To illustrate the dehumidification limits that are imposed by the limited quantity of fertilizer input to a crop system, consider the case of four common greenhouse crops:

[2] cop: Coefficient of performance is a dimensionless measure of efficiency of cooling system.

Solanum Lycopersicum (tomato), *Lactuca Sativa* (lettuce), *Ocimum Basilicum* (basil), and *Capsicum Annuum* (bell pepper). Table 2.3 provides a list of specifications for these crops including their fertilizer requirements and dehumidification load. The table presents the mass of fertilizer required for various greenhouse crops, along with the recommended concentrations (w_2) suitable for fertigation. It also includes the dehumidification load (Δm^*) associated with each crop and the corresponding plant spacing. This spacing information allows for the calculation of planting density, which is later used in the results section to estimate energy savings per unit area.

Table 2.3. Fertilizer requirements for plant crops along with their dehumidification load from evapotranspiration[3] [56-59]. Fertilizer inputs include calcium nitrate $Ca(NO_3)_2$, dipotassium phosphate K_2HPO_4, and potassium chloride KCl.

Plant Crop	Fertilizer Required | Initial Concentration | Final Concentration m_D (g/plant/day) | w_1(g/kg) | w_2 (g/kg)			Humidity Load Δm^* (kg/plant/day)	Spacing (plants /m^2)
	$Ca(NO_3)_2$	K_2HPO_4	KCl		
Tomato	0.519 | 1000 | 1	0.530 | 1490 | 0.60	0.081 | 280 | 0.70	0.28	3.5
Lettuce	0.280 | 1000 | 0.50	0.185 | 1490 | 0.05	0.034 | 280 | 0.30	0.31	25
Basil	0.320 | 1000 | 0.52	0.010 | 1490 | 0.40	0.038 | 280 | 0.44	0.72	25
Bell pepper	0.183 | 1000 | 0.35	0.010 | 1490 | 0.53	0.110 | 280 | 0.18	1.4	1.7

Figure 2.8 shows the resulting dehumidification capacity relative to the dehumidification load $\Delta m'/\Delta m^*$. As shown, in some cases the dehumidification capacity of a plant's fertilizer input satisfies or exceeds the load, such as for tomato and lettuce. But in other cases, like basil and pepper, the capacity is less than the load. For these latter two examples, it may seem natural to simply add the dehumidification capacity of each of the individual fertilizer inputs in order to approach 100 % of the load. However, this does not reflect the fact that in practice fertilizers are not diluted individually but rather diluted

[3] evapotranspiration: It is the process where water moves into the air through evaporation from soil and transpiration from plants.

as a mixture. Therefore, it is more appropriate to consider the largest of the individual fertilizer volumes as the overall dehumidification capacity. In this case, we can see that fertilizer-based liquid desiccant can handle 100 % of the dehumidification load for tomato and lettuce and only handle 85 % and 44 % of the load for basil and pepper, respectively.

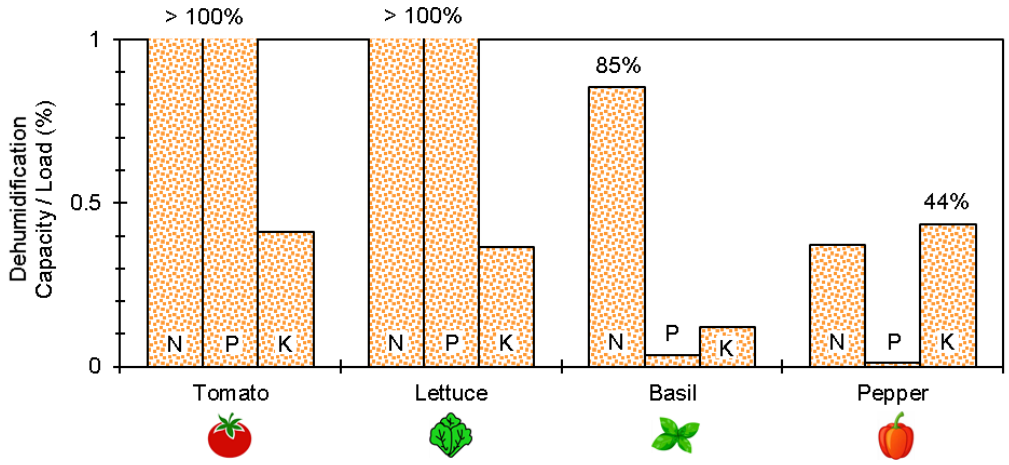

Figure 2.8 Dehumidification capacity of fertilizer-based liquid desiccant relative to the dehumidification load $\Delta m'/\Delta m^*$ for various plant crops. Fertilizer inputs include calcium nitrate (N), dipotassium phosphate (P), and potassium chloride (K). Input conditions are summarized in Table 2.3.

This ratio of dehumidification capacity to load has important implications for the proposed fertilizer-based desiccant process and its potential for energy savings. To illustrate, consider the same four plant crops and their weighted thermal load obtained from equation (2.21) and plotted in Figure 2.9. As shown, in all cases, the thermal load is less than the reference of using conventional liquid desiccant. For the crops that use enough fertilizer to handle the entire dehumidification load (i.e., tomato and lettuce), thermal energy loads are cut in half relative to conventional desiccant.

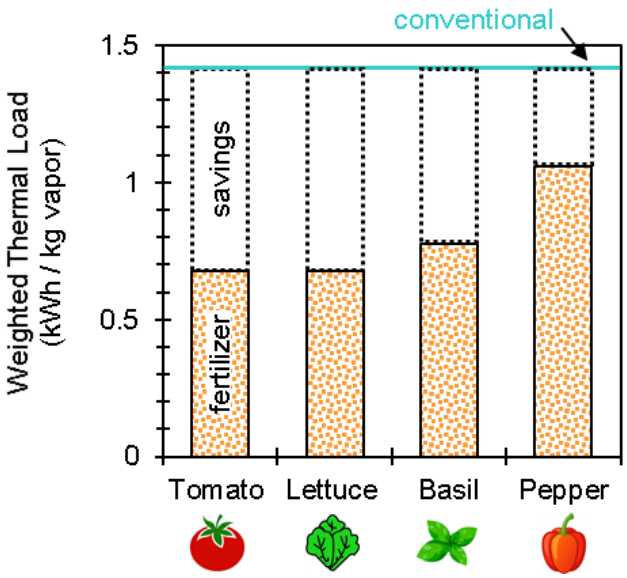

Figure 2.9 Weighted thermal load of dehumidification using fertilizer-based desiccant for four common plant crops. The thermal load using conventional liquid desiccant is shown for comparison and savings are highlighted. Input conditions are summarized in Table 2.3.

2.3.2 Energy Savings for Common Greenhouse Crops

To illustrate the energy savings that are possible for fertilizer-based liquid desiccants, consider again the case of four common greenhouse crops from Table 2.3. Figure 2.10 shows the energy savings that can be achieved by switching from conventional liquid desiccants (which require regeneration) to fertilizer-based liquid desiccants (which can be diluted and then replaced with additional fertilizer input). As shown, thermal savings per unit mass of water vapor removed are greatest for tomato and lettuce (~ 0.67 kWh/kg vapor), where fertilizer quantities are significant enough to handle the whole dehumidification load of these crops.

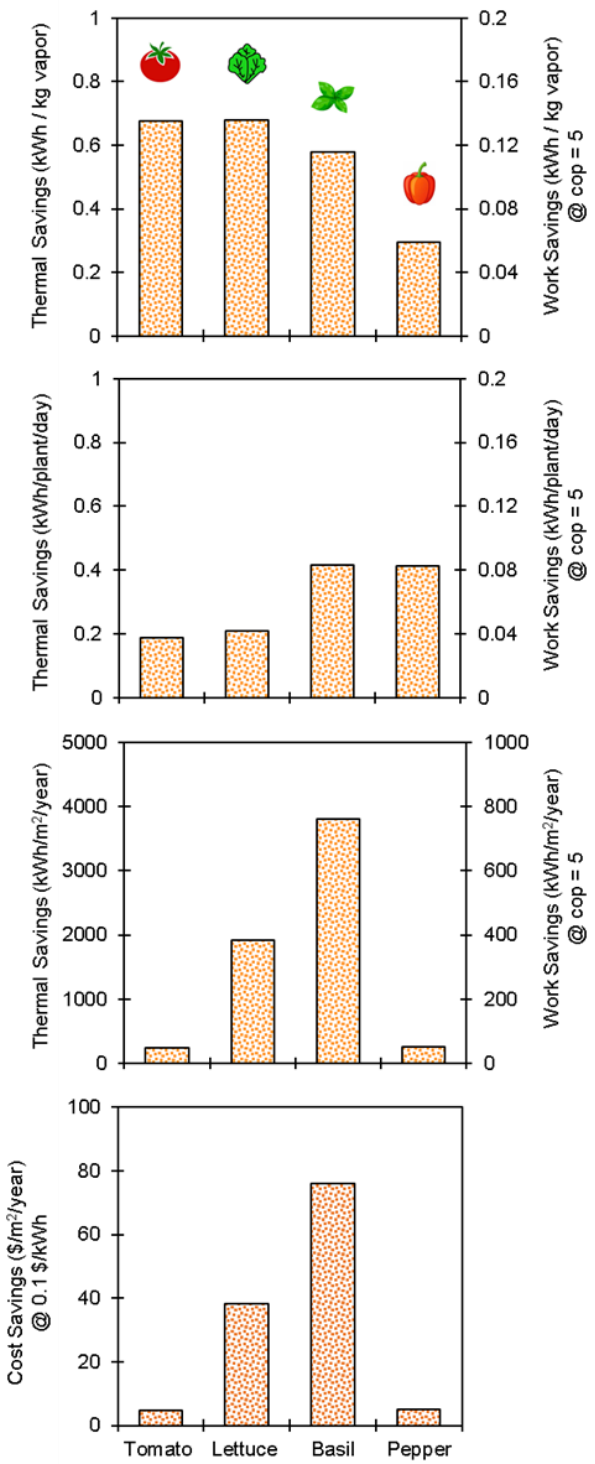

Figure 2.10 Energy savings from using fertilizer-based liquid desiccant for dehumidification, instead of conventional liquid desiccant. Thermal savings are shown per kg of water vapor removed, per plant per day, and per m^2 per year. Work savings assume a coefficient of performance cop = 5. Cost savings assume an electricity rate of 0.1 $/kWh.

When this is the case, the thermal load of dehumidification is half of what it would be if using conventional liquid desiccant. Interestingly, on a per plant basis, the thermal savings are greatest for basil and pepper (~ 0.42 kWh/plant/day) because these plants have the greatest dehumidification load caused by evapotranspiration. Finally, on a per m^2 basis, savings are greatest for lettuce and basil (1920 and 3800 kWh/m^2/year respectively) due to their high planting density. Perhaps more importantly that these differences between crops are the fact that for all crops, switching from conventional to fertilizer-based liquid desiccant has the potential to generate significant savings. Assuming that thermal loads are handled by a heat pump with $\mathrm{cop} = 5$, and assuming work (i.e., electricity) has a value of 0.1 \$/kWh, we estimate that cost savings can range from 5 to 76 \$/m^2/year. For a commercial greenhouse or indoor farm with several acres of grow space, these cost savings can be very significant. A cop value of 5 is used in this analysis as it represents the performance of highly efficient, state-of-the-art cooling systems.

2.3.3 Generalized Plots for Energy Savings from Fertilizer-Based Liquid Desiccants

The energy saving results reported above are highly case specific. They are unique to four particular crops and to various assumptions about how these crops will be cultivated. These assumptions include the amount of fertilizer input, the dehumidification loads that will be generated by evapotranspiration, plant spacing, the desired concentration of fertilizer solution, and the temperature and humidity at which the plant environment is kept. All of these variables have some influence on the potential energy savings of switching from conventional to fertilizer-based liquid desiccant. Importantly, these variables are highly circumstantial. For the same plant crop, these input variables can be

very different based on region, climate and weather, and based on plant cultivation methods.

In light of this variability, Figure 2.11 provides a general evaluation of the thermal load of dehumidification with fertilizer desiccant and the related energy savings over conventional desiccant. In Figure 2.11, the weighed thermal load and energy savings are plotted as a function of (i) the final fertilizer concentration to be delivered to plants w_2 (shown on the x axis), (ii) the dehumidification load Δm^* (shown with different contour lines), and (iii) the quantity of fertilizer input m_d (shown on separate sub figures). As shown, the weighted thermal load has a minimum value equal to the specific enthalpy of water, $\Delta\dot{Q}/\Delta\dot{m} = h_{H2O}$. However, this is only achieved if the dehumidification capacity of the fertilizer is enough to handle the dehumidification load of the plants. If the amount of fertilizer input m_d is low, or if the fertilizer cannot be diluted to low concentration w_2, then the weighted thermal load increases from the minimum line and pulls away more and more as the dehumidification load Δm^* increases. Similarly for the savings, there is a maximum savings for any given dehumidification load. But if the amount of fertilizer input m_d is reduced or if the fertilizer cannot be diluted to low concentration w_2, then the savings fall off.

For reference, markers are included for the four plant crops previously considered: tomato, lettuce, basil, and bell pepper. Results are consistent with the results presented earlier, except for small discrepancies that occur because we have only generated figures for four discrete values of m_d = 0.1, 0.3, 0.5, and 0.7 g/plant/day, but fertilizer inputs for the selected crop differ slightly from these discrete values. This is also the reason why we have added two markers for bell pepper, since the fertilizer input for it falls between the

discrete values of m_d = 0.1 and 0.3 g/plant/day. In this way, Figure 2.11 provides a useful tool that can be used by growers and others to consider the merit of switching from conventional liquid desiccant to fertilizer-based solution. In general, the energy savings are sensitive to the fertilizer amount, dehumidification load and the final fertilizer concentration but these energy savings are controlled by the evapotranspiration rate and the crop preferred fertilizer concentrations.

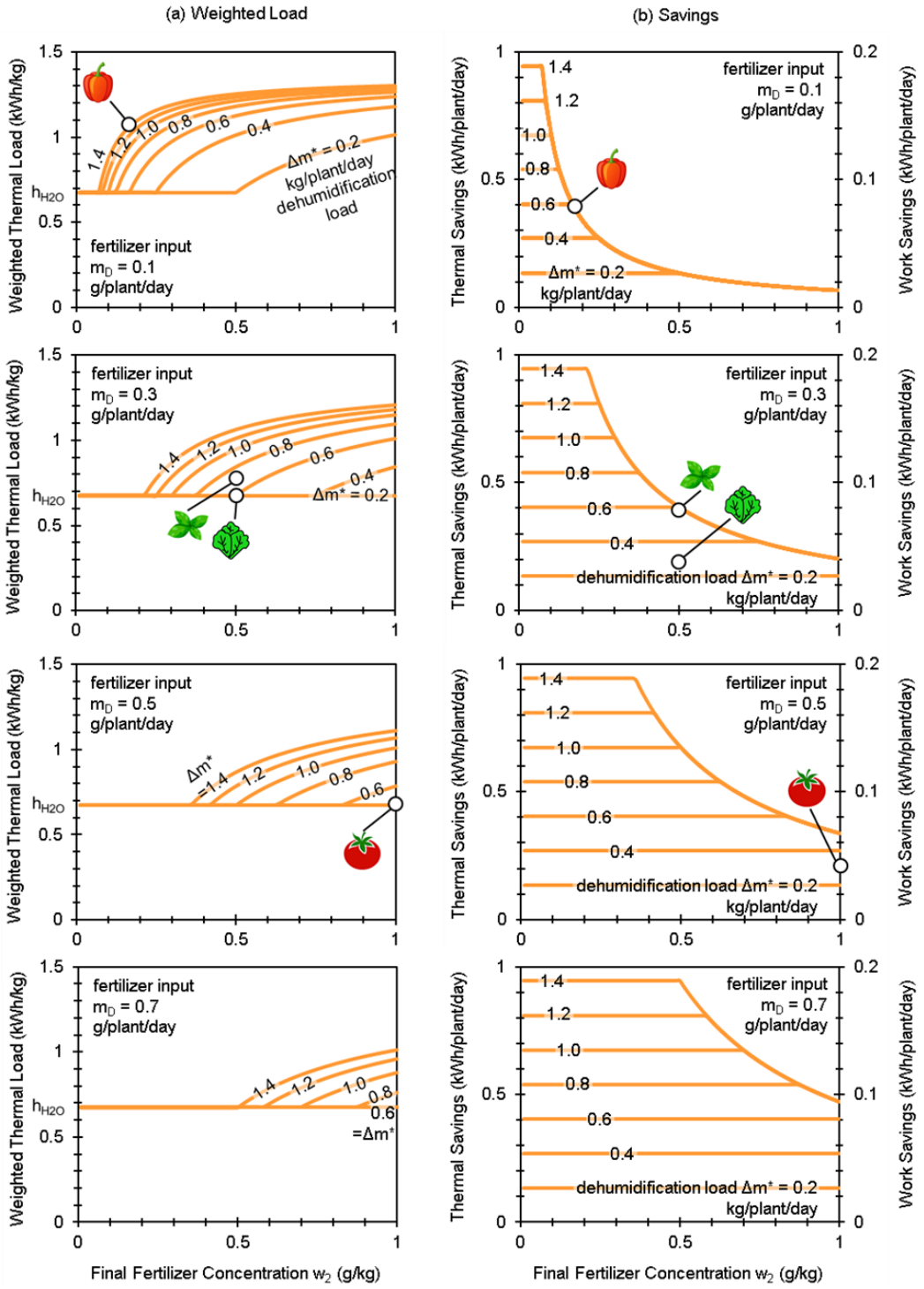

Figure 2.11 (a) Weighted energy load of fertilizer-based liquid desiccant, and (b) energy savings of switching from conventional desiccant to fertilizer-based liquid desiccant. Thermal energy is shown on the left axis, and work is shown on the right axis (assuming a coefficient of performance $\mathrm{cop} = 5$). Results are shown for different fertilizer input quantities, dehumidification loads, and desired fertilizer concentrations.

2.4 Conclusions

This study evaluates the fundamental thermodynamic limits of using fertilizer-based liquid desiccant for dehumidification of controlled plant environments. The principal goal of this analysis was to determine whether plant systems use enough fertilizer to handle the dehumidification load generated by evapotranspiration. And if so, to determine what energy savings can be achieved by switching from conventional liquid desiccant to fertilizer-based solution.

Using several common crops for case study, we show that in some cases, the capacity available from fertilizer input is sufficient to handle the dehumidification load. When this is satisfied, the thermal load of dehumidification is approximately cut in half by switching from conventional desiccant to fertilizer-based solution. This is because conventional desiccant needs to be heated for regeneration and then re-cooled for dehumidification, whereas fertilizer-based desiccant can simply be cooled in a batch process and consumed by plants when diluted enough. For crops like tomato and lettuce, which have a favorable mass balance, we show that ~ 0.7 kWh of thermal energy is saved per kg of water vapor removal.

On the other hand, we also consider crops that have an unfavorable mass balance, where fertilizer input is insufficient to handle the dehumidification load. For these crops, a second, parallel dehumidification system is needed to handle the balance of the dehumidification load. In addition to adding cost and complexity, this also limits the potential for energy savings to only that portion of the load that is handled. Interestingly, results show that the savings can nonetheless be significant, especially if the humidity load is large. For example, for basil and bell pepper, where fertilizer can only handle 85

and 45 % of their loads respectively, we nonetheless report thermal savings of ~0.4 kWh/plant/day. Assuming thermal loads are handled with a coefficient of performance of 5, these thermal savings translate to ~29 kWh/plant/year of electricity savings. For large, commercial greenhouses with many plants, these electricity savings can be quite significant.

Since these cases studies are highly specific, we also provide a series of charts that can be used to evaluate the potential of fertilizer desiccants more generally, over a range of plant system conditions. These charts show that crops that have both high evapotranspiration and high fertilizer input will have the most to gain by switching from conventional desiccant to fertilizer. These charts also serve as a useful evaluation tool to help growers and engineers obtain an initial estimate of whether fertilizer desiccant may be worth further consideration for them.

Altogether, these results are encouraging for the future of fertilizer-based liquid desiccant dehumidification. Critically, they show that the thermodynamic mass and energy balance of inputs and loads are generally favorable. This should spur further investigation of other important questions related to design, operation, control, integration, etc. In particular, we recommend technoeconomic analysis as an important next step for consideration. It remains to be seen whether the potential energy savings are sufficient to justify investment in this novel dehumidification technology.

2.5 Supplementary Information

2.5.1 Supplementary Note 2.1: Gibbs Free Energy of Separating Water Vapor from Humid Air

The Gibbs free energy of an ideal gas mixture is given by,

$$G = \sum_i n_i \left[\mu_i^o + R\,T \ln \frac{n_i}{n_{total}}\right] \tag{S2.1}$$

Where n_i is the moles of component i, μ_i^o is the chemical potential of pure i at standard temperature and pressure, and n_{total} is the total number of moles in the mixture. For a homogenous mixture of dry air and water vapor, let n_{air} be the moles of dry air and n_{H2O} be the moles of water vapor, then for initial state we get:

$$\begin{aligned} G_{initial} = {} & n_{air}\left[\mu_{air}^o + R\,T \ln\left(\frac{n_{air}}{n_{air}+n_{H2O}}\right)\right] \\ & + n_{H2O}\left[\mu_{H2O}^o + R\,T \ln\left(\frac{n_{H2O}}{n_{air}+n_{H2O}}\right)\right] \end{aligned} \tag{S2.2}$$

For final state, the mixture is separated into two parts, namely the removed portion of water, and the remaining mixture. If we assume that the separation process is perfectly selective, then the removed part will consist of pure water, while the remaining part contains all of the original quantity of air. The Gibbs free energy of the final state is then the sum of these two parts.

$$G_{final} = G_{removed} + G_{remaining} \tag{S2.3}$$

$$G_{removed} = r\,n_{H2O}\left[\mu_{H2O}^o + R\,T \ln\left(\frac{\Delta n_{H2O}}{\Delta n_{H2O}}\right)\right] = r\,n_{H2O}\,\mu_{H2O}^o \tag{S2.4}$$

Then the Gibbs energy of the remaining air-vapor mixture can be written as:

$$\begin{aligned} G_{remaining} = {} & n_{air}\left[\mu_{air}^o + R\,T \ln\left(\frac{n_{air}}{n_{air}+(1-r)\,n_{H2O}}\right)\right] \\ & + n_{H2O}\,(1-r)\left[\mu_{H2O}^o + R\,T \ln\left(\frac{(1-r)\,n_{H2O}}{n_{air}+(1-r)\,n_{H2O}}\right)\right] \end{aligned} \tag{S2.5}$$

Where r is the recovery ratio, which is the mole ratio of water vapor removed relative to the initial amount contained in the mixture $\Delta n_{H2O}/n_{H2O}$.

The change in Gibbs free energy is then the difference between the initial and final states.

$$\Delta G = G_{final} - G_{initial} \tag{S2.6}$$

$$\begin{aligned}\Delta G = {} & r\, n_{H2O}\, \mu^{o}_{H2O} + n_{air}\left[\mu^{o}_{air} + R\, T \ln\left(\frac{n_{air}}{n_{air} + (1-r)\, n_{H2O}}\right)\right] \\ & + n_{H2O}\,(1-r)\left[\mu^{o}_{H2O} + R\, T \ln\left(\frac{(1-r)\, n_{H2O}}{n_{air} + (1-r)\, n_{H2O}}\right)\right] \\ & - n_{air}\left[\mu^{o}_{air} + R\, T \ln\left(\frac{n_{air}}{n_{air} + n_{H2O}}\right)\right] \\ & - n_{H2O}\left[\mu^{o}_{H2O} + R\, T \ln\left(\frac{n_{H2O}}{n_{air} + n_{H2O}}\right)\right]\end{aligned} \tag{S2.7}$$

Now solving for the chemical potential terms μ_i^o, we can observe that they are balanced and equal to zero.

$$r\, n_{H2O}\, \mu^{o}_{H2O} + (1-r)\, n_{H2O}\, \mu^{o}_{H2O} - n_{H2O}\, \mu^{o}_{H2O} = 0 \tag{S2.8}$$

$$n_{air}\, \mu^{o}_{air} - n_{air}\, \mu^{o}_{air} = 0 \tag{S2.9}$$

This allows us to reduce equation (S2.7).

$$\begin{aligned}\Delta G = {} & n_{air}\left[R\, T \ln\left(\frac{n_{air}}{n_{air} + (1-r)\, n_{H2O}}\right)\right] \\ & + n_{H2O}\,(1-r)\left[R\, T \ln\left(\frac{(1-r)\, n_{H2O}}{n_{air} + (1-r)\, n_{H2O}}\right)\right] \\ & - n_{air}\left[R\, T \ln\left(\frac{n_{air}}{n_{air} + n_{H2O}}\right)\right] - n_{H2O}\left[R\, T \ln\left(\frac{n_{H2O}}{n_{air} + n_{H2O}}\right)\right]\end{aligned} \tag{S2.10}$$

$$\Delta G = R\,T\left[n_{air}\ln\left(\frac{n_{air}}{n_{air}+(1-r)\,n_{H2O}}\right)\right.$$
$$+ n_{H2O}\,(1-r)\ln\left(\frac{(1-r)\,n_{H2O}}{n_{air}+(1-r)\,n_{H2O}}\right) \quad \text{S2.11}$$
$$\left.- n_{air}\ln\left(\frac{n_{air}}{n_{air}+n_{H2O}}\right) - n_{H2O}\ln\left(\frac{n_{H2O}}{n_{air}+n_{H2O}}\right)\right]$$

Similarly, water vapor terms:

$$\Delta G = R\,T\left[n_{air}\ln\left(\frac{n_{air}+n_{H2O}}{n_{air}+(1-r)\,n_{H2O}}\right)\right.$$
$$+ n_{H2O}\,(1-r)\ln\left(\frac{(1-r)\,n_{H2O}}{n_{air}+(1-r)\,n_{H2O}}\right) \quad \text{S2.12}$$
$$\left.- n_{H2O}\ln\left(\frac{n_{H2O}}{n_{air}+n_{H2O}}\right)\right]$$

Finally, for convenience, the expression for the Gibbs energy of separation can be normalized per unit mass of water vapor removed from the mixture, which is given by $\Delta m = \Delta n_{H2O}\,M_{H2O} = r\,n_{H2O}\,M_{H2O}$, where M is molar mass.

$$\frac{\Delta G}{\Delta m} = \frac{R\,T}{r\,n_{H2O}\,M_{H2O}}\left[n_{air}\ln\left(\frac{n_{air}+n_{H2O}}{n_{air}+(1-r)\,n_{H2O}}\right)\right.$$
$$+ n_{H2O}\,(1-r)\ln\left(\frac{(1-r)\,n_{H2O}}{n_{air}+(1-r)\,n_{H2O}}\right) \quad \text{S2.13}$$
$$\left.- n_{H2O}\ln\left(\frac{n_{H2O}}{n_{air}+n_{H2O}}\right)\right]$$

Now we need to normalize with the mass of vapor removed, where mass of vapor is given as:

$$\Delta m = r n_{H2O} M_w \quad \text{S2.13a}$$

Where, M_{H2O} is the molar mass of water vapor. Then, the normalized minimum work can be written as:

$$\frac{\Delta G}{\Delta m} = \frac{R\,T}{M_{H2O}}\,\frac{1}{r}\left[\frac{1}{x_{H2O}}\ln\left(\frac{1+x_{H2O}}{1+(1-r)\,x_{H2O}}\right)\right.$$
$$\left.+\,(1-r)\ln\left(\frac{(1-r)\,x_{H2O}}{1+(1-r)\,x_{H2O}}\right)-\ln(x_{H2O})\right] \quad \text{S2.14}$$

2.5.2 Supplementary Note 2.2: Energy Balance of Conventional Liquid Desiccant Dehumidification

The energy requirements of the conventional liquid desiccant system illustrated in Figure S2.1 can be determined by considering the energy balance of its individual components. Equations (S2.15) -(S2.21) describe the energy balance across the dehumidification unit, the chiller, the regeneration unit, and the heater.

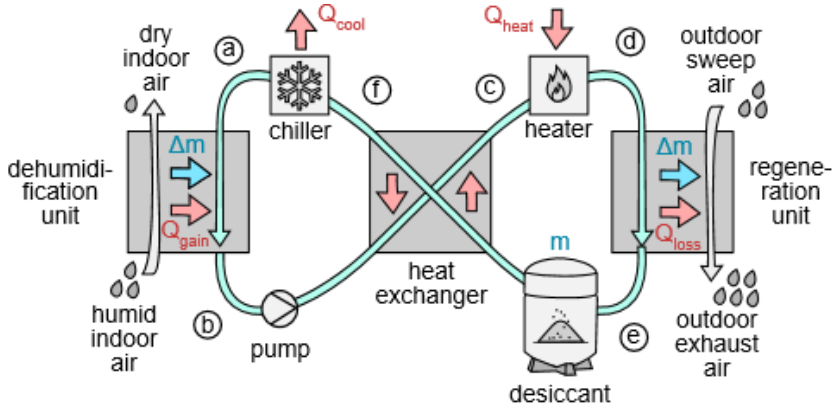

Figure S2.1 Conventional liquid desiccant cycle. (a-b) Air is dehumidified as water vapor and heat are transferred to the desiccant. (b-c) Liquid desiccant is pumped through a heat exchanger and then (c-d) a heater to raise the vapor pressure of the desiccant above exhaust air conditions. (d-e) Liquid desiccant is regenerated as water vapor and heat are dumped to the exhaust air stream. (e-f) Liquid desiccant is circulated through a heat exchanger and then (f-a) a chiller to reduce the vapor pressure to the target operating point.

Equation (S2.15) describes the energy balance of liquid desiccant through the chiller, where subscripts f and a denote the inlet and outlet. As shown, the change in energy will

be a function of the heat removed from the liquid desiccant $\dot{Q}_{cooling}$. The result of this will be a decrease in the specific energy e which will be in the form of enthalpy h, and which can be observed by a drop in temperature T at some average specific heat capacity c_p.

$$\Delta\dot{E}_{a-f} = \dot{E}_a - \dot{E}_f \quad \text{S2.15a}$$

$$\Delta\dot{E}_{a-f} = -\dot{Q}_{cooling} \quad \text{S2.15b}$$

$$\Delta\dot{E}_{a-f} = \dot{m}\, e_a - \dot{m}\, e_f \quad \text{S2.15c}$$

$$\Delta\dot{E}_{a-f} = \dot{m}\, h_a - \dot{m}\, h_f \quad \text{S2.15d}$$

$$\dot{Q}_{cooling} = \dot{m}\, h_f - \dot{m}\, h_a \quad \text{S2.15e}$$

Equation (S2.16) describes the energy balance of liquid desiccant through the dehumidification unit, where subscripts a and b denote the inlet and outlet. As shown, the change in energy will be a function of the heat transfer from the warm air to the cool desiccant $\dot{Q}_{gain}$, and the mass transfer of pure water vapor $\Delta\dot{m}$ with its associated enthalpy h_{H2O}. The result of this will be an increase in the specific energy e which will be in the form of enthalpy h.

$$\Delta\dot{E}_{b-a} = \dot{E}_b - \dot{E}_a \quad \text{S2.16a}$$

$$\Delta\dot{E}_{b-a} = \dot{Q}_{gain} + \Delta\dot{m}\, h_{H2O} \quad \text{S2.16b}$$

$$\Delta\dot{E}_{b-a} = (\dot{m} + \Delta\dot{m})\, e_b - \dot{m}\, e_a \quad \text{S2.16c}$$

$$\Delta\dot{E}_{b-a} = (\dot{m} + \Delta\dot{m})\, h_b - \dot{m}\, h_a \quad \text{S2.16d}$$

$$\dot{Q}_{gain} + \Delta\dot{m}\, h_{H2O} = (\dot{m} + \Delta\dot{m})\, h_b - \dot{m}h_a \quad \text{S2.16e}$$

Equation (S2.17) describes the energy balance of liquid desiccant through the heat exchanger, where subscripts b and c denote the inlet and outlet. As shown, the change in

energy will be a function of the heat transfer to the desiccant Q_{HX}. The result of this will be an increase in the specific energy e which will be in the form of enthalpy h.

$$\Delta\dot{E}_{c-b} = \dot{E}_c - \dot{E}_b \quad \text{S2.17a}$$

$$\Delta\dot{E}_{c-b} = \dot{Q}_{HX} \quad \text{S2.17b}$$

$$\Delta\dot{E}_{c-b} = (\dot{m} + \Delta\dot{m})\, \dot{e}_c - (\dot{m} + \Delta\dot{m})\, e_b \quad \text{S2.17c}$$

$$\Delta\dot{E}_{c-b} = (\dot{m} + \Delta\dot{m})\, h_c - (\dot{m} + \Delta\dot{m})\, h_b \quad \text{S2.17d}$$

$$\dot{Q}_{HX} = (\dot{m} + \Delta\dot{m})\, h_c - (\dot{m} + \Delta\dot{m})\, h_b \quad \text{S2.17e}$$

Equation (S2.18) describes the energy balance across liquid desiccant through the heater, where subscripts c and d denote the inlet and outlet. As shown, the change in energy will be a function of the heat transfer to the liquid desiccant $\dot{Q}_{heating}$. The result of this will be an increase in the specific energy e which will be in the form of enthalpy h.

$$\Delta\dot{E}_{d-c} = \dot{E}_d - \dot{E}_c \quad \text{S2.18a}$$

$$\Delta\dot{E}_{d-c} = \dot{Q}_{heating} \quad \text{S2.18b}$$

$$\Delta\dot{E}_{d-c} = (\dot{m} + \Delta\dot{m})\, e_d - (\dot{m} + \Delta\dot{m})\, e_c \quad \text{S2.18c}$$

$$\Delta\dot{E}_{d-c} = (\dot{m} + \Delta\dot{m})\, h_d - (\dot{m} + \Delta\dot{m})\, h_c \quad \text{S2.18d}$$

$$\dot{Q}_{heating} = (\dot{m} + \Delta\dot{m})\, h_d - (\dot{m} + \Delta\dot{m})\, h_c \quad \text{S2.18e}$$

Equation (S2.19) describes the energy balance of liquid desiccant through the regeneration unit, where subscripts d and e denote the inlet and outlet. As shown, the change in energy will be a function of the heat transfer from the warm liquid desiccant to the cool exhaust air $\dot{Q}_{loss}$, and the mass transfer of pure water vapor $\Delta\dot{m}$ with its associated enthalpy h_{H2O}. The result of this will be a decrease in the specific energy e which will be in the form of enthalpy h.

$$\Delta\dot{E}_{e-d} = \dot{E}_e - \dot{E}_d \quad \text{S2.19a}$$

$$\Delta\dot{E}_{e-d} = -\dot{Q}_{loss} - \Delta\dot{m}\, h_{H2O} \quad \text{S2.19b}$$

$$\Delta\dot{E}_{e-d} = \dot{m}\, e_e - (\dot{m} + \Delta\dot{m})\, e_d \quad \text{S2.19c}$$

$$\Delta\dot{E}_{e-d} = \dot{m}\, h_e - (\dot{m} + \Delta\dot{m})\, h_d \quad \text{S2.19d}$$

$$\dot{Q}_{loss} = (\dot{m} + \Delta\dot{m})\, h_d - \dot{m}\, h_e - \Delta\dot{m}\, h_{H2O} \quad \text{S2.19e}$$

Equation (S2.20) describes the energy balance of liquid desiccant through the heat exchanger, where subscripts e and f denote the inlet and outlet. As shown, the change in energy will be a function of the heat removed from the desiccant $\dot{Q}_{HX}$. The result of this will be a decrease in the specific energy e which will be in the form of enthalpy h.

$$\Delta\dot{E}_{f-e} = \dot{E}_f - \dot{E}_e \quad \text{S2.20a}$$

$$\Delta\dot{E}_{f-e} = -\dot{Q}_{HX} \quad \text{S2.20b}$$

$$\Delta\dot{E}_{f-e} = \dot{m}\, e_f - \dot{m}\, e_e \quad \text{S2.20c}$$

$$\Delta\dot{E}_{f-e} = \dot{m}\, h_f - \dot{m}\, h_e \quad \text{S2.20d}$$

$$\dot{Q}_{HX} = \dot{m}\, h_e - \dot{m}\, h_f \quad \text{S2.20e}$$

Both equations (S2.17) and (S2.20) describe the energy balance of the heat exchanger. In addition, the heat transfer from one fluid to the other can be described in terms of the heat exchanger effectiveness ε and the maximum heat transfer possible between the hot and cold fluids $\dot{Q}_{max}$, as in equation (S2.21). Treating the liquid desiccant as incompressible and the specific heat capacity of fluid c_p as constant, we can express the change in temperature T associated with heat transfer in terms of the change in enthalpy c_p.

$$\dot{Q}_{HX} = \varepsilon\, \dot{Q}_{max} \quad \text{S2.21a}$$

$$\dot{Q}_{HX} = \varepsilon\,(\dot{m} + \Delta\dot{m})\,c_p\,(T_e - T_b) \qquad \text{S2.21b}$$

$$\dot{Q}_{HX} = \varepsilon\,(\dot{m} + \Delta\dot{m})\,(h_e - h_b) \qquad \text{S2.21c}$$

Now, taking equations (S2.15)-(S2.21) we can obtain an expression for the cooling load. It is helpful to obtain the expression in terms of the enthalpy at the entrance of the dehumidification unit h_a, the enthalpy at the entrance of the regeneration unit h_d, and the initial mass of liquid desiccant m, because all of these input parameters are defined at the design stage.

$$\dot{Q}_{cooling} = \dot{m}\,h_f - \dot{m}\,h_a \qquad \text{S2.15}$$

$$\dot{Q}_{cooling} = \left[\dot{m}\,h_e - \dot{Q}_{HX}\right] - \dot{m}\,h_a \qquad \text{S2.15+S2.20}$$

$$\dot{Q}_{cooling} = \dot{m}\,h_e - [\varepsilon\,(\dot{m} + \Delta\dot{m})\,(h_e - h_b)] - \dot{m}\,h_a \qquad \text{S2.15+S2.20+S2.21}$$

$$\dot{Q}_{cooling} = \left(\dot{m} - \varepsilon\,(\dot{m} + \Delta\dot{m})\right) h_e + \varepsilon\,(\dot{m} + \Delta\dot{m})\,h_b - \dot{m}\,h_a \qquad \text{S2.15+S2.20+S2.21}$$

$$\dot{Q}_{cooling} = \Big(\dot{m} - \varepsilon\,(\dot{m} + \Delta\dot{m})\Big)\left[\frac{-\dot{Q}_{loss} + (\dot{m} + \Delta\dot{m})\,h_d - \Delta\dot{m}\,h_{H2O}}{\dot{m}}\right] + \varepsilon\,(\dot{m} + \Delta\dot{m})\left[\frac{\dot{Q}_{gain} + \dot{m}\,h_a + \Delta\dot{m}\,h_{H2O}}{(\dot{m} + \Delta\dot{m})}\right] - \dot{m}\,h_a \qquad \text{S2.15+S2.16+ S2.19+S2.20+S2.21}$$

$$\dot{Q}_{cooling} = \left(1 - \varepsilon\left(1 + \frac{\Delta\dot{m}}{\dot{m}}\right)\right)(\dot{m} + \Delta\dot{m})\,h_d - (1 - \varepsilon)\,\dot{m}\,h_a + \varepsilon\,\dot{Q}_{gain} - \left(1 - \varepsilon\left(1 + \frac{\Delta\dot{m}}{\dot{m}}\right)\right) Q_{loss} - \left(1 - \varepsilon\left(1 + \frac{\Delta\dot{m}}{\dot{m}}\right) - \varepsilon\right)\Delta\dot{m}\,h_{H2O} \qquad \text{S2.22a}$$

And similarly, for the heating load:

$$\dot{Q}_{heating} = (\dot{m} + \Delta\dot{m})\, h_d - (\dot{m} + \Delta\dot{m})\, h_c \qquad \text{S2.18}$$

$$\dot{Q}_{heating} = (\dot{m} + \Delta\dot{m})\, h_d - [Q_{HX} + (\dot{m} + \Delta\dot{m})\, h_b] \qquad \text{S2.17+S2.18}$$

$$\dot{Q}_{heating} = (\dot{m} + \Delta\dot{m})\, h_d - [\varepsilon\, (\dot{m} + \Delta\dot{m})\, (h_e - h_b)] - (\dot{m} + \Delta\dot{m})\, h_b \qquad \text{S2.17+S2.18+S2.21}$$

$$\dot{Q}_{heating} = (\dot{m} + \Delta\dot{m})\, h_d - \varepsilon\, (\dot{m} + \Delta\dot{m})\, h_e - (1 - \varepsilon)\, (\dot{m} + \Delta\dot{m})\, h_b \qquad \text{S2.18+S2.17+S2.21}$$

$$\dot{Q}_{heating} = (\dot{m} + \Delta\dot{m})\, h_d - \varepsilon\, (\dot{m} + \Delta\dot{m}) \left[\frac{-\dot{Q}_{loss} + (\dot{m} + \Delta\dot{m})\, h_d - \Delta\dot{m}\, h_{H2O}}{m}\right] - (1 - \varepsilon)\, (\dot{m} + \Delta\dot{m}) \left[\frac{\dot{Q}_{gain} + \dot{m}\, h_a + \Delta\dot{m}\, h_{H2O}}{(\dot{m} + \Delta\dot{m})}\right] \qquad \text{S2.16+S2.17+S2.18+S2.19+S2.21}$$

$$Q_{heating} = \left(1 - \varepsilon\, \left(1 + \frac{\Delta\dot{m}}{\dot{m}}\right)\right) (\dot{m} + \Delta\dot{m})\, h_d - (1 - \varepsilon)\, \dot{m}\, h_a + \varepsilon\, \left(1 + \frac{\Delta\dot{m}}{\dot{m}}\right) \dot{Q}_{loss} - (1 - \varepsilon)\, \dot{Q}_{gain} - \left(1 - \varepsilon\, \left(1 + \frac{\Delta\dot{m}}{\dot{m}}\right) - \varepsilon\right) \Delta\dot{m}\, h_{H2O} \qquad \text{S2.23a}$$

Then for the simple case where an ideal heat exchanger has an effectiveness $\varepsilon = 1$, and where the dehumidification unit and regeneration unit are adiabatic so that $\dot{Q}_{gain} = \dot{Q}_{loss} = 0$, the expressions for cooling and heating loads can be simplified as follows.

$$\dot{Q}_{cooling} = \left(1 + \frac{\Delta\dot{m}}{\dot{m}}\right) \Delta\dot{m}\, h_{H2O} - \left(1 + \frac{\Delta\dot{m}}{\dot{m}}\right) \Delta\dot{m}\, h_d \qquad \text{S2.24a}$$

$$\dot{Q}_{heating} = \left(1 + \frac{\Delta\dot{m}}{\dot{m}}\right) \Delta\dot{m}\, h_{H2O} - \left(1 + \frac{\Delta\dot{m}}{\dot{m}}\right) \Delta\dot{m}\, h_d \quad \text{S2.24b}$$

For convenience, the cooling and heating loads can be normalized per unit mass of vapor permeate to obtain equations (2.24c) and (2.24d).

$$\frac{\dot{Q}_{cooling}}{\Delta\dot{m}} = \left(1 + \frac{\Delta\dot{m}}{\dot{m}}\right) (h_{H2O} - h_d) \quad \text{S2.24c}$$

$$\frac{\dot{Q}_{heating}}{\Delta\dot{m}} = \left(1 + \frac{\Delta\dot{m}}{\dot{m}}\right) (h_{H2O} - h_d) \quad \text{S2.24d}$$

2.5.3 Supplementary Note 2.3: Energy Balance of Fertilizer-Based Liquid Desiccant Dehumidification

Since the proposed fertilizer-based liquid desiccant system (illustrated in Figure S2.2) is a batch process (rather than a cycle like for conventional liquid desiccant), its energy requirements are best determined by considering the energy balance of the liquid desiccant from start (super concentrated fertilizer solution near its solubility limit) to finish (diluted fertilizer solution that is ready for plants).

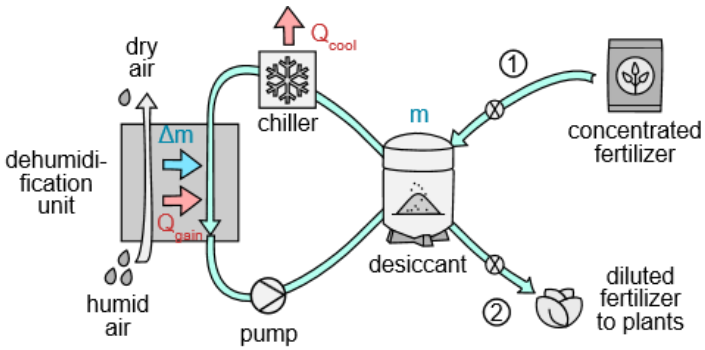

Figure S2.2 Fertilizer-based liquid desiccant dehumidification cycle. (1) An initial quantity of fertilizer is introduced to the system and cooled to achieve some target vapor pressure. Air is dehumidified as water vapor (and heat) are transferred to the desiccant. Liquid desiccant is recirculated through a chiller to reduce the vapor pressure to meet the target operating point. (2) At its final state, after sufficient dilution, the fertilizer solution is delivered to plants and a new batch of concentrated fertilizer is input to the system.

Equation (S2.25) describes the energy balance between the initial and final states of the liquid desiccant solution, as denoted by subscripts 1 and 2. As shown, the change in energy is equal to the balance between heat gain from the warm air to the cool desiccant $\dot{Q}_{gain}$, mass transfer of pure water vapor Δm with its associated enthalpy h_{H2O}, and heat removed by active cooling $\dot{Q}_{cooling}$.

$$\Delta \dot{E}_{2-1} = \dot{E}_2 - \dot{E}_1 \quad \text{S2.25a}$$

$$\Delta \dot{E}_{2-1} = h_{H2O}\, \Delta \dot{m} + \dot{Q}_{gain} - \dot{Q}_{cooling} \quad \text{S2.25b}$$

Treating the liquid desiccant as an incompressible fluid, we can express the change in energy of the solution as a function of its mass m, specific heat capacity c_p, and temperature T to obtain equation (S2.26). All three of the variables $\dot{m}$, c_p, and T change from the initial to final states of the batch process, where the relationship between them depends on the way in which the batch process is operated, as discussed in detail in Section 2.4.3.

$$\int_1^2 \dot{m}\, c_p\, dT = h_{H2O}\, \Delta \dot{m} + \dot{Q}_{gain} - \dot{Q}_{cooling} \quad \text{S2.26a}$$

In any case, the cooling load can then be obtained by reorganizing the above expression. Also, for convenience, the load is normalized per unit mass of vapor permeate $\Delta \dot{m} = \dot{m}_2 - \dot{m}_1$.

$$\dot{Q}_{cooling} = h_{H2O}\, \Delta \dot{m} + \dot{Q}_{gain} - \int_1^2 \dot{m}\, cp\, dT \quad \text{S2.26b}$$

$$\frac{\dot{Q}_{cooling}}{\Delta \dot{m}} = h_{H2O} + \frac{\dot{Q}_{gain}}{\Delta \dot{m}} - \frac{1}{\Delta \dot{m}} \int_1^2 \dot{m}\, cp\, dT \quad \text{S2.26c}$$

CHAPTER THREE

NUMERICAL MODELING: SIMULATING TRANSPORT DYNAMICS TO EVALUATE THE SPECIFIC ENERGY USE OF FERTILIZER-BASED LIQUID DESICCANT TO DEHUMIDIFY INDOOR PLANT ENVIRONMENTS

3.1 Introduction

As mentioned in previous chapters of this dissertation, maintaining proper humidity levels in plant environments is crucial for crop productivity, quality and health which needs water vapor removal at a rate similar to plant evapotranspiration [60]. While fresh air ventilation can be used for this, closed systems are often preferred to prevent pests and contaminant entry. In closed systems, water vapor removal is typically brought using conventional air conditioning systems [61,62] and through various desiccant-based cycles [63-69]. With all these technologies, one of the primary challenges is to reduce energy intensity for dehumidification, so as to reduce operating costs, as highlighted in Chapter One. For measuring this energy intensity, one common energy efficiency metric is the specific energy use of dehumidification which is ratio of amount of energy consumed to water vapor removed from the humid air environment. Lab-scale systems have reported values between 0.3-0.9 kWh/kg under optimized conditions [70-72], whereas commercial systems often range from 1-2 kWh/kg [73]. In contrast, recent indoor farming regulations require 0.37-0.55 kWh/kg [73]. This suggests the need for more improved technologies for dehumidification in indoor farming.

In an effort to improve the energy efficiency of greenhouse dehumidification, our lab recently introduced the novel concept of using concentrated fertilizer solution as a liquid desiccant agent [30]. Figure 3.1 illustrates one schematic of the concept in a membrane-

based dehumidification process. As shown, fertilizer solution is circulated through a membrane module where the low vapor pressure of the cool concentrated desiccant draws water vapor across the membrane, out of the indoor air. A chiller is used to remove the heat of condensation released from the phase change of water vapor that occurs on the desiccant surface and thereby maintains a relatively cool fertilizer desiccant with low vapor pressure. When fertilizer solution is sufficiently diluted, it is replaced by a fresh batch of fertilizer and then delivered directly to plants where it provides valuable nutrients in addition to closing the water cycle by recycling water vapor for irrigation. The concept was experimentally validated in our lab's previous work, and dehumidification was confirmed across a range of typical greenhouse conditions using a variety of common fertilizers [30].

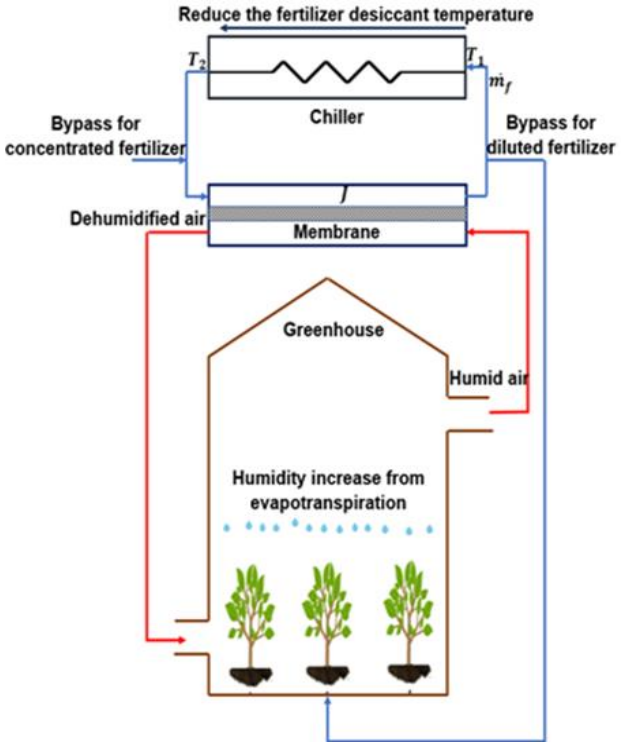

Figure 3.1 Water vapor permeate can be drawn from a humid air stream across a selective polymer membrane by a vapor pressure gradient established by a concentrated fertilizer-based liquid desiccant solution.

A more detailed process and psychrometric diagram is also provided in Figure 3.2. As shown, the principal advantage of the proposed dehumidification process is that it avoids the need for overcooling air to the dewpoint and then re-heating as with conventional air conditioning, and it avoids the need for thermal regeneration and then re-cooling of the liquid desiccant solution as with typical liquid desiccant processes. Therefore, while important energy savings are theoretically possible, no systematic analysis of the system's specific energy of dehumidification has yet been published in the scientific literature. While Chapter Two establishes thermodynamic limits and energy savings under the assumption of no heat gain but only enthalpy transfer from water vapor, this chapter presents a more realistic evaluation by simulation of heat flux as heat gain across the membrane.

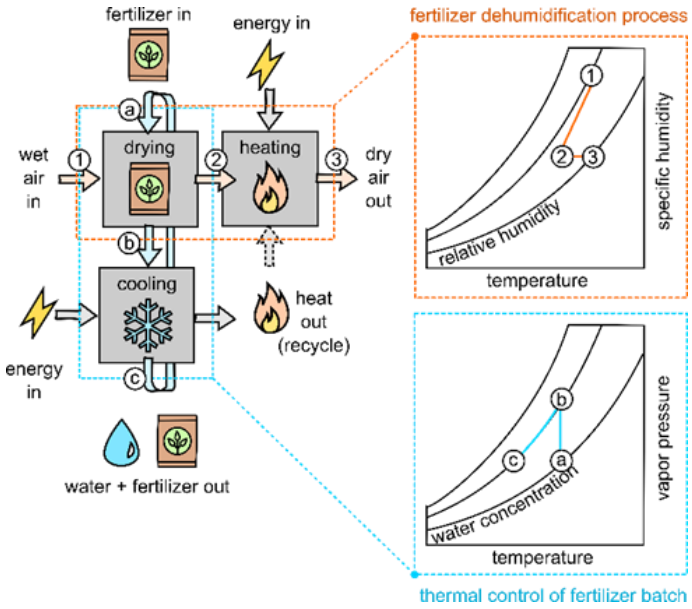

Figure 3.2 Process and psychrometric diagrams of fertilizer dehumidification system. (1)-(2): Humidity is absorbed by cool fertilizer liquid desiccant solution, reducing air humidity and reducing temperature due to thermal diffusion. (2)-(3): Air is reheated to ambient temperatures via a heat pump or from waste heat. (a)-(b): Fertilizer desiccant solution is diluted as water vapor is absorbed, reducing its concentration and increasing its vapor pressure. (b)-(c): Fertilizer solution at the new concentration is cooled to restore the target vapor pressure.

The purpose of this study is therefore to evaluate theoretical specific energy use of dehumidification for fertilizer-based liquid desiccant dehumidification using a more realistic approach that was neglected in thermodynamic analysis. This builds on our lab's previous work, which introduced the concept and provided evidence of successful dehumidification, but which importantly did not include any evaluation of the concept's specific energy use [30]. This is the gap that this Chapter will address. For the first time, this important performance metric will be studied here and provide insight into the potential for this technology to compete with other dehumidification systems. Fundamental mass and heat transport dynamics of the process are defined, and a numerical model is validated and then used to simulate energy performance in response to a range of operating conditions and a selection of membrane properties.

3.2 Theory

3.2.1 Specific Energy of Dehumidification

In a membrane-based dehumidification system, a polymer core separates a concentrated desiccant solution from a humid air feed stream as shown in Figure 3.3. Water vapor from the air stream migrates to the membrane's surface, diffuses through it, and then desorbs and condenses on the liquid desiccant surface due to a differential vapor pressure between the air stream and the liquid desiccant solution.

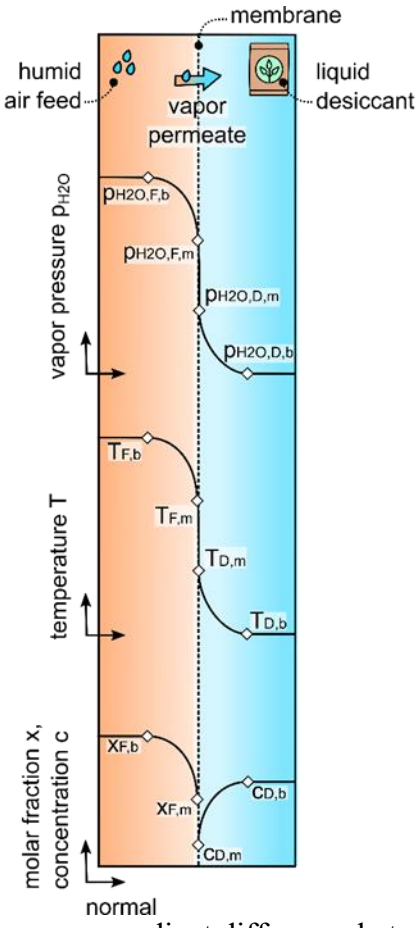

Figure 3.3. The water vapor pressure gradient difference between the liquid desiccant and the humid feed air drives the vapor flux in a membrane-based liquid desiccant dehumidification process. The vapor pressure difference across the membrane is determined by the non-linear temperature and concentration gradients.

Because the driving vapor pressure is strongly dependent on temperature, it is generally necessary to maintain cool liquid desiccant. This is especially important in the proposed fertilizer-based liquid desiccant process, where temperature is used to maintain the target vapor pressure, even as the batch of fertilizer solution is diluted. This thermal gradient across the membrane improves the rate of water vapor transfer, but also leads to heat transfer, and the associated thermal load must be managed by actively cooling the liquid desiccant. The result of these dynamics is a tradeoff between the rate of water vapor mass transfer and the rate of thermal energy transfer, which are both proportional

to desiccant temperature. The ratio of these two dynamics can be expressed as the specific energy of dehumidification q, as defined in equation (3.1), and optimized as a function of temperature, as illustrated in Figure 3.4.

$$q = \frac{\dot{Q}}{\Delta \dot{m}} \tag{3.1}$$

Where $\dot{Q}$ is the amount of heat transferred to the liquid desiccant per unit time, which is the cooling load, and $\Delta \dot{m}$ is the amount of water removed from the humid air, both of which are defined in equations (3.2) and (3.10). Because many technologies can handle cooling loads with coefficients of performance greater than unity, it is also helpful to consider the specific electric energy (work) normalized over the coefficient of performance, i.e., $w = q/\,\mathrm{cop}$. Where coefficient of performance, cop is defined as the measure of cooling efficiency.

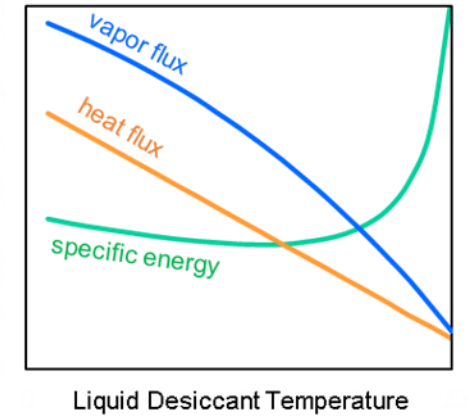

Figure 3.4. Water vapor flux and thermal energy flux towards the liquid desiccant solution are both increased by cool desiccant temperatures. The balance of these two-competing metrics can be expressed as the specific energy of dehumidification and optimized as a function of temperature.

3.2.2 Vapor Transfer Across the Membrane

In a membrane-based dehumidification system, water vapor transfer from humid feed air towards concentrated liquid desiccant is driven by diffusion along a vapor pressure

gradient. When normalized per unit membrane surface area, the rate of water vapor transfer can be expressed as vapor flux J.

$$J = \frac{\Delta \dot{m}}{a} = \dot{m}_{diffusion} \tag{3.2a}$$

$$J = \frac{\Delta \dot{m}}{a} = K\,\Delta p_{H2O} \tag{3.2b}$$

Where a is the membrane surface area, K is the mass transfer coefficient of water vapor transport, and Δp_{H2O} is the vapor pressure difference across the membrane and fluid boundary layers. The vapor pressure of the humid feed air can be obtained as a fraction of atmospheric pressure as per Dalton's law or as a fraction of the saturation pressure, as described in equation (3.3). The vapor pressure of the liquid desiccant solution can be obtained from the Kohler equation [75,76], as described in equation (3.4).

$$p_{H2O,F} = x\,p = RH\,p_o \tag{3.3}$$

$$p_{H2O,d} = p_o \exp\left(\frac{V_m}{R\,T}(p - \pi)\right) \tag{3.4}$$

Where x is the mole fraction of water vapor, p is pressure, RH is the relative humidity, and p_o is the equilibrium vapor pressure, R is the gas constant, V_m is the molar volume of water, T is temperature, and π is osmotic pressure. In the equations (3.3) and (3.4), the subscripts F and d represent the feed (air) and fertilizer desiccant, respectively.

While other models have also been proposed, the equilibrium vapor pressure p_o and the osmotic pressure π, can be classically obtained from the Antoine equation and the Van't Hoff equation.

$$p_o = 10^{\left(A_o - \frac{B_o}{C_o + T}\right)} \tag{3.5}$$

$$\pi = i\,R\,T\,c \tag{3.6}$$

Where A_o, B_o, and C_o are empirical constants, i is the number of ions, and c is the ion concentration in the solution.

In cases where a rough estimate of flux is satisfactory, the vapor pressures in equations (3.3) and (3.4) can be calculated from the properties, temperatures, and concentrations of the bulk fluids. However, in cases where a more accurate model of flux is desired, boundary layer dynamics should be considered, to obtain vapor pressures as a result of temperatures, concentrations, and other fluid properties at the membrane surfaces.

In this case, a lumped element approach is taken and vapor diffusion across the membrane and also the fluid boundary layers is considered. This is done by considering the water vapor pressure difference Δp_{H2O} across each of their respective mass transfer coefficients K. Where K_m, K_F, and K_D are mass transfer coefficients for the membrane, the feed air boundary layer, and liquid desiccant boundary layer, respectively, each of which are defined in equations (3.7)-(3.9).

$$K_m = B/L \tag{3.7}$$

$$K_F = 0.0732\,Re^{0.6}\,Sc^{0.33}\,\frac{p}{p'}\frac{T'}{T}\frac{D}{d^{0.4}} \tag{3.8}$$

$$K_D \approx 0 \tag{3.9}$$

The expression for the membrane mass transfer coefficient K_m is obtained from the simple ratio of membrane vapor permeability B and thickness L. The air feed mass transfer coefficient K_F is given here by an empirical expression previously proposed for gas flow in hollow fiber membranes [77-79], where Re is the Reynolds number of air based on hydraulic diameter, Sc is the Schmidt number, D is the diffusivity of water

vapor, d is the hydraulic diameter, and p' and T' are standard pressure and temperature. The use of equation (3.8) assumes that the fluid is turbulent, the solute concentration does not significantly affect the fluid properties, and convective mass transfer is the dominant transport mechanism. And the mass transfer coefficient for the liquid desiccant is neglected $K_D \sim 0$, since the boundary layer gradient of water concentration is minimal [80].

3.2.3 Heat Transfer Across the Membrane

In a membrane-based dehumidification system, thermal energy transfer to the liquid desiccant solution is driven primarily by diffusion along a temperature gradient between the warm feed air and the cool liquid desiccant, as well as by vapor mass transfer that carries both latent and sensible heat across the membrane. When normalized per unit membrane surface area, the rate of thermal energy transfer can be expressed as heat flux $\dot{q}$.

$$\dot{q} = \frac{\dot{Q}}{a} = \dot{q}_{diffusion} + \frac{\Delta \dot{m}}{a} \times h_{H2O} \tag{3.10a}$$

$$\dot{q} = \frac{\dot{Q}}{a} = \frac{\Delta T}{R_{th}} + J \times h_{H2O} \tag{3.10b}$$

Where $\dot{q}_{diffusion}$ is the temperature-driven thermal diffusion through the membrane, $J \times h_{H2O}$ is the heat carried by the water vapor mass that permeates across the membrane. Expressions for each of these three thermal energy transfer mechanisms are provided in equation (3.10b), where ΔT is the temperature difference across the membrane and fluid boundary layers with thermal resistivity R_{th}, and h_{H2O} is the specific enthalpy.

As stated previously, in cases where only an estimate of heat flux is needed, the temperatures and other fluid properties in equation (3.10) can be taken from the bulk fluids. However, to improve modeling accuracy, it is necessary to consider the non-linear temperature gradient across the fluid boundary layers, which will act to reduce heat flux (as well as mass flux).

In this case, a lumped element approach is taken and heat transfer across the membrane and the fluid boundary layers are considered. This is done by considering the temperature difference ΔT across each of their respective thermal resistivity R_{th} normalized over area a. Where $R_{th,m}$, $R_{th,F}$, and $R_{th,d}$ are thermal resistivities for the membrane, the feed air boundary layer, and liquid desiccant boundary layer, respectively, each of which are defined in equations (3.11) -(3.13).

$$R_{th,m} = L/k \tag{3.11}$$

$$R_{th,F} = {H_F}^{-1} = \left(0.023 \frac{k}{d} Re^{0.8} Pr^{0.3}\right)^{-1} \tag{3.12}$$

$$R_{th,d} = {H_D}^{-1} = \left(0.36 \frac{k}{d} Re^{0.55} Pr^{0.33}\right)^{-1} \tag{3.13}$$

Where k is the thermal conductivity of either the membrane or the boundary layer fluid, H is the convection coefficient which is given here by empirical expressions previously proposed for shell and tube configurations [81,82], and Pr is the Prandtl number for respective fluids. Equation (3.12) is for air side, while (3.13) is for fertilizer desiccant side.

3.3 Methods and Materials

3.3.1 Finite Difference Analysis

A numerical approach was employed to evaluate the specific energy use of dehumidification as a result of water vapor flux and heat flux in the fertilizer-based liquid desiccant system. A theoretical model of mass and heat transport dynamics was developed using equations (3.1)-(3.13) using the control volume shown in Figure 3.5 along with the heat and mass transfer circuit. The model was applied using discrete element analysis in 2-dimensions, including the direction normal to the membrane surface, and the direction axial to the membrane surface as shown in Figure 3.5.

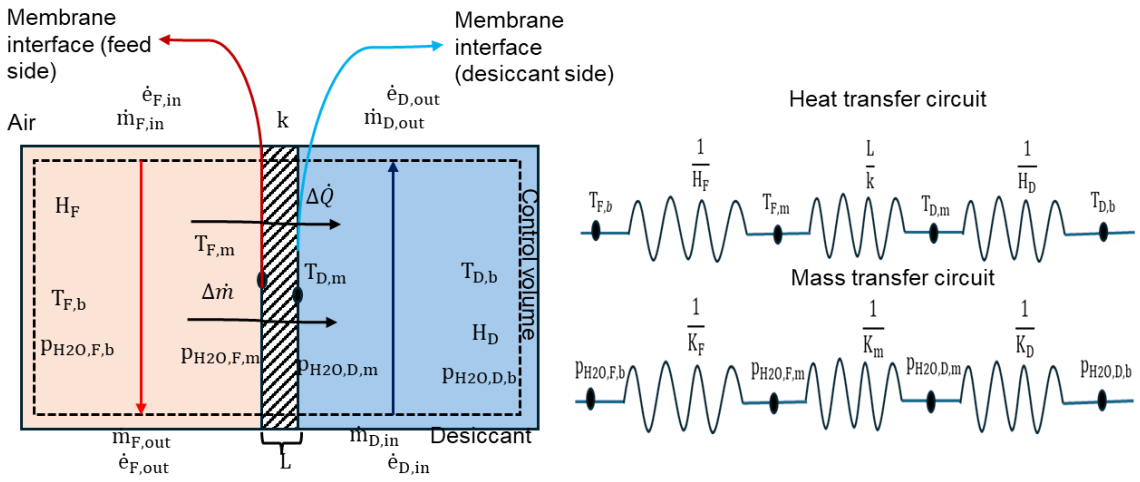

Figure 3.5 Control volume diagram for theoretical mass and heat transport dynamics along with the heat and mass transfer circuit used in finite element analysis

In the normal direction, concentration and temperature gradients develop due to different mass and thermal diffusivity rates across the membrane and its boundary layers. The normal profile was discretized into lumped elements, and a steady-state mass and energy balance was defined at both the air feed membrane surface and the liquid desiccant membrane surface. The governing equations of this balance are provided in Table 3.1 with the help of Figure 3.5, where the subscript b is used to define pressure and

temperature of the bulk fluid, and subscript m is used to specify properties at the membrane surface. In the air side, the convective heat transfer from air and the sensible heat carried by the vapor is conducted through membrane and the sensible heat flux continues through the membrane. On the desiccant side, heat conduction through membrane and sensible heat of permeated vapor is transferred to the bulk desiccant through convection, sensible heat transport and heat release due to vapor condensation on the surface of desiccant.

Table 3.1 Steady state mass and energy balance at the membrane surfaces.

	Mass balance	Energy balance
Air feed membrane surface	$K_F\left(p_{H2O,F,b} - p_{H2O,F,m}\right) = K_m\left(p_{H2O,F,m} - p_{H2O,D,m}\right)$	$H_F\left(T_{F,b} - T_{F,m}\right) + \frac{\Delta\dot{m}}{a}\left(h_{F,b}\right) = \frac{k}{L}\left(T_{F,m} - T_{D,m}\right) + \frac{\Delta\dot{m}}{a}\left(h_{F,m}\right)$
Liquid desiccant membrane surface	$K_m\left(p_{H2O,F,m} - p_{H2O,D,m}\right) = K_D\left(p_{H2O,D,m} - p_{H2O,D,b}\right)$	$\frac{k}{L}\left(T_{F,m} - T_{D,m}\right) + \frac{\Delta\dot{m}}{a}\left(h_{F,m}\right) = H_D\left(T_{D,m} - T_{D,b}\right) + \frac{\Delta\dot{m}}{a}\ h_{D,m}$

In the axial direction, concentration and temperature gradients develop due to the accumulation of water permeate and heat as the bulk liquid desiccant advances (and conversely the depletion of water permeate and heat from the bulk air feed). The axial profile was discretized into finite difference, and a steady-state mass and energy balance was defined for each element of bulk fluid flow along the membrane surface. The governing equations of this balance are provided in Table 3.2, and the discretized equations in the axial directions are provided from 3.14-3.17:

$$\dot{m}_F\left(x_{H2O,j+1} - x_{H2O,j}\right) = \Delta\dot{m}_j \tag{3.14}$$

$$\dot{m}_d\left(c_{H2O,j+1} - c_{H2O,j}\right) = \Delta\dot{m}_j \tag{3.15}$$

$$\dot{m}_F\left(h_{F,j+1} - h_{F,j}\right) = -\dot{Q}_j - \Delta\dot{m}_j h_{h2O} \tag{3.16}$$

$$\dot{m}_d\left(h_{d,j+1} - h_{d,j}\right) = \dot{Q}_j + \Delta\dot{m}_j h_{h2O} \quad 3.17$$

Where, x_{H2O} is the mole fraction of water vapor in the air, c is the concentration of water vapor in the solution, $\dot{Q}$ is the heat transferred. In the equations (3.14-3.17), j represents the node the in the discretization and h is the enthalpy.

Table 3.2 Steady state mass and energy balance for bulk air feed and liquid desiccant flow axial to the membrane surface.

	Mass balance	Energy balance
Air feed bulk fluid	$\dot{m}_{F,out} = \dot{m}_{F,in} - \Delta\dot{m}$	$\dot{m}_{F,in}\,\dot{e}_{F,out} = \dot{m}_{F,out}\,\dot{e}_{F,in} - \dot{Q}$
Liquid desiccant bulk fluid	$\dot{m}_{D,out} = \dot{m}_{D,in} + \Delta\dot{m}$	$\dot{m}_{D,out}\,e_{D,out} = \dot{m}_{D,in}\,e_{D,in} + \dot{Q}$

3.3.2 Numerical Methods

The coupled mass and heat transport model was implemented in MATLAB (R2018a, MathWorks, Natick, MA) to simulate the fertilizer-based liquid desiccant dehumidification process. A finite difference method was used to discretize the governing equations, and a nested iterative algorithm was developed to solve the heat and mass transfer coupled system. The overall computational framework is outlined in Figure 3.6. The model begins by initializing all the input parameters, including air and desiccant flow properties, membrane characteristics, and boundary conditions. An initial guess is made for the water vapor flux, which is required to estimate the local membrane surface temperatures. An initial guess was needed due to the flow conditions being counter flow. Since the surface temperatures themselves are functions of the vapor flux due to coupled heat and mass transfer, a nested iterative loop is used to refine the flux estimation until convergence ($\left|\frac{(Jc-Jg)}{Jg}\right| \leq 10^{-3}$) is achieved for each discrete axial segment of the membrane. A marching algorithm is then applied along the membrane length to update

local air and desiccant temperatures and concentrations based on the mass and energy balances. This procedure accounts for axial variation and polarization effects along the flow direction.

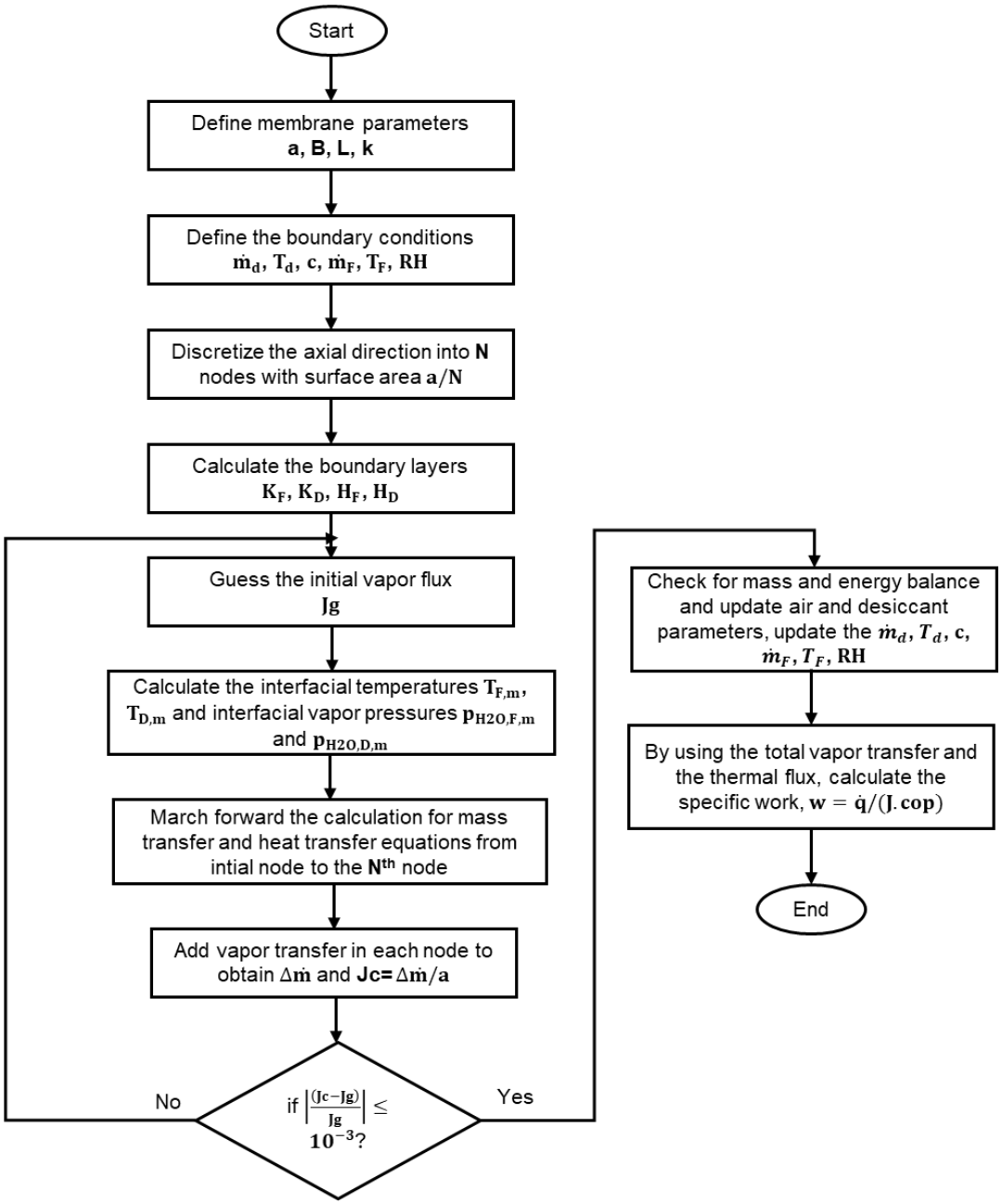

Figure 3.6 Finite difference model used to numerically solve heat and mass transfer across each finite membrane element and determine the resulting energy and mass balance of each control volume throughout the liquid desiccant and air feed boundary layers.

3.3.3 Simulation Parameters

A number of different scenarios were simulated to evaluate performance, particularly the specific energy of dehumidification, over a range of operating and environmental conditions. A summary of the membrane characteristics and simulation input parameters is provided in Table 3.3. Unless otherwise specified, all results refer to these baseline conditions. The baseline is defined so as to be consistent with laboratory test conditions used in previous study [30] and was experimentally validated as described in Section 3.3.4. A hollow fiber module with a dense polydimethylsiloxane membrane was selected for the baseline scenario.

Table 3.3 Baseline simulation input parameters

Membrane	
Configuration	hollow fiber
Material	polydimethylsiloxane
Vapor permeability B	3.94×10^{-6} g m^{-2} s^{-1} Pa^{-1}
Thermal conductivity k	0.19 W m^{-1} K^{-1}
Membrane area a	1 m^2
Fiber thickness L	55×10^{-6} m
Fiber diameter d	300×10^{-6} m
Number of fibers	12,600
Shell channel diameter	6×10^{-2} m
Liquid Desiccant	
Flow direction	counter
Mass flow $\dot{m}_d$	2 lpm
Fertilizer solute	$Ca(NO_3)_2$ $4H_2O$
Concentration c	945 g/l (75 % solubility)
Temperature T_d	15 °C
Coefficient of performance cop	5
Air Feed Supply	
Mass flow $\dot{m}_F$	5 slpm
Humidity RH	70 %
Temperature T_F	25 °C

3.3.4 Experimental Validations

Experimental validation of the mass and heat transport model was completed for baseline conditions using a laboratory test bench as shown in Figure 3.7. At the heart of the system is a commercial polydimethylsiloxane hollow fiber membrane module (PDMSXA-1.0, PermSelect, Ann Arbor MI).

Feed is circulated through the membrane fibers from a compressed air source. Air feed is heated and humidified to the target test conditions via an inline electric heater with a variable dc power source, and via bubbling through columns of deionized water. A mass and energy balance of the air feed is considered by measuring mass flow rate (GH-32907-69 mass flow controller, Masterflex, Radnor, PA), temperature in and out (MT-6340-30 thermal resistance sensors, TWTADE, Suzhou, China), and relative humidity in and out (AM2315 capacitive humidity sensors, Aosong Electronics, Guangzhou, China).

Liquid desiccant is pumped through the shell side of the membrane module from a reservoir of fertilizer solution prepared from deionized water and calcium nitrate tetrahydrate (98 % pure, Fisher-Scientific, Pittsburgh, PA). Liquid desiccant is cooled to the target temperature via circulation through a thermostatically controlled bath (TC550-SD, Brookfield, Middleboro, MA). A mass and energy balance of the liquid desiccant is considered by measuring temperature in and out (800-32/140-1188 thermal resistance sensors, Noshok, Berea, OH).

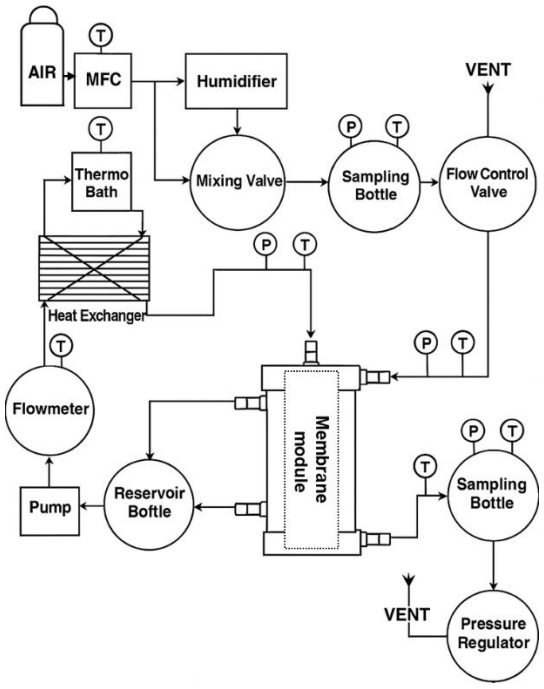

Figure 3.7. Liquid desiccant dehumidification test bench at Oakland University laboratory, used to experimentally validate the base case scenario defined in Table 3.3.

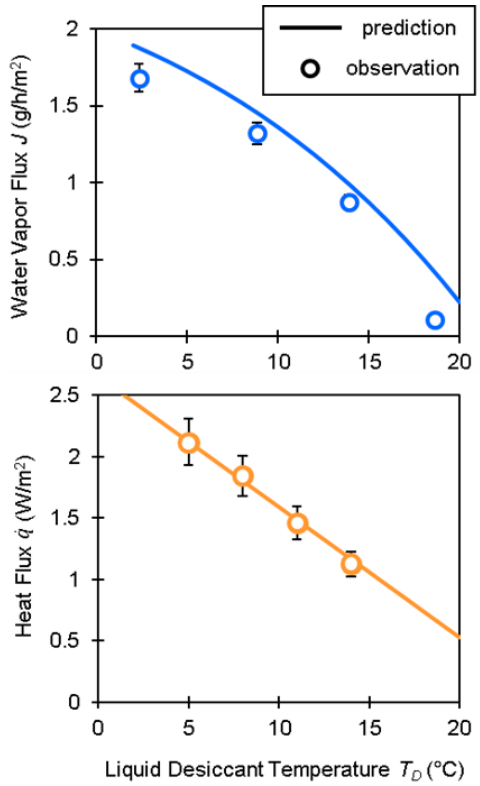

Figure 3.8 Water vapor flux and heat flux as predicted by the transport model and as observed by laboratory testing under base case conditions defined in Table 3.3.

Figure 3.8 shows the water vapor and heat flux that are predicted by the transport model as well as the experimental observation of these from the experimental mass and energy balance. A significant level of consistency is observed between the results. Some degree of discrepancy is evident, but this may arise from inherent limitations within the chosen transport model correlations, as well as uncertainties inherent in the accuracy of the collected data. For reference, a complete data set is provided in Supplementary Notes 3.6.1 and 3.6.2, showing raw data, analysis, and propagation of uncertainty.

3.4 Results and Discussions

3.4.1 Specific Work Input of Dehumidification

Figure 3.9 shows the specific energy use results for fertilizer-based dehumidification given the base case conditions previously specified in Table 3.3. As shown, water vapor flux increases significantly as liquid desiccant solution is cooled, and simultaneously, a significant increase in heat flux is observed. For example, vapor flux increases from 0.2 to 1.3 $g/m^2/h$ as desiccant temperature is halved from 20 to 10 °C, but heat flux also increases from 0.55 to 1.65 W/m^2. The balance of these two competing dynamics is observed in the specific work use of dehumidification, where a minimum of 0.24 Wh/g is achieved at 13 °C, assuming the cooling load can be handled with a coefficient of performance $\mathrm{cop} = 5$. The effect of higher or lower cop is also shown. These specific energy results compare favorably against both the thermodynamic limit of dehumidification which is 0.14 Wh/g for this case, and the new California greenhouse standards which range from 0.37 to 0.55 Wh/g.

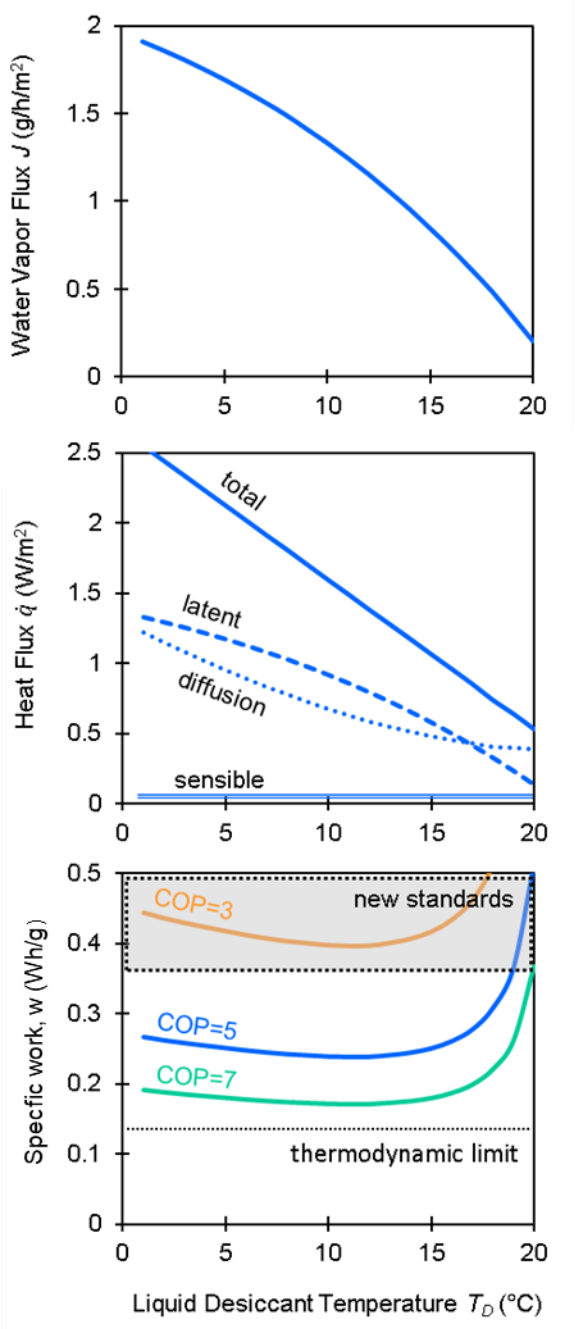

Figure 3.9 Water vapor and heat flux received by a fertilizer-based liquid desiccant solution across a range of desiccant temperatures. Specific work input for dehumidification is obtained from the ratio of heat flux to vapor flux, and normalized over the assumed coefficient of performance of the cooling technology. The thermodynamic limit of dehumidification, and new energy efficiency standards are provided for reference. Unless otherwise specified, default simulation parameters are specified in Table 3.3.

As shown, total heat flux is linearly proportional to the liquid desiccant temperature. A linear profile like this is characteristic of a heat transfer process that is approaching thermal equilibrium. In this case, the air feed has low thermal capacity (relative to that of the liquid desiccant), and the membrane is somewhat oversized (relative to the feed flow rate) providing ample surface area for heat transfer. Under these conditions, air feed leaves the membrane module at temperatures approximately equal to the liquid desiccant inlet. This is confirmed by reviewing the raw data, such as provided in Supplementary Notes 3.6.1 and 3.6.2, which shows that $T_{F,out} \rightarrow T_{D,in}$. The total heat flux curve is therefore only a representation of the thermal equilibrium limit, which is a linear function of the liquid desiccant temperature.

Figure 3.9 also shows the relative contribution of different heat transfer mechanisms to the total flux. These mechanisms include (1) diffusion of heat across the membrane (dotted line), (2) latent heat released from condensation of vapor permeate (hatched line), and (3) sensible heat carried by the vapor mass transfer (double line). The third mechanism of sensible heat transfer is shown to be negligible, and therefore it is not included in further analysis. The second mechanism of latent heat transfer by condensation is of course proportional to the rate of vapor mass transfer, and as shown the latent heat flux curve follows the vapor flux curve. Interestingly, any change in latent heat flux is countered by an opposite change in thermal diffusion which establishes thermal equilibrium and generates the linear plot for total flux that is explained above.

3.4.2 Liquid Desiccant Dilution

One of the primary features of fertilizer-based liquid desiccant is that, unlike conventional desiccant, its concentration is not maintained via an energy intensive

heating and cooling regeneration cycle. Instead, a batch of fertilizer desiccant is recirculated through the membrane dehumidification system, recovering water vapor from the indoor plant environment, until the solution is sufficiently diluted for delivery to the plants. However, as the concentration of desiccant drops, so does its dehumidification potential. The transient nature of this process (dilution with water vapor addition) has an important effect on its specific energy use, as well as on its ability to match plant evapotranspiration rates, which are also highly dynamic.

Figure 3.10 shows water vapor flux and the resulting specific energy use of dehumidification, as fertilizer concentration is diluted from near the solubility limit down to 10 % and then 0.1 % solubility. Such low concentrations are on the order of what is typically desired for safe delivery of fertilizers to plants. For example, in the case of $Ca(NO_3)_2$ which is selected for this study, it is typically delivered to plants at concentrations of ~ 1 g/l, equivalent to ~ 0.1 % of solubility [83].

As expected, vapor flux drops as solution is diluted, and the resulting specific energy and work of dehumidification increases. In addition, we observe that the minimum specific energy point and work shifts to lower temperatures at low concentrations. This suggests the need to progressively cool the fertilizer solution, as the batch process advances and the solution is diluted. To illustrate, consider the case where fertilizer solution is maintained at a constant 13 °C as it is diluted. In this case, water vapor flux would drop from 1.12 to 0.86 g/m^2/h, and as a result the specific work would increase from 0.23 to 0.30 Wh/g. If however, the fertilizer temperature is progressively reduced from 13 to 10 °C as the solution is diluted, vapor transfer would be maintained at a nearly

constant rate, and the specific work would only increase from 0.23 to 0.27 Wh/g as seen in Figure 3.10.

Interestingly, total heat flux remains constant across all the different concentrations. This may appear to be somewhat counter intuitive since latent heat transfer by condensation is proportional to the rate of vapor mass transfer, which drops as desiccant concentration is reduced. However, we observe here that any drop in the latent heat of condensation is followed by an equal and opposite increase in thermal diffusion, such that total flux will remain constant. This is because the process is operating near its thermal equilibrium limit, as explained in Section 3.4.1. Under these conditions, thermal diffusion can be quite significant. This is well illustrated in Figure 3.10 at temperatures of around 20 °C, where even in the absence of condensation, when mass transfer is reduced to zero due to low concentration desiccant, thermal equilibrium is established by diffusion alone and total flux remains constant.

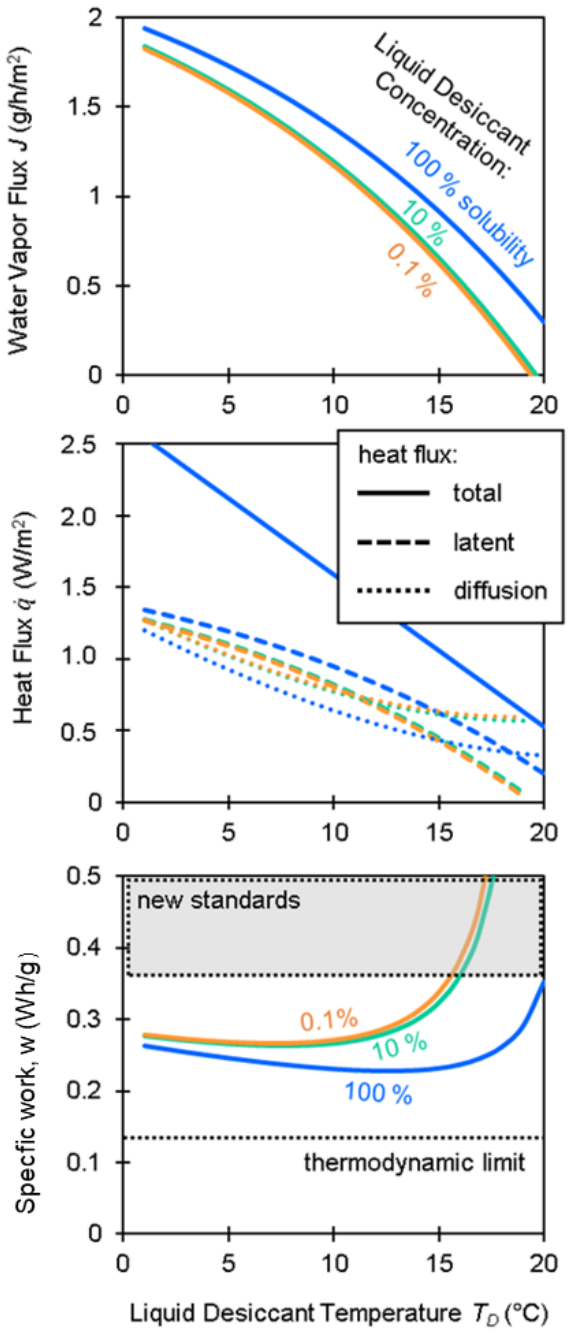

Figure 3.10. Water vapor and heat flux received by a fertilizer-based liquid desiccant solution across a range of fertilizer solution concentrations. Specific work input for dehumidification is obtained from the ratio of heat flux to vapor flux, and normalized over the coefficient of performance of the cooling technology. The thermodynamic limit of dehumidification, and new energy efficiency standards are provided for reference. Unless otherwise specified, default simulation parameters are specified in Table 3.3.

3.4.3 Liquid Desiccant and Air Feed Circulation Rates

Performance of the proposed fertilizer-based dehumidification system can be optimized by careful control of operating conditions, including the circulation rates of liquid desiccant and air feed. For example, axial gradients of temperature and concentration can be mitigated by reducing the residence time of fluids in the membrane system. In addition, boundary layers and their associated transport resistances can be reduced by maintaining high velocities and high Reynolds numbers.

Figure 3.11 shows the effect that different circulation rates have on dehumidification performance. As shown, a small improvement in vapor flux is noted from higher liquid desiccant circulation rates. This is driven by a reduction in concentration polarization due to improved mixing that occurs at higher Reynolds numbers. There is no observed effect on heat flux, because again the circulating air reaches thermal equilibrium with the liquid desiccant temperature, and any difference in heat of condensation is only offset by more or less diffusion.

A more important change in performance is observed in response to different air circulation rates. Performance is much more sensitive to air circulation because air temperatures vary over the surface of the membrane before converging towards the liquid desiccant temperature at thermal equilibrium. Greater circulation rates for the air feed allow it to maintain relatively uniform temperatures over a greater portion of the membrane surface, thereby improving flux, but conversely this also means that a greater mass of air is cooled to the liquid desiccant equilibrium temperature, which represents more thermal energy transfer. For example, an increase in air circulation rates from 1 to 10 lpm is shown to cause an increase in vapor and heat flux from 0.34 to 1.31 g/ m^2/h and

0.25 to 2.55 W/m^2, respectively (at liquid desiccant temperatures of 13 °C). This particular tradeoff is unfavorable, and from among the cases considered, the lowest specific energy use and work input results are obtained at low air flow rates of 1 lpm, in which case very impressive results as low as 0.15 Wh/g are predicted.

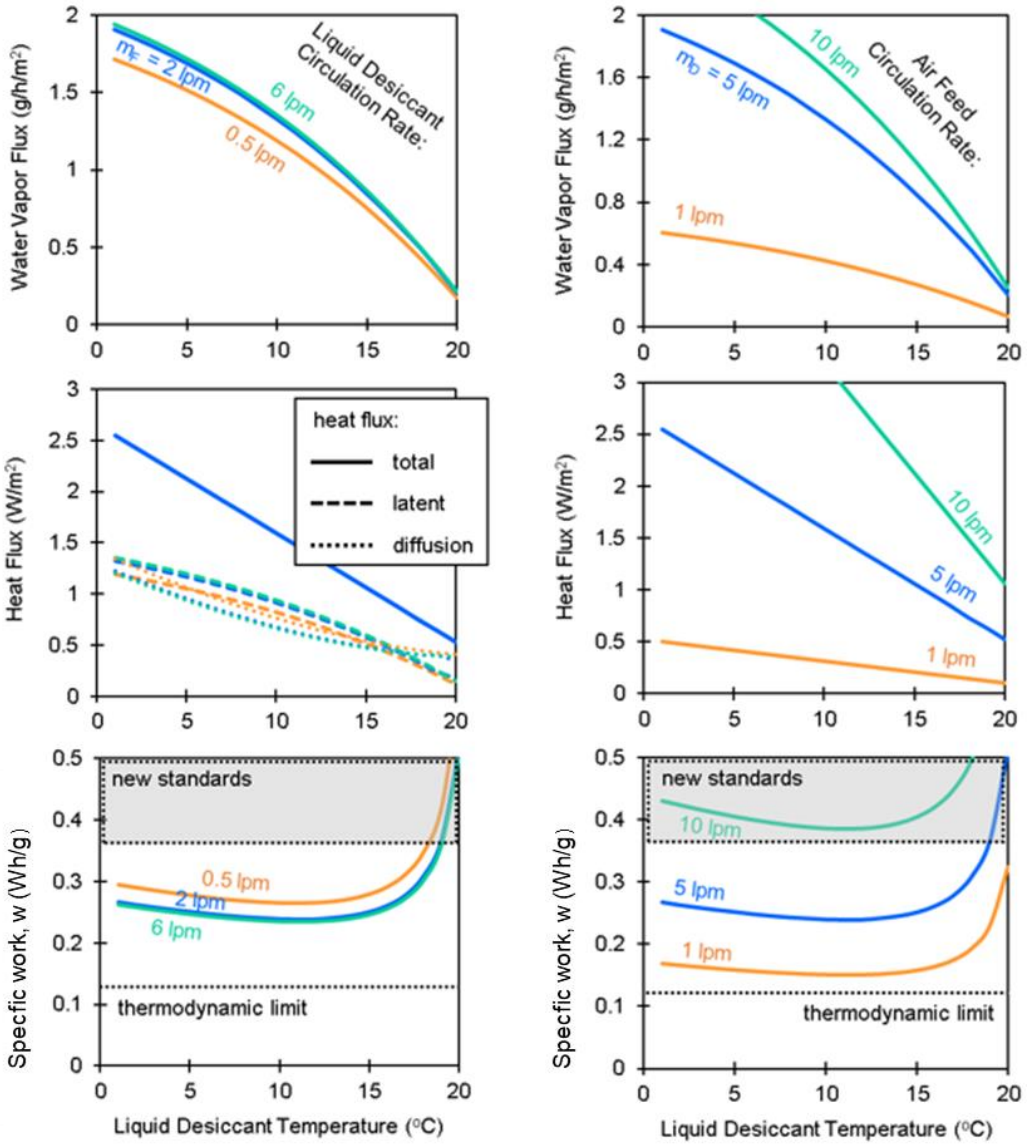

Figure 3.11. Water vapor and heat flux received by a fertilizer-based liquid desiccant solution across a range of circulation rates for both the liquid desiccant and the air feed. Specific work of dehumidification is obtained from the ratio of heat flux to vapor flux, and normalized over the coefficient of performance of the cooling technology. The thermodynamic limit of dehumidification, and new energy efficiency standards are provided for reference.

These results indicate the need to optimize operating parameters including the air feed and liquid desiccant circulation rates. Low circulation rates were favored here, but the conditions for minimum specific energy will be highly case specific and scaled proportionate to the membrane surface area and channel geometry. Importantly, we do not consider here the effect of friction losses, which would impose an energy penalty for high circulation rates. This would need to be considered in further optimization.

3.4.4 High Performance Membranes

Fertilizer-based liquid desiccants can be applied in a number of desiccant systems (such as spray dehumidification and evaporative coolers) but in this study a membrane dehumidification system is featured [84,85]. As a result, membrane selection will be a significant factor in the performance of the dehumidification system. Ideally, a membrane will exhibit very high water vapor permeability to encourage dehumidification mass transfer, but very low thermal conductivity so as to minimize the desiccant cooling load by mitigating thermal diffusion [86].

Figure 3.12 shows dehumidification for a selection of three different membrane materials. Performance of the default polydimethylsiloxane (PDMS) membrane is compared against a high permeability polyether block amide (PEBAX) membrane, and a low permeability polyether sulfone (PES) membrane. As shown, the membrane's vapor permeability has a significant impact on performance. This is clear from the large difference in vapor flux that is observed for the different membranes. To illustrate, consider operation at 15 °C where vapor flux increases from 0.85 $g/m^2/h$ for PDMS to 1.30 $g/m^2/h$ for PEBAX, and as a result the specific work reduces from 0.25 to 0.16 Wh/g. This approaches the thermodynamic limit of dehumidification. Moreover, the

specific energy use profile of PEBAX appears to be relatively better over a range of liquid desiccant temperatures ranging from approximately 5 to 15 °C. This can provide some advantages and operational flexibility for controlling a future dehumidification prototype that will need to balance dehumidification efficiency and dehumidification rate.

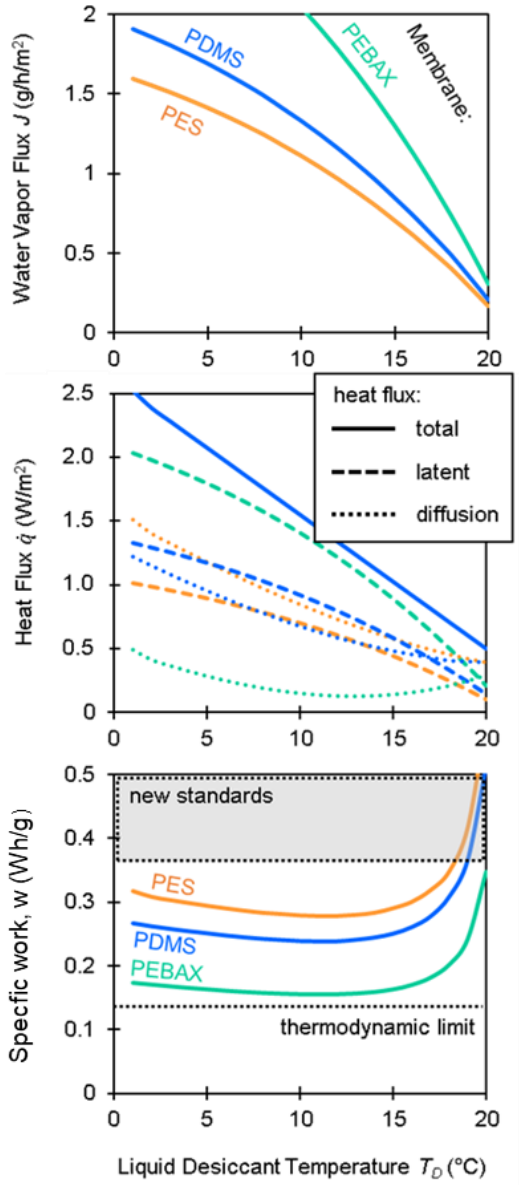

Figure 3.12 Water vapor and heat flux received by a fertilizer-based liquid desiccant solution across a selection of different membranes. Polyether block amide (PEBAX) has vapor permeability $B = 5.48 \times 10^{-6}$ g m^{-2} s^{-1} Pa^{-1} [87]. Polydimethylsiloxane (PDMS) has vapor permeability $B = 3.94 \times 10^{-6}$ g m^{-2} s^{-1} Pa^{-1} [88]. Polyether sulfone (PES) has vapor permeability $B = 0.49 \times 10^{-6}$ g m^{-2} s^{-1} Pa^{-1} [89,90].

3.5 Conclusions

This study evaluates the performance and specific energy use of fertilizer-based liquid desiccants for dehumidification of indoor plant environments. The novel fertilizer concept is applied here to a membrane-based dehumidification process that has been modeled and experimentally validated. Performance is simulated across a range of operating conditions, with particular consideration for the liquid desiccant temperature. Other variables include the liquid desiccant concentration, the liquid desiccant and air feed circulation rates, and the membrane material. Mass and heat transfer are accounted for and energy efficiency is evaluated in terms of the specific energy of dehumidification, which is the ratio of the water vapor removed from the air versus the heat that is transferred to the cool liquid desiccant (which must then be rejected from the system via a cooling unit with some coefficient of performance).

Specific energy use and work input were found to be highly dependent on liquid desiccant temperature. At lower desiccant temperatures, vapor pressure is reduced, and hence additional vapor transfer is promoted. However, cooling the liquid desiccant also drives additional heat transfer from the warm feed air. This tradeoff is clearly illustrated throughout the results, and there is shown to be an optimal liquid desiccant temperature that will maximize the ratio of vapor removal to heat transfer, thereby minimizing the specific energy of dehumidification. Minimum specific work input between 0.16-0.24 kWh/kg was achieved across the various cases studied. This compares very favorably with the thermodynamic limit of enthalpy of condensation of 0.14 kWh/kg. It also compares favorably with other dehumidification technologies available on the market

[73] and satisfies new energy efficiency standards for indoor plant cultivation which require between 0.37-0.55 kWh/kg [25,74].

Across the range of parameters considered, the liquid desiccant temperature for the minimum specific energy and work appeared between 7 and 14 ^{o}C, but it is highly case specific. For example, at different fertilizer concentrations, the minimum specific energy was achieved at different liquid desiccant temperatures. In general, lower fertilizer concentration leads to decreased vapor flux and increased specific energy use, and the minimum specific energy point is shifted to a lower desiccant temperature. This suggests that liquid desiccant temperature should be actively controlled throughout a fertilizer dehumidification batch process, because as water vapor is removed from the air and accumulated by the liquid desiccant, the fertilizer concentration will reduce in real time. Active control of liquid desiccant temperature could be done to (i) ensure efficient operation at the minimum specific energy point, and (ii) ensure vapor removal rates are sufficient to maintain target greenhouse conditions. Such dynamic control would need to account for not only changes in the liquid desiccant concentration (which is diluted over time), but also for changes in the environmental conditions (as the rates of plant evapotranspiration are expected to vary throughout the day and throughout the plant lifecycle). Such active control strategies should be considered in future work.

Vapor flux associated with operation at the minimum specific energy points ranged from 1.2 to 1.6 g/m^2 /h. These vapor removal rates are relatively modest and other membrane-based desiccant studies have reported much higher flux [40,91]. However, lower vapor flux is somewhat to be expected in this study because membrane surface area is somewhat oversized relative to the air feed circulation rates. Other studies that used

similar amounts of membrane area relative to feed circulation, have obtained similar vapor flux as reported here [92]. This dynamic is clearly illustrated in the analysis of the air feed circulation rates, which showed much better vapor flux when air feed flow rates were increased. Vapor flux is an important metric because it provides an indicator of the amount of membrane area, and hence capital, that would be required to scale up the system and achieve a certain target dehumidification capacity as required by the greenhouse. Other variables considered in this study included the liquid desiccant circulation rate and the membrane material. Changes in the liquid desiccant circulation rates had only a minor effect on performance. This suggests that the liquid desiccant circulation rates are excessive and should be optimized in proportion to the membrane surface area and geometry. For the membrane material, PEBAX outperformed PDMS and PES in terms of both vapor flux and specific energy use. These findings established that materials with higher vapor permeability enabled greater water vapor transfer, consequently reducing the specific energy required for dehumidification.

In conclusion, this work contributes to the literature by providing the first ever specific energy analysis of using fertilizer-based liquid desiccants for dehumidification. The results are encouraging and justify further research and development of the concept. In particular, we recommend future work to prototype the technology and integrate the proposed real-time control of liquid desiccant temperature.

3.6 Supplementary Note

3.6.1 Supplementary Note 3.1: Sample Test Data, Analytical Methods, and Uncertainty Analysis for Validation of the Vapor Transport Model

The proposed mass transport model was validated using a series of tests performed on the Oakland University laboratory bench. Figure S3.1 shows raw data collected for a sample test trial, and Table S3.1 provides a detailed outline of how data is analyzed, including how experimental uncertainty is propagated throughout the analysis. Vapor flux was evaluated by considering a mass balance of the air feed.

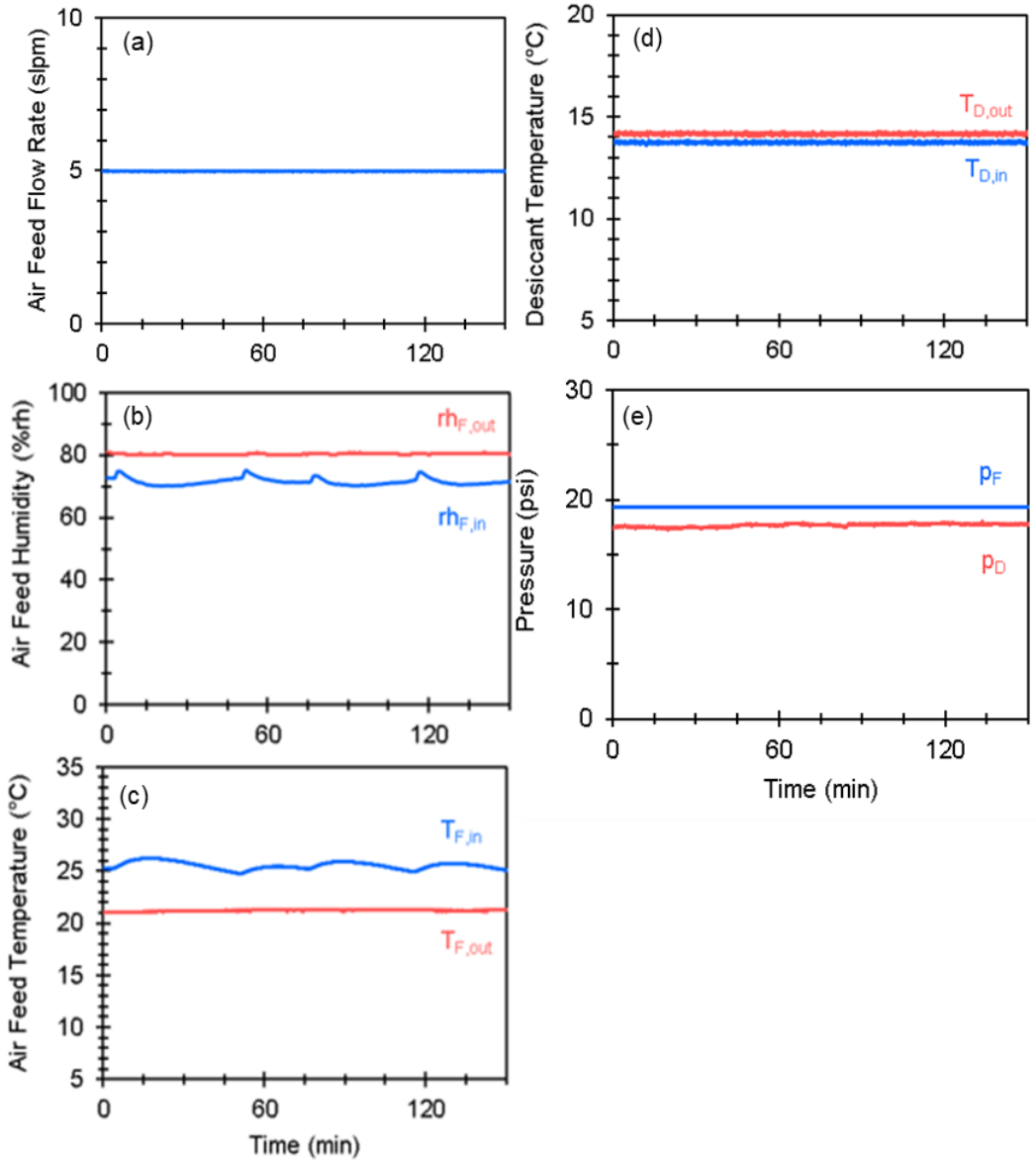

Figure S3.1 Raw Test data. (a) Air feed flow rate: measured by mass flow controller GH-32907-69, Masterflex, Radnor, PA, (b-c) Air feed relative humidity and temperature: measured by AM2315 i2C, Aosong, Guangzhou, China, (d) Liquid desiccant temperature: measured by 800-32/140-11880256, Noshok, Berea, OH and (e) Pressure of the air feed and desiccant measured by: GC557F0142CD, Ashcroft, Stratford, CT.

Table S3.1 Raw test data and analysis

Parameter	Value	Measurement or Analysis
Test preparation		
Liquid desiccant water mass $m_{D,w}$	980.4 ± 0.1 g	Balance (AX8201, Ohaus, Parsippany, NJ), 8000 ± 0.1 g

Table S3.1—continued

Parameter	Value	Measurement or Analysis
Liquid desiccant salt mass $m_{D,s}$	951.2 ± 0.1 g	Balance (AX8201, Ohaus, Parsippany, NJ), 8000 ± 0.1 g
Liquid desiccant concentration c_D	0.97 ± 0.00014 g/g	$c_D = \frac{m_{D,s}}{m_{D,w}}$ $\frac{\delta c_D}{c_D} = \sqrt{\left(\frac{\delta m_{D,s}}{m_{D,s}}\right)^2 + \left(\frac{\delta m_{D,w}}{m_{D,w}}\right)^2}$
Average trial results		
Air feed flow rate $\dot{V}_F$	4.99 ± 0.05 slpm	Mass flow controller (GH-32907-69, Masterflex, Radnor, PA), 5 slpm ± (0.8 % reading + 0.2 % full scale)
Air feed temperature at inlet $T_{F,in}$	25.5 ± 1 °C	Thermistor temperature sensor (AM2315, Aosong, Guangzhou, China), 125 ± 1 °C
Air feed temperature at outlet $T_{F,out}$	21.1 ± 1 °C	Thermistor temperature sensor (AM2315, Aosong, Guangzhou, China), 125 ± 1 °C
Air feed humidity at inlet $rh_{F,in}$	71.3 ± 2 %rh	Capacitive humidity sensor (AM2315, Aosong, Guangzhou, China), 100 ± 2 %rh
Air feed humidity at outlet $rh_{F,out}$	80.3 ± 2 %rh	Capacitive humidity sensor (AM2315, Aosong, Guangzhou, China), 100 ± 2 %rh
Air feed pressure p_F	17.66 ± 0.38 psia	Pressure transducer (GC557F0142CD, Ashcroft, Stratford, CT), 75 ± 0.38 psi
Liquid desiccant flow rate $\dot{V}_D$	2.08 ± 0.19 slpm	Flowmeter (8051K107, McMaster-Carr, Elmhurst, IL), 1.6 ± 0.05 gpm
Liquid desiccant temperature at inlet $T_{D,in}$	13.7 ± 0.3 °C	Thermal resistance sensor, (800-32/140-1188, Noshok, Berea, OH), 60 ± 0.3 °C
Liquid desiccant temperature at outlet TD,out	14.2 ± 0.3 °C	Thermal resistance sensor, (800-32/140-1188, Noshok, Berea, OH), 60 ± 0.3 °C
Liquid desiccant pressure pD	19.30 ± 0.38 psia	Pressure transducer (GC557F0142CD, Ashcroft, Stratford, CT), 75 ± 0.38 psid
Mass balance analysis		
Water vapor content of air feed at inlet $x_{H2O,in}$	0.015 mol_{H2O}/mol ± 8.3 %	$x_{H2O,in} = rh_{in}\ \frac{p_{sat,in}}{p_F}$ where $p_{sat,in} = 10^{A-\left(\frac{B}{C+T_{F,in}}\right)}$ $\delta x_{H2O,in} = \left(\sqrt{\left(\frac{p_{sat,in}}{p_F}\Delta rh_{in}\right)^2 + \left(\frac{rh_{in}}{p_F}\Delta p_{sat,in}\right)^2 + \left(-\frac{rh_{in}p_{sat,in}\Delta p_F}{(p_F)^2}\right)^2}\right)$ where, A, B and C are the constants of the Antoine equation which can be obtained from the references and vary with T

Table S3.1—continued

Parameter	Value	Measurement or Analysis
Water vapor mass flow of air feed at inlet $\dot{m}_{F,H2O,in}$	3.75 g/h ± 8.53 %	$\dot{m}_{F,H2O,in} = \dot{m}_F \left(\frac{x_{H2O,in}}{1-x_{H2O,in}}\right) \frac{M_{H2O}}{M_{air}}$, $\delta\dot{m}_{F,H2O,in} = \sqrt{\left(0.6 \frac{x_{H2O,in}}{1-x_{H2O,in}} \Delta\dot{m}_F\right)^2 + \left(0.6 \frac{\dot{m}_F}{(1-x_{H2O,in})^2} \Delta x_{H2O,in}\right)^2}$
Water vapor content of air feed at outlet $x_{H2O,out}$	0.0116 mol_{H2O}/mol ± 9.38 %	$x_{H2O,out} = rh_{out} \frac{p_{sat,out}}{p_F}$ where $p_{sat,out} = 10^{A-\left(\frac{B}{C+T_{F,out}}\right)}$ $\delta x_{H2O,out} = \left(\sqrt{\left(\frac{p_{sat,out}}{p_F} \Delta rh_{out}\right)^2 + \left(\frac{rh_{out}}{p_F} \Delta p_{sat,out}\right)^2 + \left(-\frac{rh_{out} p_{sat,out} \Delta p_F}{(p_F)^2}\right)^2}\right)$
Water vapor mass flow of air feed at inlet $\dot{m}_{F,H2O,out}$	2.88 g/h ± 9.38 %	$\dot{m}_{F,H2O,out} = \dot{m}_F \left(\frac{x_{H2O,out}}{1-x_{H2O,out}}\right) \frac{M_{H2O}}{M_{air}}$ $\delta\dot{m}_{F,H2O,in} = \sqrt{\left(0.6 \frac{x_{H2O,out}}{1-x_{H2O,out}} \Delta\dot{m}_F\right)^2 + \left(0.6 \frac{\dot{m}_F}{(1-x_{H2O,out})^2} \Delta x_{H2O,out}\right)^2}$
Water vapor flux J	0.872 $g/m^2/h$ ± 45 %	$J = \frac{\dot{m}_{F,H2O,in} - \dot{m}_{F,H2O,out}}{a}$ $\delta J = \sqrt{\left(\delta\dot{m}_{F,H2O,in}\right)^2 + \left(\delta\dot{m}_{F,H2O,out}\right)^2}$

3.6.2 Supplementary Note 3.2: Sample Test Data, Analytical Methods, and Uncertainty Analysis for Validation of the Heat Transport Model

The proposed heat transport model was validated using a series of tests performed on the Oakland University laboratory bench. Figure S3.2 shows raw data collected for a sample test trial, and Table S3.2 provides a detailed outline of how data is analyzed, including how experimental uncertainty is propagated throughout the analysis. Heat fluxes were evaluated by considering a mass and thermal energy balance of the air feed.

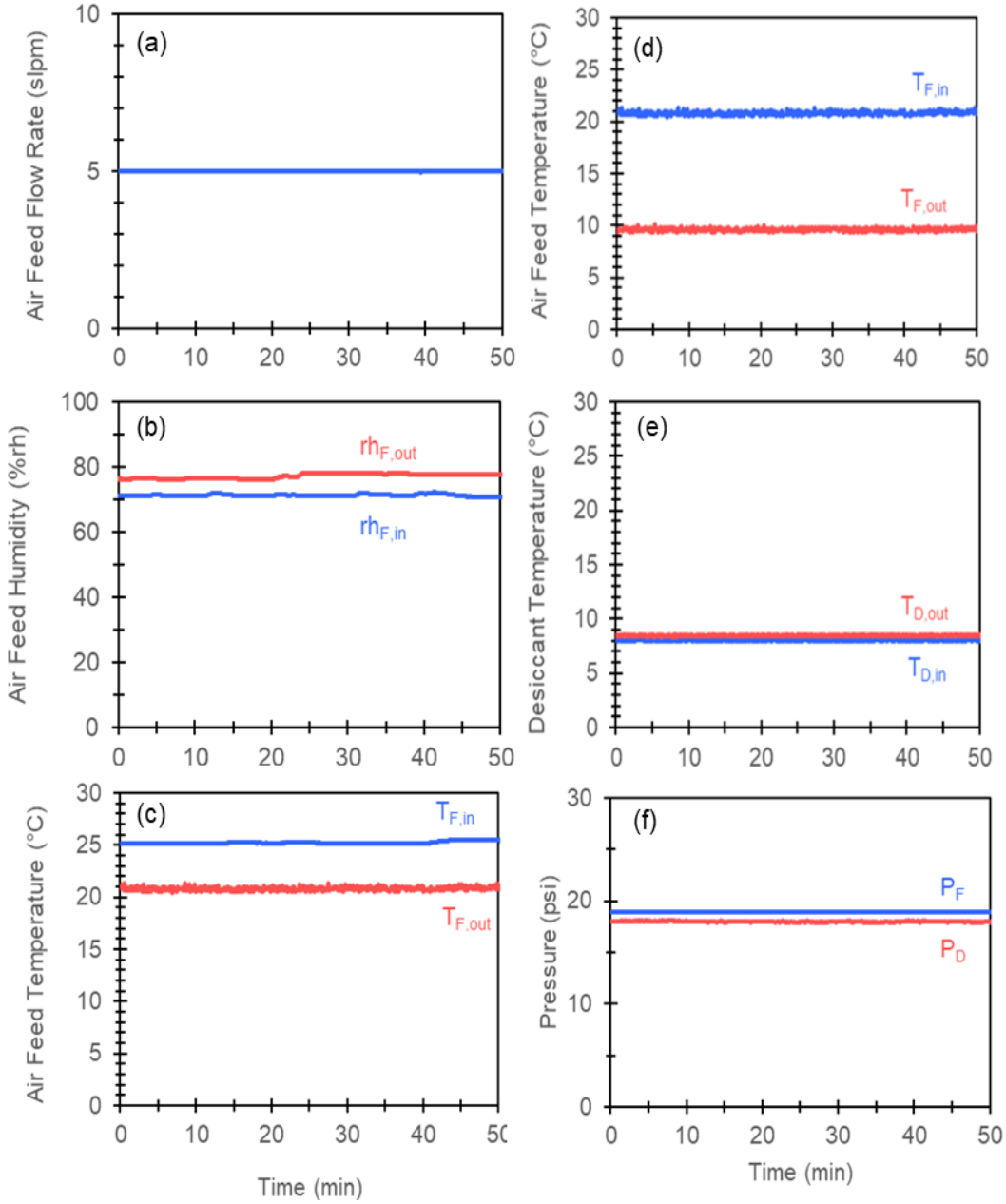

Figure S3.2 Raw Test data. (a) Air feed flow rate: measured by mass flow controller GH-32907-69, Masterflex, Radnor, PA, (b-c) Air feed relative humidity and temperature: measured by AM2315 i2C, Aosong, Guangzhou, China, (d) Air temperature at membrane ports: measured by MT-6340-30, TWTADE, Suzhou, China (e) Liquid desiccant temperature: measured by 800-32/140-11880256, Noshok, Berea, OH and (f) Pressure of the air feed and desiccant measured by: GC557F0142CD, Ashcroft, Stratford, CT. The data are instantaneously taken over the period of 50 minutes. There are some noises in the data due to the configuration of sensors. Air flow rate was smooth because of the better control from the mass flow controller that is situated between the compressed airline and the box where the air is conditioned.

Table S3.2 Raw test data

Parameter	Value	Measurement or Analysis
Test preparation		
Liquid desiccant water mass $m_{D,w}$	980.4 ± 0.1 g	Balance (AX8201, Ohaus, Parsippany, NJ), 8000 ± 0.1 g
Liquid desiccant salt mass $m_{D,s}$	1.3 ± 0.1 g	Balance (AX8201, Ohaus, Parsippany, NJ), 8000 ± 0.1 g
Liquid desiccant concentration c_D	0.001 ± 0.00014 g/g	$c_D = \frac{m_{D,s}}{m_{D,w}}$ $\frac{\delta c_D}{c_D} = \sqrt{\left(\frac{\delta m_{D,s}}{m_{D,s}}\right)^2 + \left(\frac{\delta m_{D,w}}{m_{D,w}}\right)^2}$
Average trial results		
Air feed flow rate $\dot{V}_F$	4.99 ± 0.05 slpm	Mass flow controller (GH-32907-69, Masterflex, Radnor, PA), 5 slpm ± (0.8 % reading + 0.2 % full scale)
Air feed temperature at inlet $T_{F,in}$	20.82 ± 0.5 °C	(MT-6340-30, TWTADE, Suzhou, China), Full scale oC±0.3% Full scale (Transmitter side)
Air feed humidity at inlet $rh_{F,in}$ @ $T_{rh,in}$	71.2 ± 2 %rh @ 25.25 ± 0.1 °C	Capacitive humidity sensor (AM2315, Aosong, Guangzhou, China), 100 ± 2 %rh
Air feed temperature at outlet $T_{F,out}$	9.60 ± 0.5 °C	(MT-6340-30, TWTADE, Suzhou, China) Full scale oC±0.3% Full scale (Transmitter side)
Air feed humidity at outlet $rh_{F,out}$@ $T_{rh,out}$	77.2 ± 2 %rh @ 19.81 ± 0.1 °C	Capacitive humidity sensor (AM2315, Aosong, Guangzhou, China), 100 ± 2 %rh
Air feed pressure p_F	17.9 ± 0.38 psia	Pressure transducer (GC557F0142CD, Ashcroft, Stratford, CT), 75 ± 0.38 psi
Liquid desiccant flow rate $\dot{V}_D$	2.08 ± 0.19 slpm	Flowmeter (8051K107, McMaster-Carr, Elmhurst, IL), 1.6 ± 0.05 gpm
Air feed pressure p_F	17.9 ± 0.38 psia	Pressure transducer (GC557F0142CD, Ashcroft, Stratford, CT), 75 ± 0.38 psi

Table S3.2—continued

Parameter	Value	Measurement or Analysis
Liquid desiccant temperature at inlet $T_{D,in}$	8.02 ± 0.3 °C	Thermal resistance sensor, (800-32/140-1188, Noshok, Berea, OH), 60 ± 0.3 °C
Liquid desiccant flow rate $\dot{V}_D$	2.08 ± 0.19 slpm	Flowmeter (8051K107, McMaster-Carr, Elmhurst, IL), 1.6 ± 0.05 gpm
Liquid desiccant temperature at outlet $T_{D,out}$	8.45 ± 0.3 °C	Thermal resistance sensor, (800-32/140-1188, Noshok, Berea, OH), 60 ± 0.3 °C
Liquid desiccant pressure p_D	18.9 ± 0.38 psia	Pressure transducer (GC557F0142CD, Ashcroft, Stratford, CT), 75 ± 0.38 psid
Mass balance analysis		
Water vapor content of air feed at inlet $x_{H2O,in}$	0.0177 mol_{H2O}/mol ± 7.5 %	$x_{H2O,in} = rh_{in}\frac{p_{sat,in}}{p_F}$ where $p_{sat,in} = 10^{A-\left(\frac{B}{C+T_{rh,in}}\right)}$ $\delta x_{H2O,in} = \left(\sqrt{\left(\frac{p_{sat,in}}{p_F}\Delta rh_{in}\right)^2 + \left(\frac{rh_{in}}{p_F}\Delta p_{sat,in}\right)^2 + \left(-\frac{rh_{in}p_{sat,in}\Delta p_F}{(p_F)^2}\right)^2}\right)$
Water vapor mass flow of air feed at inlet $\dot{m}_{F,H2O,in}$	4.22 g/h ± 8.02 %	$\dot{m}_{F,H2O,in} = \dot{m}_F\left(\frac{x_{H2O,in}}{1-x_{H2O,in}}\right)\frac{M_{H2O}}{M_{air}}$, $\delta\dot{m}_{F,H2O,in} = \sqrt{\left(0.6\frac{x_{H2O,in}}{1-x_{H2O,in}}\Delta\dot{m}_F\right)^2 + \left(0.6\frac{\dot{m}_F}{(1-x_{H2O,in})^2}\Delta x_{H2O,in}\right)^2}$
Water vapor content of air feed at outlet $x_{H2O,out}$	0.013 mol_{H2O}/mol ± 8.74 %	$x_{H2O,out} = rh_{out}\frac{p_{sat,out}}{p_F}$ where $p_{sat,out} = 10^{A-\left(\frac{B}{C+T_{F,out}}\right)}$ $\delta x_{H2O,out} = \left(\sqrt{\left(\frac{p_{sat,out}}{p_F}\Delta rh_{out}\right)^2 + \left(\frac{rh_{out}}{p_F}\Delta p_{sat,out}\right)^2 + \left(-\frac{rh_{out}p_{sat,out}\Delta p_F}{(p_F)^2}\right)^2}\right)$
Water vapor mass flow of air feed at outlet $\dot{m}_{F,H2O,out}$	3.27 g/h ± 7.46 %	$\dot{m}_{F,H2O,out} = \dot{m}_F\left(\frac{x_{H2O,out}}{1-x_{H2O,out}}\right)\frac{M_{H2O}}{M_{air}}$ $\delta\dot{m}_{F,H2O,in} = \sqrt{\left(0.6\frac{x_{H2O,out}}{1-x_{H2O,out}}\Delta\dot{m}_F\right)^2 + \left(0.6\frac{\dot{m}_F}{(1-x_{H2O,out})^2}\Delta x_{H2O,out}\right)^2}$

Table S3.2—continued

Parameter	Value	Measurement or Analysis
Water vapor flux J	0.95 g/m^2/h ± 41.63 %	$J = \frac{\dot{m}_{F,H2O,in} - \dot{m}_{F,H2O,out}}{a}$ where a = 1 m^2 $\delta J = \sqrt{\left(\delta\dot{m}_{F,H2O,in}\right)^2 + \left(\delta\dot{m}_{F,H2O,out}\right)^2}$
Heat flux $\dot{q}$	1.84 W/m^2 ± 49.29 %	$\dot{q} = \left(\dot{m}_F c_p T_{F,in} - \left(\dot{m}_F - \dot{m}_{F,H2O,in} + \dot{m}_{F,H2O,out}\right) c_p T_{F,out} + \left(\dot{m}_{F,H2O,in} - \dot{m}_{F,H2O,out}\right) \times 1\right)/a$ $\delta\dot{q} = \sqrt{\left(\frac{\Delta\dot{m}_F c_p \Delta T_F}{a}\right)^2 + \left(\frac{\Delta T_{F,in}\dot{m}_F c_p}{a}\right)^2 + \left(\frac{-\Delta T_{F,out}\left(\dot{m}_F - \dot{m}_{F,H2O,in} + \dot{m}_{F,H2O,o}\right.}{a}\right.}$ $+ \left(\frac{\Delta\dot{m}_{F,H2O,in}\left(c_{pT_{F,out}} + 1\right)}{a}\right)^2 + \left(\frac{\Delta\dot{m}_{F,H2O,out}\left(-c_{pT_{F,out}} - 1\right)}{a}\right)^2$

CHAPTER FOUR

EXPERIMENTAL ANALYSIS: MEASURING THE ENERGY EFFICIENCY OF USING A NOVEL FERTILIZER-BASED LIQUID DESICCANT SYSTEM TO DEHUMIDIFY INDOOR PLANT ENVIRONMENTS

4.1 Introduction

It is now well understood the need for proper humidity control for optimal crop growth and quality, as mentioned in previous chapters and documented in the literature [93,94]. Common indoor farming dehumidification methods are also well known [95], which typically come with high energy costs. To address this, we previously introduced the concept of using fertilizer-based liquid desiccants [30,47]. A simple schematic of that process is shown in Figure 4.1. This idea builds on earlier studies highlighting the significant free energy potential of concentrated fertilizers for various applications [56,96-98]. In Chapter Two thermodynamic limits and maximum energy savings are established, while in Chapter Three, a theoretical transport model with simulation of the membrane assisted fertilizer-based liquid desiccant dehumidification is presented for specific energy calculation. However, until now, the energy efficiency of the process has not been experimentally confirmed. The goal of this study is therefore to complete the first-ever experimental analysis to calculate the specific energy use of dehumidification of fertilizer-based liquid desiccant dehumidification. To accomplish this, a laboratory test bench was developed and used to conduct a comprehensive and detailed experimental analysis of the energy use of dehumidification per unit of water vapor removal.

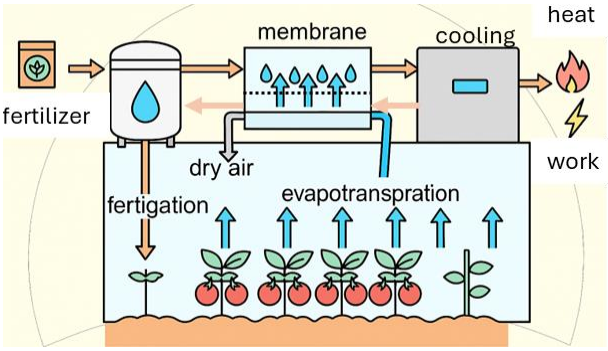

Figure 4.1 Humidity is removed from the indoor plant environment by using a concentrated fertilizer solution to draw water vapor across a selective membrane. A chiller (or some other heat sink) is used to keep desiccant cool by removing the energy that is transferred from the warm air to the cool desiccant.

In evaluating the specific energy use of the process, there are several important dynamics that must be considered. First, in our previous work we have shown that specific energy use is highly sensitive to liquid desiccant temperature. At cool temperatures, dehumidification accelerates, which is desirable, but so does the rate of heat transfer from warm air to cool desiccant, which is undesirable. Some particular temperature will balance these competing dynamics and yield the minimum specific energy use of dehumidification. This tradeoff is illustrated in Figure 4.2. Until now this dynamic has been understudied in the literature and has received limited attention in experimental research [99-101]. Therefore, in this study we experimentally evaluate the energy use of dehumidification as a function of liquid desiccant temperature and consider the implications this has on the need for active controls to be integrated.

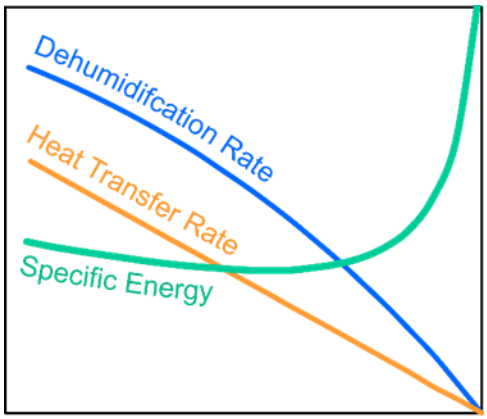

Figure 4.2 Dehumidification performance is influenced by liquid desiccant temperature. Cooling desiccant improves the dehumidification rate but also increases heat gains, which require energy to remove. The ratio of energy input to vapor output is the specific energy use, and it can be minimized at some particular desiccant temperature.

Second, energy efficiency will be influenced by the fertilizer concentration. This is expected from the literature related to more general liquid desiccant systems, which usually include thermal regeneration of the desiccant to maintain constant concentration and consistent performance [102,103]. In this case however, fertilizer desiccant is to be recirculated and diluted from very high initial concentrations down to very low final concentrations that are suitable for plant fertigation. Therefore, our experimental analysis also evaluates specific energy use under a range of fertilizer concentrations. This is done for both simple single solute fertilizers as well as for complex fertilizer blends, marking the first time that dehumidification has been demonstrated with fertilizer blends.

Finally, experimental results are reported and compared to other common dehumidification technologies providing context to the energy efficiency results. We conclude by discussing the implications of these potential energy savings and what might come next for fertilizer-based dehumidification. This will pave a path for future research on fertilizer-based liquid desiccant systems using different approaches.

4.2 Materials and Methods

4.2.1 Laboratory Test Bench

A laboratory-scale liquid desiccant test bench at Oakland University was used to evaluate the specific energy and work of the proposed fertilizer-based dehumidification system. A visual and schematic of the laboratory system is provided in Figure 4.3. The bench consists of a 5-port hollow fiber membrane module (with 2 lumen ports and 3 shell-side ports) that is supplied with warm feed air through the lumen and cool liquid desiccant solution through the shell.

On the liquid desiccant side, a positive displacement diaphragm pump (SFDP1-030-045-33, Seaflo, Xiamen, China) is used to circulate fluid from a 2-L reservoir. A mass flow meter (8051K107, McMaster-Carr, Elmhurst, IL) is used to measure the liquid desiccant flow rate, which is controlled by varying the DC voltage supplied to the pump motor. An inline accumulator tank (SFAT-075-125-01, Seaflo, Xiamen, China) is used to smooth the flow by damping the vibrations. To cool the liquid desiccant, it is circulated through a stacked-plate heat exchanger (35115K62, McMaster-Carr, Elmhurst, IL) that is supplied with a working fluid flowing in thermostatically controlled bath (TC550-SD, Brookfield, Middleboro, MA). Desiccant temperature is measured at both the membrane inlet and outlet using inline thermal resistance sensors (800-32/140-1188, Noshok, Berea, OH) which are mounted inside thermowells (75-025-316SS, Noshok, Berea, OH) for protection. Foam tubing is used to insulate all the desiccant lines to minimize heat gain from the ambient environment.

On the gas side, air is supplied from a compressed air source and a mass flow controller (GH-32907-69, Masterflex, Radnor, PA) is used to regulate the circulation rate.

Temperature of the air feed is controlled by circulating the gas through an inline electric resistance heater (AHP-3742, Omega, Norwalk, CT) with a DC voltage applied to it. Humidity of the air feed is controlled by bubbling a portion of the gas through inline columns of deionized water, and then blending the humid air stream with dry air in some proportion that is adjusted by a series of valves. Temperature and humidity are measured at both the membrane inlet and outlet using resistive temperature detectors (MT-6340-30, TWTADE, Suzhou, China) and capacitive humidity sensors (AM2315, Aosong Electronics, Guangzhou, China). Pressure of the feed is monitored via a differential pressure transducer (GC557F0142CD, Ashcroft, Stratford, CT) and kept approximately equal to the liquid desiccant pressure using a pressure regulator valve.

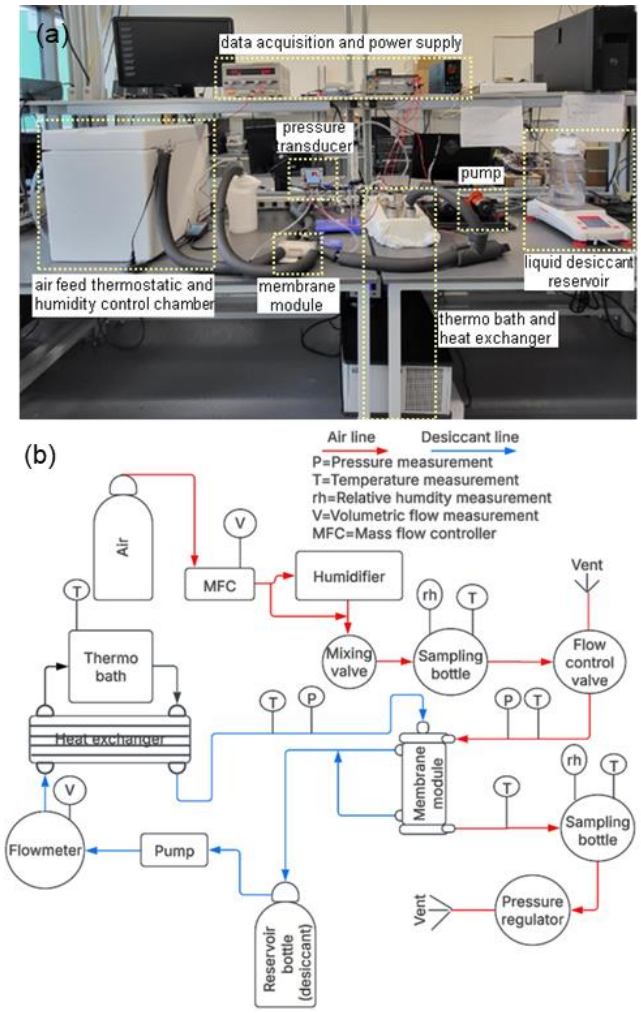

Figure 4.3 (a) Photo and (b) schematic of the liquid desiccant dehumidification test bench.

Table 4.1 provides a summary of all sensors and instrumentations with their specifications. A data acquisition module (OM-USB-1608FS, Omega, Norwalk, CT) connected to a PC is used to record the sensor data. The data acquisition module has 8 analog-to-digital converter channels configured in the range of ± 5 V to accommodate sensors, which output either 0-5 VDC or 4-20 mA signals. A detailed wiring diagram with all sensors and data acquisitions is included in Supplementary Note 4.1.

A commercial membrane module (PDMSXA-1.0, PermSelect, Ann Arbor MI) was selected for this study. The module consists of dense polydimethylsiloxane membrane

fibers. Fibers are composed of dense polydimethylsiloxane membranes. Supplementary Note 4.2 provides a schematic of the membrane module and a microscopic view of the membrane hollow fibers. Table 4.2 provides a summary of key membrane specifications.

Table 4.1 Sensor and instrumentation specifications

Instrument	Manufacturer	Model number	Full scale ± Uncertainty
Liquid desiccant			
Mass flow meter	McMaster-Carr	8051K107	1.6 ± 0.05 gpm
Thermal resistance sensor	Noshok	800-32/140-1188	60 ± 0.3 °C
Air feed			
Mass flow controller	Aalborg	GFC17	5 ± 0.05 slpm
Resistive temperature detector	TWTADE	MT-6340-30	200 ± 0.5 °C
Capacitive humidity sensor	Aosong Electronics	AM2315	100 ± 2 %
Differential pressure transducer	Ashcroft	GC557F0142CD	75 ± 0.38 psi

Table 4.2 Membrane specifications

Material	Polydimethylsiloxane
Module type	Hollow fiber
Membrane area	1 m^2
Fiber length	0.14 m
Fiber diameter (outer)	300×10^{-6} m
Fiber thickness	55×10^{-6} m
Number of fibers	12,600
Flow orientation	Counter flow

4.2.2 Data Analysis

Raw data was analyzed to determine the dehumidification rate and the specific energy of dehumidification under a range of operating conditions. Specific energy use q is defined as the ratio of the rate of energy transfer $\dot{Q}$ relative to the rate of dehumidification $\Delta\dot{m}$ (equation 4.1). Energy is transferred to the liquid desiccant by both heat transfer and mass transfer, and must then be removed. This change in energy represents a cooling load that will be handled by a chiller or heat pump with some coefficient of performance cop, and therefore the specific work w can be obtained from equation (4.2).

$$q = \frac{\dot{Q}}{\Delta \dot{m}} \tag{4.1}$$

$$w = \frac{q}{cop} \tag{4.2}$$

The rate of dehumidification is determined by taking a mass balance of the water vapor at the membrane inlet and outlet, as shown in equation (4.3) and (4.4) (see detailed derivation in Supplementary Note 4.3). For convenience, the dehumidification rate can be normalized over the membrane surface area a and expressed as vapor flux $J = \Delta \dot{m}/a$.

$$\Delta \dot{m} = \dot{m}_{H2O,in} - \dot{m}_{H2O,out} \tag{4.3}$$

$$\Delta \dot{m} = \dot{m}_F \left(\frac{RH_{in}\, p_{sat,in}}{p_F - RH_{in}\, p_{sat,in}} - \frac{RH_{out}\, p_{sat,out}}{p_F - RH_{out}\, p_{sat,out}} \right) \frac{M_{H2O}}{M_{air}} \tag{4.4}$$

Where $\dot{m}_F$ is the mass flow rate of the air feed, RH is the relative humidity at the membrane inlet and outlet, M is the molar mass of water and air, and p_F is the pressure of the air feed. p_{sat} the saturation pressure of air at the membrane inlet and outlet.

The rate of energy transfer is determined by taking an energy balance of the warm feed air at the membrane inlet and outlet, which is equal to the change in energy of the desiccant, as shown in equations (4.5) and (4.6) (see detailed derivation in Supplementary Note 4.4). Energy transfer includes heat transfer from the warm air to the cool desiccant $\dot{Q}$ as well as the enthalpy h_{H2O} carried by the mass of water vapor transfer. For convenience, the energy transfer rate can be normalized over the membrane surface area and expressed as energy flux $\dot{Q}/a$.

$$\dot{Q} = \dot{Q}_{sensible} + \Delta \dot{m}\, h_{H2O} \tag{4.5}$$

$$\dot{Q} = \dot{m}_F cp_{air} (T_{in} - T_{out}) + \Delta \dot{m}\, h_{H2O} \tag{4.6}$$

Where cp and T are the specific heat and temperature of air at the membrane inlet and outlet, and h_{H2O} is the specific enthalpy of saturated vapor at the outlet temperature. Again, thermophysical properties can be obtained from the NIST database or other such thermodynamic references [104].

A set of raw data is provided in Supplementary Note 4.5 with sample calculations to illustrate how equations (4.1) -(4.6) are used to evaluate specific energy and specific work. In addition, a detailed description of how experimental uncertainty [105,106] propagates throughout the analysis is provided in Supplementary Note 4.5.

4.2.3 Test Conditions

Dehumidification performance and energy efficiency were evaluated across a range of liquid desiccant temperatures for three common standard fertilizer solutions, including (1) single solute calcium nitrate $Ca(NO_3)_2 \cdot 4H_2O$ (99 % purity, Fisher Scientific, Waltham, MA), (2) a custom blend with KNO_3, $MgSO_4$, and K_2HPO_4 (99 % purity, Fisher Scientific, Waltham, MA), and (3) a complete commercial blend (SuperThrive Grow®, Dyna-Gro, Richmond CA). To represent dilution of the fertilizer, which is expected to reduce performance as a given batch is recirculated, concentration was varied from near saturation down to some low concentration near the target for plant fertigation. Table 4.3 provides a summary of all test conditions, including the range of concentrations considered for each fertilizer. The table also shows baseline test conditions that are held constant throughout experiments (unless otherwise specified). Air temperatures and humidity are typical for an indoor plant environment. Pressure is adjusted so as to negate any transmembrane pressure that results from differential resistances on the desiccant and air circulation channels.

Table 4.3 Test Conditions

Baseline test conditions	
Desiccant circulation rate	2 lpm
Air circulation rate	5 slpm
Desiccant pressure	30 kPa (gauge)
Air Pressure	30 kPa (gauge)
Pressure difference	0
Air temperature	25 °C
Air relative humidity	70 %
Variable test conditions	
Desiccant temperature	3 – 19 °C
Desiccant concentration	
Fertilizer (1): $Ca(NO_3)_2 \cdot 4H_2O$	1 – 1000 g/l
Fertilizer (2): Custom blend KNO_3:$MgSO_4$:K_2HPO_4 39:38:23 parts by mass	2.3 – 230 g/l
Fertilizer (3): Commercial blend SuperThrive Grow®	2.5 – 25 ml/l

4.3 Results

4.3.1 Dehumidification with a Single Solute Fertilizer

Dehumidification performance and specific energy use were evaluated for a variety of different fertilizer-based liquid desiccants. Figure 4.4 shows the results for calcium nitrate $Ca(NO_3)_2.4H_2O$, which is a common, single solute fertilizer. Dehumidification is successfully achieved across a range of desiccant concentrations and temperatures, as denoted by a positive vapor flux. Notably, dehumidification is only achieved at temperatures lower than $T_D \sim 17$ °C, with negative vapor flux (humidification of air)

occurring closer to room temperature. An important increase in dehumidification rates is observed as the liquid desiccant is cooled.

For example, Figure 4.4(a) shows the case of fertilizer solution at super concentrated levels of c_D = 1000 g/l, which is near the solubility limit. In this case, vapor flux reaches as high as J = 2.1 ± 0.2 g/h/m^2 as the temperature decreases to T_D = 3.1 ± 0.3 °C. However, while such an increase in dehumidification is desirable, cooling of the desiccant leads to an important increase in heat transfer, with energy flux reaching up to $\dot{Q}$/a = 3.0 ± 0.1 W/m^2 for the previous example. The interplay between these two dynamics is evident from the specific energy use, and the specific energy can be minimized when the benefit of more rapid dehumidification is balanced against the energy cost of more rapid heat transfer.

For the same example in Figure 4.4(a), a minimum specific energy of q = 1.47 ± 0.19 kWh/kg is achieved at a desiccant temperature of T_d = 8.0 ± 0.3 °C. Assuming a coefficient of performance cop = 5, this translates to a minimum specific work of w = 0.29 ± 0.03 kWh/kg. A coefficient of performance cop = 5 is chosen based on the performance range of highly efficient cooling systems, such as energy efficient commercial heat pumps. For reference, given the temperatures observed at the minimum specific energy point, a heat pump operating at the maximum Carnot efficiency would approach approximately cop ~ 16.

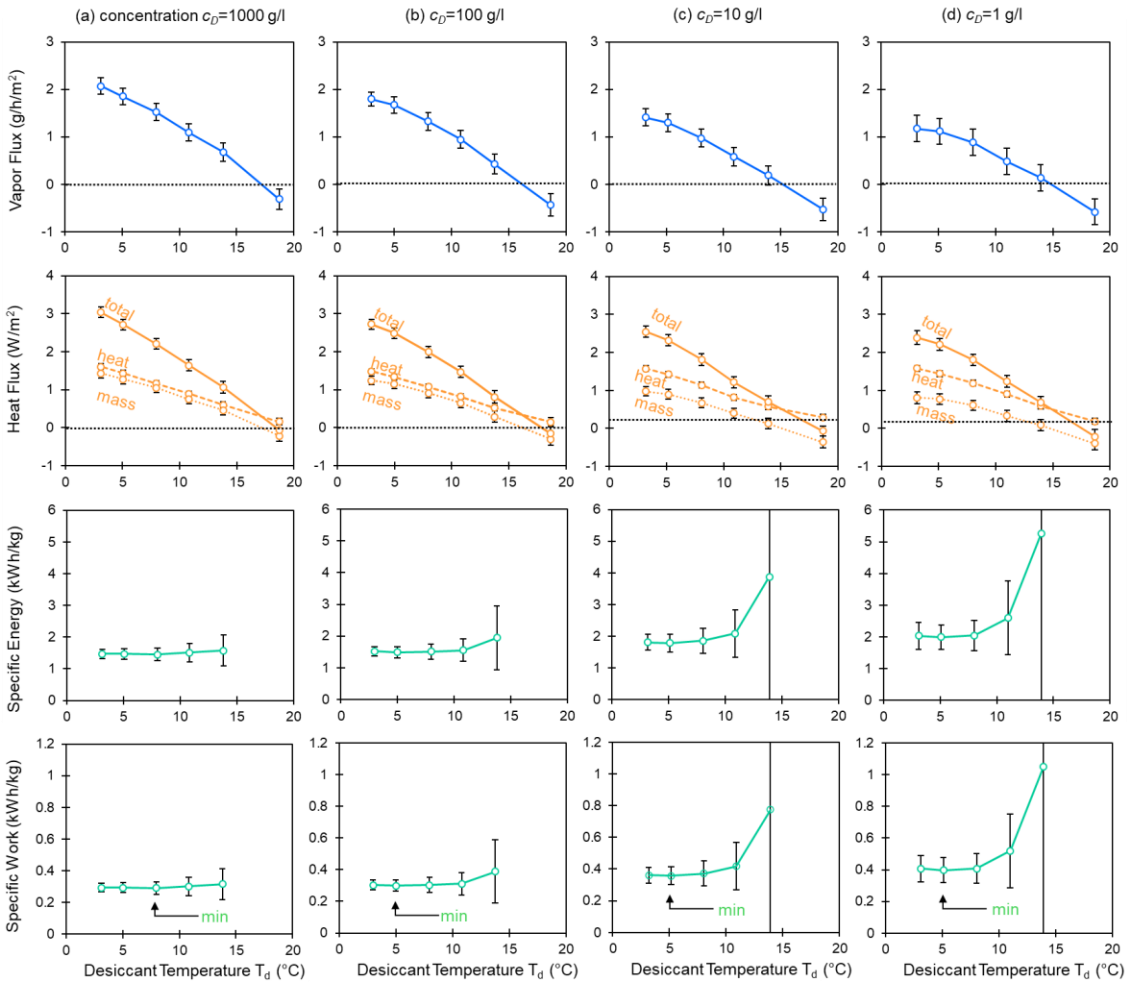

Figure 4.4 Dehumidification performance of fertilizer-based liquid desiccant using single solute calcium nitrate at a range of concentrations including (a) c_D = 1000, (b) 100, (c) 10, and (d) 1 g/l. Baseline test conditions are specified in Table 4.3. Specific work assumes a coefficient of performance cop = 5.

Figure 4.4 also illustrates that energy flux has a near linear correlation with the temperature of the desiccant solution, indicative of a process approaching thermal equilibrium. In this scenario, the air feed, with its low thermal capacity compared to the liquid desiccant, exits the membrane module at temperatures closely resembling those at the liquid desiccant inlet (see data in Supplementary Note 4.5). The figure depicts the proportional contributions of distinct energy transfer mechanisms to the overall or total energy flux: heat transfer across the membrane and enthalpy transfer from mass flux. The

second mechanism, relates directly to the water vapor flux and therefore shows a trend similar to the mass flux itself. Both the heat and enthalpy fluxes demonstrate a linear inverse correlation with fertilizer solution temperature, where decreasing solution temperature increases sensible and latent heat fluxes due to the enhanced water transport and heat transfer.

Figure 4.4 (a)-(d) also illustrates the effect of diluting fertilizer solution from an initial super concentration of c_D = 1000 g/l down to a level that is appropriate for delivery to plants c_D = 1 g/l [90]. This is important because dilution of the desiccant is one of the key differences between the proposed dehumidification system and other common liquid desiccant systems. Traditionally, liquid desiccants are maintained at a constant concentration through an energy-intensive heating and cooling regeneration cycle. But in this process, a batch of fertilizer desiccant is recirculated, capturing water vapor from the indoor plant environment until it is diluted enough to be safely delivered to the plants. Of course, as the desiccant concentration diminishes, so does its dehumidification efficacy.

For example, as concentration drops to c_D = 1 g/l as shown in Figure 4.4(d), the maximum rate of dehumidification observed is J = 1.1 ± 0.2 g/h/m^2. This is almost half of what it is at the initial concentration. This transient dynamic significantly impacts both the ability of the system to match evapotranspiration rates of the plants, and its energy efficiency. For example, as the concentration drops to c_D = 1 g/l, the minimum work of dehumidification increases to w = 0.39 ± 0.08 kWh/kg, up almost 38 % from the initial super concentration. Notably, this minimum work occurs at a desiccant temperature of T_d = 5.1 ± 0.3 °C, which is cooler than the best temperature for the initial super concentration. In general, we can observe that the minimum specific energy point occurs

at a lower temperature as the fertilizer solution is diluted, suggesting the need to control desiccant temperature throughout the batch process.

4.3.2 Dehumidification with Multi-Ion Fertilizer Blends

Single solutes are usually mixed together and delivered to plants as a complete and balanced blend. Therefore, it is important to consider the performance of such solutions in the proposed dehumidification system. Figure 4.5 shows the results for a commercial off-the-shelf fertilizer blend, and Figure 4.6 shows the results for a custom blend that approximates the standard recipe known as Hoagland B solution [107]. In both cases, positive vapor flux indicates that dehumidification is successfully achieved. This is the first experimental demonstration of dehumidification with a blended fertilizer solution.

Consider first the results using the commercial fertilizer product in Figure 4.5. The results are shown for the recommended concentration of 2.5 ml of fertilizer solution diluted in 1 l of water, as well as for ×10 this strength. A 7 % drop in the dehumidification rate is observed with the dilution, as vapor flux goes from 1.9 ± 0.2 $g/m^2/h$ down to 1.7 ± 0.2 $g/m^2/h$. This change is not very high because both concentrations are relatively similar without drastic difference. A more significant discrepancy might be observed at higher fertilizer concentrations but efforts to test this failed due to fertilizer precipitation on the membrane surfaces and throughout the liquid desiccant system as shown in Supplementary Note 4.6. To avoid precipitation, the desiccant solution should be maintained at a pH between 6 and 8, which usually can be done by adding a buffer solution to prevent ionic interactions in the solution. However, the impact of buffer on dehumidification performance requires future investigation. It is

also recommended to periodically flush the system with deionize water to prevent any maintenance related issues like corrosion.

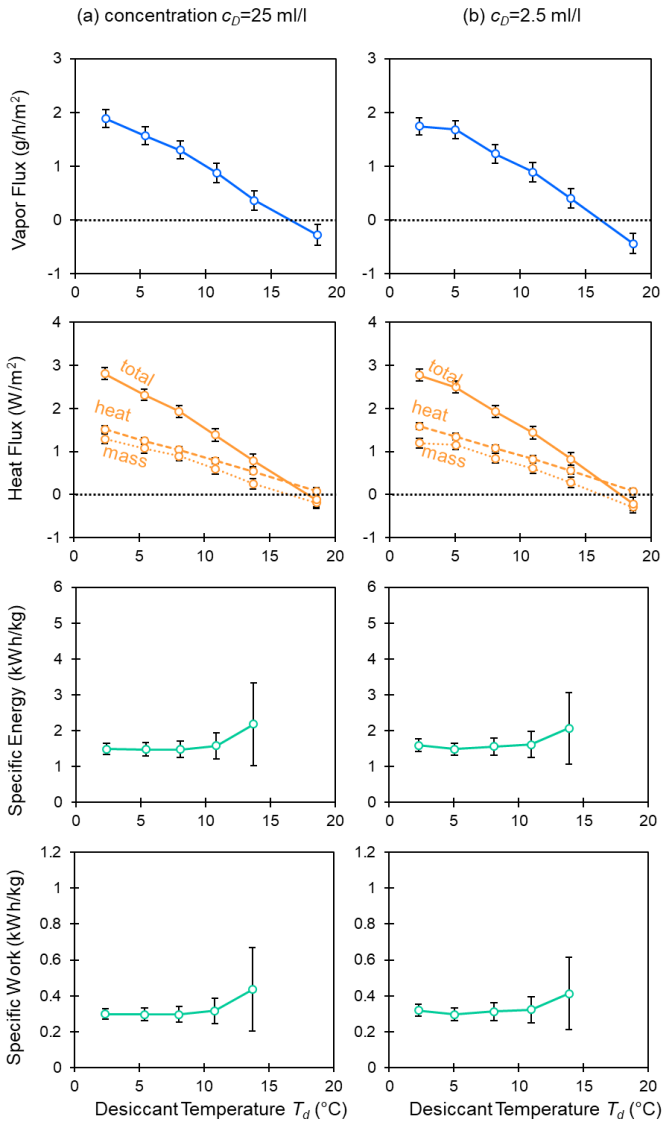

Figure 4.5 Dehumidification performance of fertilizer-based liquid desiccant using a commercial fertilizer blend (SuperThrive Grow®, Dyna-Gro, Richmond CA) diluted to (a) 25, and (b) 2.5 ml/l. Baseline test conditions are specified in Table 4.3. Specific work assumes a coefficient of performance cop = 5.

Specific energy use was almost the same at both concentrations, with a minimum of e = 1.5 ± 0.17 kWh/kg observed. Assuming a coefficient of performance of cop = 5, this translates to specific work input of w = 0.29 ± 0.03 kWh/kg. Interestingly, the minimum

energy point occurs at a cooler temperature for the more diluted solution (T_D = 8.0 ± 0.3 °C compared to 5.4 ± 0.3 °C). This shift occurs due to the balance between removing water vapor from the air and supplying energy to cool down the fertilizer solution. The slope of the specific work curve for this blend is steeper at higher temperatures and flattens out at lower temperatures, indicating a range of temperatures over which temperature has trivial effects on the energy efficiency but a very significant impact on water vapor flux.

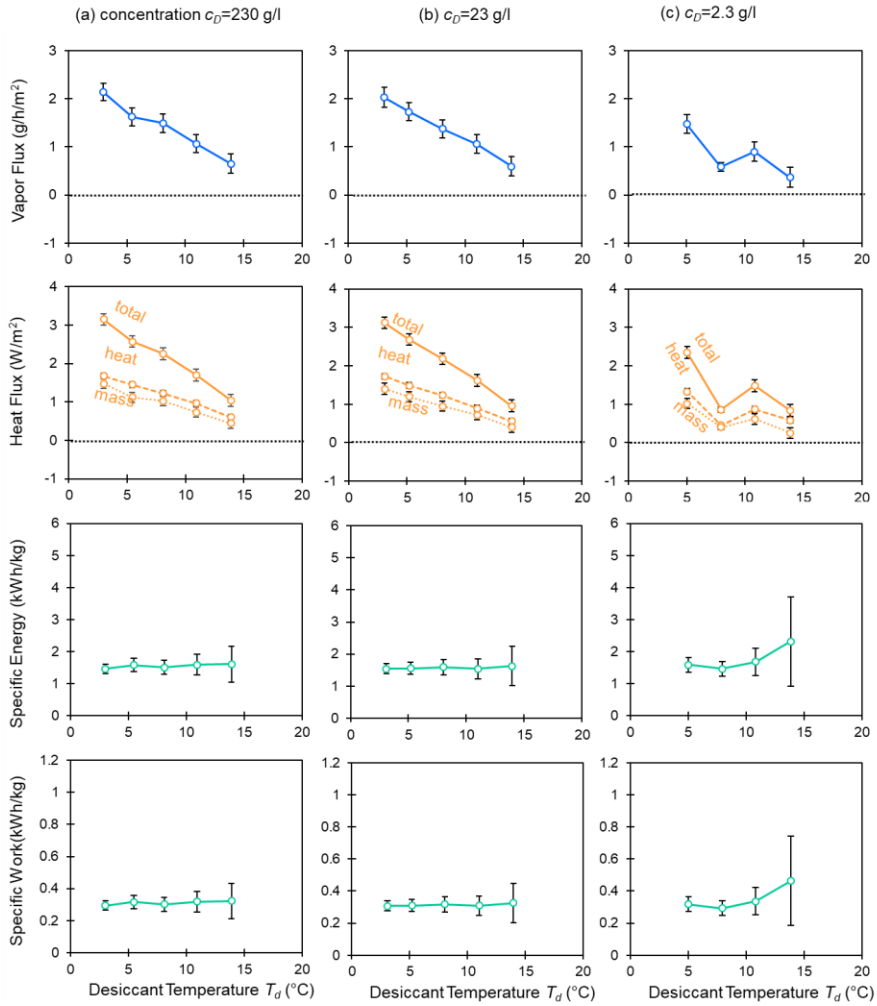

Figure 4.6 Dehumidification performance of fertilizer-based liquid desiccant using a custom fertilizer blend (KNO_3:$MgSO_4$:K_2HPO_4 at 39:38:23 parts by mass) diluted to (a) c_D = 230, (b) 23, and (c) 2.3 g/l. Baseline test conditions are specified in Table 4.3. Specific work assumes a coefficient of performance cop = 5.

Next, consider the results using a custom fertilizer blend. A number of concentrations are shown in Figures 4.6 (a), (b), and (c) with the lowest concentration being equivalent to the strength typically provided to plants. Many of the same trends are observed as with the other fertilizers. As expected, the vapor flux decreases because of the drop in concentration, from a maximum of 2.1 ± 0.2 g/m^2/h at high concentration down to 1.5 ± 0.2 g/m^2/h at low concentration. A proportional drop in energy flux is observed with this due to the reduced enthalpy transfer from mass flux. The maximum total energy flux dropped from 3.15 ± 0.14 W/m^2 at higher concentration to 2.34 ± 0.15 W/m^2 at lower concentration. The minimum specific work input w = 0.29 ± 0.03 kWh/kg is obtained at temperatures of T_D = 2.9 ± 0.3 °C at high concentration and 7.9 ± 0.3 °C at low concentration. Importantly, at lower concentrations, the specific energy use and specific work input profiles exhibit a steeper slope, indicating heightened sensitivity to variations in temperature and concentration. Conversely, at higher concentrations, the profiles flatten, demonstrating that temperature has a minimal effect on the specific energy use and the system reaches a saturation point where additional energy input yields diminishing returns in performance.

4.4 Discussion

4.4.1 Real-Time Temperature Control for Improved Batch Performance

Unlike conventional liquid desiccant systems that regenerate solution to maintain constant concentration, the proposed system recirculates a given batch of fertilizer desiccant and allows it to be gradually diluted. As shown throughout the results, dehumidification performance will vary because of this, and the minimum specific work

input will shift to a different temperature as concentration drops. Figure 4.7 shows dehumidification performance as a function of fertilizer concentration, assuming that temperature is adjusted to track the point of minimum specific work input throughout the batch process. The general trends show that as fertilizer becomes more and more diluted, dehumidification rates drop and specific work of dehumidification increases. Deviation from this trend can be explained by experimental uncertainty. The figure also shows liquid desiccant temperature being adjusted in response to changing concentration. For example, for calcium nitrate in Figure 4.7(a), desiccant is cooled from an initial temperature of 7.9 ± 0.3 °C down to 5.1 ± 0.3 °C. For the custom blend shown in Figure 4.7(b), desiccant is warmed from an initial temperature of 2.9 ± 0.3 °C up to 7.9 ± 0.3 °C and for commercial blend in Figure 4.7(c), temperature is cooled from initial temperature of 8.1 ± 0.3 °C to 5.0 ± 0.3 °C. For custom blend, the increase in temperature may be an anomaly due to experimental uncertainty and ion chemistry. Nevertheless, these observations underscore the need to control liquid desiccant temperature as fertilizer is diluted throughout the batch process. Smart controls and automation can greatly assist with this and should be implemented in future work.

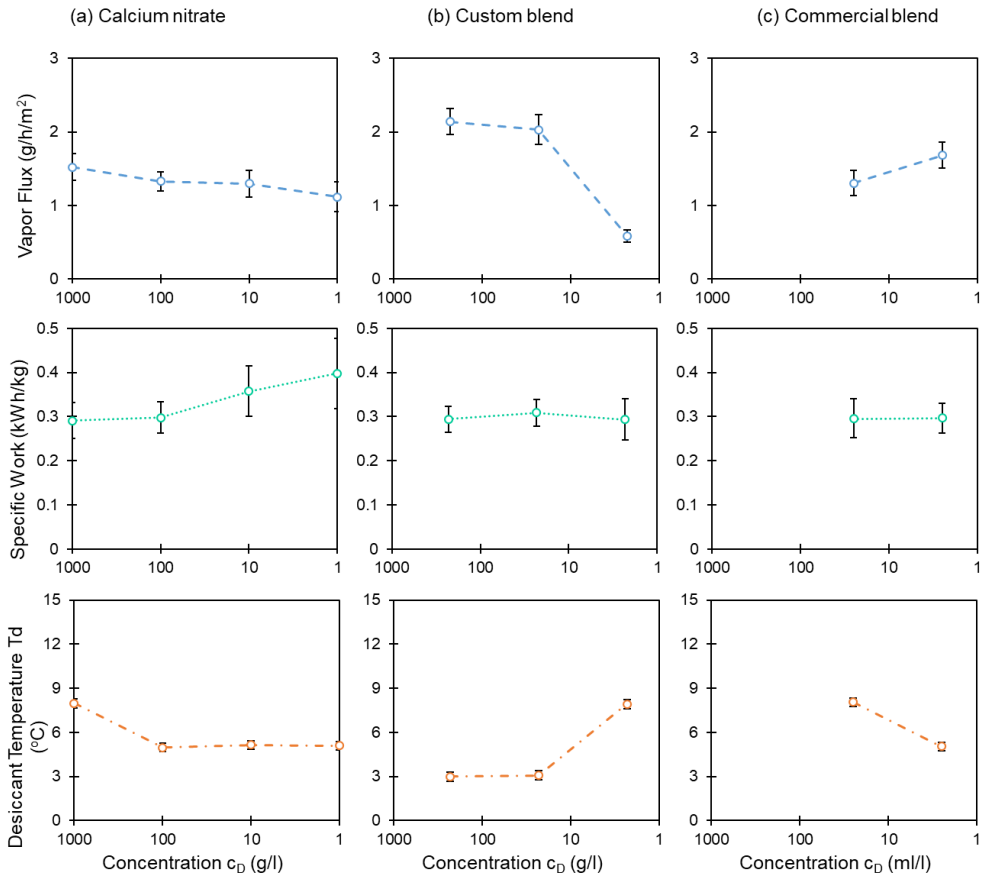

Figure 4.7 Dehumidification performance as a function of concentration, which drops as fertilizer desiccant is recirculated throughout the batch process. Baseline test conditions are specified in Table 4.3. Specific work assumes a coefficient of performance, cop = 5.

4.4.2 Comparison to the Current State of the Art

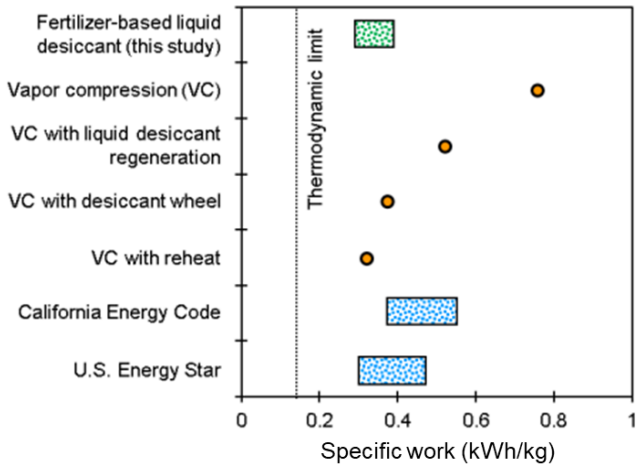

Figure 4.8 Specific work of dehumidification for the proposed fertilizer-based liquid desiccant system (assuming coefficient of performance cop=5) as compared to other dehumidification technologies [42] and standards [46,74].

Assuming that temperature is actively controlled as concentration drops throughout the batch process, experimental results throughout this study show minimum specific work input of dehumidification ranging from 0.29 to 0.39 kWh/kg. Figure 4.8 compares these experimental results to the specific energy use of other dehumidification technologies reported in the literature. Although highly sensitive to test conditions, such as target temperatures and humidity, these results provide a useful benchmark for evaluating our system's performance. As shown, the proposed fertilizer-based dehumidification system compares very favorably, achieving lower specific work of dehumidification than a variety of common vapor compression cycles [42].

In addition, the proposed technology appears to satisfy energy efficiency targets as specified by the U.S. Energy Star program (requires between 0.30 and 0.47 kWh/kg) and by the most recent California Energy Code (requires between 0.37 and 0.55 kWh/kg) [46,74]. The thermodynamic limit of dehumidification is also provided for reference [47]. The principal reasons for improved performance are (1) the proposed fertilizer-based desiccant system avoids the need for energy intensive thermal regeneration, which is characteristic of other desiccant processes, and (2) the system is capable of dehumidifying without bringing air to its saturation point, as with conventional vapor compression systems, which then often require re-heating of the air product.

4.5 Conclusions

In this study, we have successfully demonstrated the efficacy of fertilizer-based liquid desiccant for dehumidification across various concentrations and temperatures, including multi-ion fertilizer blends, marking the first-ever detailed experimental validation of such

an approach. The experimental analysis has revealed major trends indicating the impact of desiccant temperature on the water removal rate from air. Notably, cooling the desiccant leads to a rise in vapor flux, albeit accompanied by rise in heat flux. This highlights the importance of striking an optimal balance to minimize specific energy use, a critical consideration for efficient operation.

Furthermore, desiccant concentration emerges as another pivotal factor, expected to undergo fluctuations throughout the batch process. As the concentration decreases, so does the dehumidification efficacy, necessitating frequent updates with new fertilizer batches to sustain performance at desired levels. Temperature control throughout the process emerges as a crucial determinant of consistent dehumidification performance due to its impact on vapor flux, energy requirements, desiccant stability, particularly evident in multi-ion solutions.

The experimental investigation achieved a minimum specific work of 0.29 kWh/kg, comparing favorably with the thermodynamic limit of 0.14 kWh/kg, updated California greenhouse standards, NREL prediction models, and state-of-the-art dehumidification technologies [42,46,47,74]. Although competitive, it is crucial to evaluate the thermodynamic limits imposed by plants' limited fertilizer needs. Optimizing this balance and determining the optimal frequency for introducing new fertilizer batches will enhance the system's efficiency and sustainability, representing a promising scope for future research.

4.6 Supplementary Information

4.6.1 Supplementary Note 4.1: Wiring and Data Acquisition

Figure S4.1 provides a detailed wiring diagram for all sensors and data acquisition.

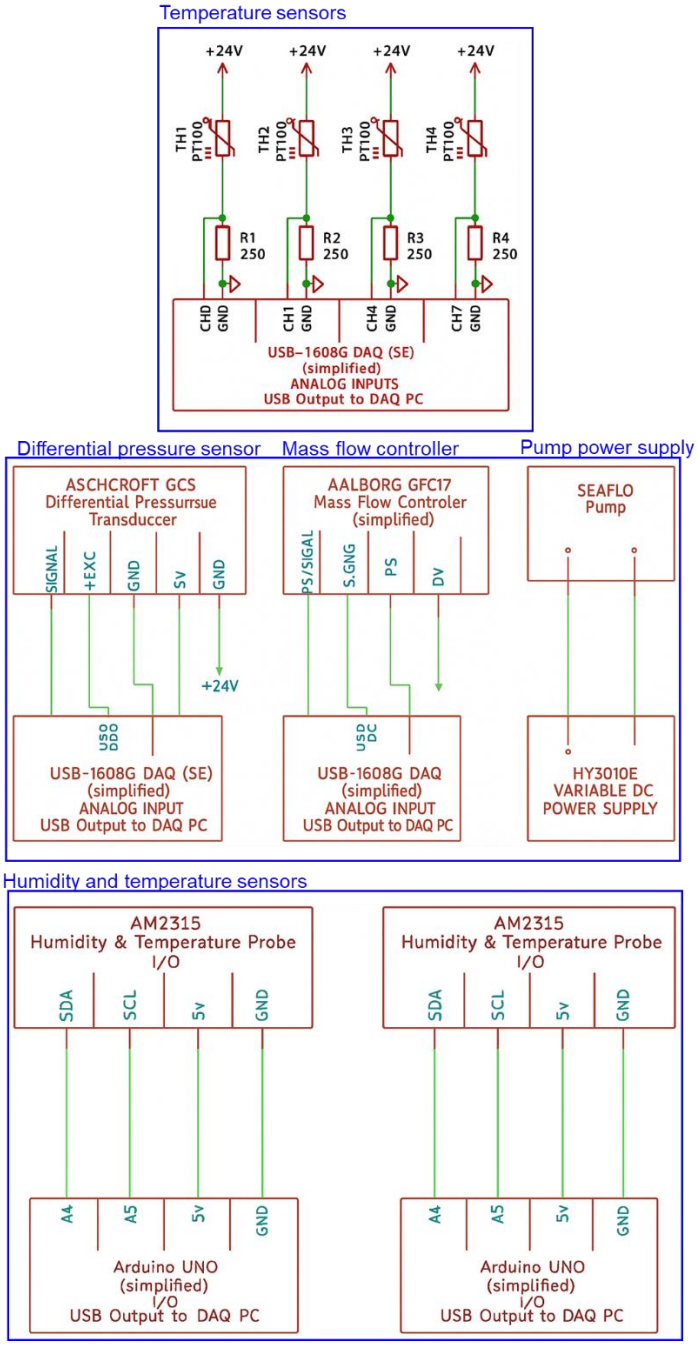

Figure S4.1 Instrumentation and data acquisition wiring schematic of all temperature, humidity, differential pressure sensors, mass flow controller and pump power supply with DAQ.

4.6.2 Supplementary Note 4.2: Additional Membrane Module Details

Figure S4.2 provides a schematic of the membrane module and a microscopic view of the membrane hollow fibers.

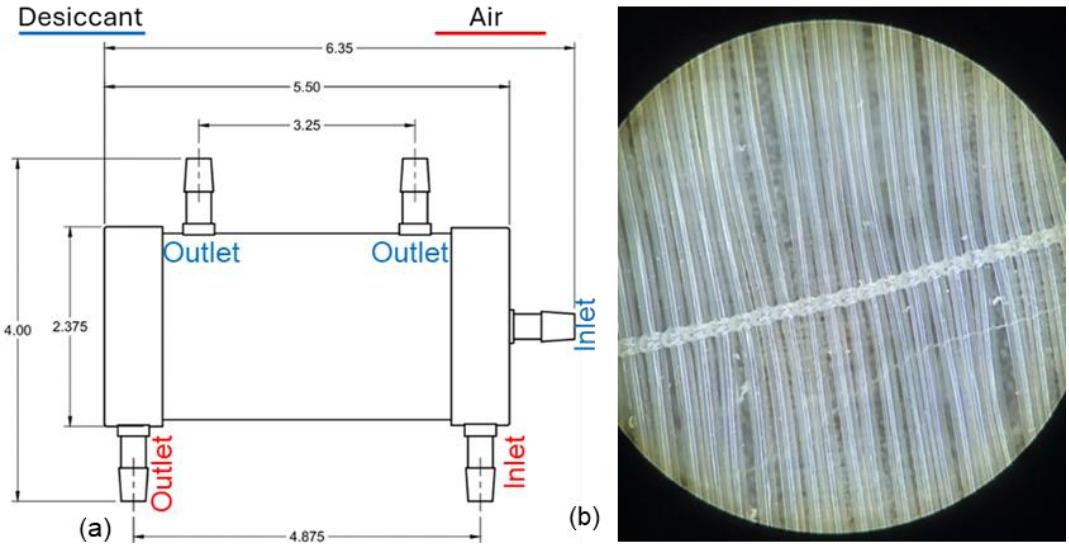

Figure S4.2 (a) Schematic view of commercial hollow fiber polydimethylsiloxane membrane module with dimensions (all dimensions in inches). (b) Microscopic view of hollow fibers lengthwise stitched together.

4.6.3 Supplementary Note 4.3: Mass Balance of the Liquid Desiccant Process

The rate of dehumidification $\Delta\dot{m}$ can be evaluated by considering the mass balance of moist air as it enters and leaves the dehumidification unit.

$$\Delta\dot{m} = \dot{m}_{in} - \dot{m}_{out} \quad \text{S4.1}$$

Assuming that moist air is composed simply of dry air and water vapor, we can separate the mass flow into these two constituents. For a perfectly selective membrane, such as we assume here, the mass of air at the inlet and outlet are equal. Then we can then relate the mass flow rate of water to the mass flow rate of dry air $\dot{m}_{air}$ via the humidity mass ratio ω.

$$\Delta\dot{m} = \left(\dot{m}_{air,in} + \dot{m}_{H2O,in}\right) - \left(\dot{m}_{air,out} + \dot{m}_{H2O,out}\right) \quad \text{S4.2}$$

$$\Delta\dot{m} = \dot{m}_{H2O,in} - \dot{m}_{H2O,out} \quad \text{S4.3}$$

$$\Delta\dot{m} = \dot{m}_{air}(\omega_{in} - \omega_{out}) \quad \text{S4.4}$$

Using the molar mass of air and water, the humidity ratio can be expressed as a molar ratio x, which can be related to the ratio of vapor pressure p_{H2O} to total feed pressure p_F, as per Dalton's law. Finally, the vapor pressure can be related to the relative humidity RH via the saturation pressure p_{sat}.

$$\Delta\dot{m} = \dot{m}_{air}(x_{in} - x_{out})\frac{M_{H2O}}{M_{air}} \quad \text{S4.5}$$

$$\Delta\dot{m} = \dot{m}_{air}\left(\frac{p_{H2O,in}}{p_{air,in}} - \frac{p_{H2O,out}}{p_{air,out}}\right)\frac{M_{H2O}}{M_{air}} \quad \text{S4.6}$$

$$\Delta\dot{m} = \dot{m}_{air}\left(\frac{RH_{in}\, p_{sat,in}}{p_F - RH_{in}\, p_{sat,in}} - \frac{RH_{out}\, p_{sat,out}}{p_F - RH_{out}\, p_{sat,out}}\right)\frac{M_{H2O}}{M_{air}} \quad \text{S4.7}$$

In cases where the total mass flow rate $\dot{m}_F$ is measured rather than the mass of dry air $\dot{m}_{air}$, the expression can be rewritten using the ratio $\frac{\dot{m}_{air}}{\dot{m}_F} = (1+\omega)^{-1}$.

$$\Delta\dot{m} = \frac{\dot{m}_{F,in}}{1+\omega_{in}}\left(\frac{RH_{in}\, p_{sat,in}}{p_F - RH_{in}\, p_{sat,in}} - \frac{RH_{out}\, p_{sat,out}}{p_F - RH_{out}\, p_{sat,out}}\right)\frac{M_{H2O}}{M_{air}} \quad \text{S4.8}$$

Or rather, for simplicity, it can also be assumed that the mass flow rate of dry air $\dot{m}_{air}$ is approximately equal to the total mass flow rate $\dot{m}_F$. In this case we obtain the following expression which can be solved using experimental data from our experimental test bench.

$$\Delta\dot{m} = \dot{m}_F\left(\frac{RH_{in}\, p_{sat,in}}{p_F - RH_{in}\, p_{sat,in}} - \frac{RH_{out}\, p_{sat,out}}{p_F - RH_{out}\, p_{sat,out}}\right)\frac{M_{H2O}}{M_{air}}\frac{M_{H2O}}{M_{air}} \quad \text{S4.9}$$

4.6.4 Supplementary Note 4.4: Energy Balance of the Liquid Desiccant Process

The cooling load of the system $\dot{Q}$ can be evaluated by considering the energy balance of moist air as it enters and leaves the dehumidification unit, where $\dot{m}$ is the mass flow rate of moist air and h is the associated enthalpy. This is the heat that would need to be removed by a chiller, requiring mechanical work.

$$\dot{Q} = \dot{E}_{out} - \dot{E}_{in} \tag{S4.10}$$

$$\dot{Q} = \dot{m}_{out}\, h_{out} - \dot{m}_{in}\, h_{in} \tag{S4.11}$$

Assuming that moist air is composed simply of dry air and water vapor, we can separate the mass flow and its associated enthalpy into these two constituents. Then the mass flow rate of water can be related to the mass flow rate of dry air $\dot{m}_{air}$ via the humidity ratio ω. And by conservation of mass, for a perfectly selective membrane, such as we assume here, the mass of air at the inlet and outlet are equal.

$$\begin{aligned}\dot{Q} = {} & \left(\dot{m}_{out,air}\, h_{out,air} + \dot{m}_{out,H2O}\, h_{out,H2O}\right) \\ & - \left(\dot{m}_{in,air}\, h_{in,air} + \dot{m}_{in,H2O}\, h_{in,H2O}\right)\end{aligned} \tag{S4.12}$$

$$\dot{Q} = \dot{m}_{air}\left[\left(h_{out,air} + \omega_{out}\, h_{out,H2O}\right) - \left(h_{in,air} + \omega_{in}\, h_{in,H2O}\right)\right] \tag{S4.13}$$

Assuming constant pressure, the specific enthalpy of dry air can be expressed in terms of the specific heat c and temperature T. And assuming low vapor pressure, as would be expected, the specific enthalpy of water can be approximated by the enthalpy of saturated vapor h_g at a given temperature.

$$\dot{Q} = \dot{m}_{air}\left[\left(c_{in,air}\, T_{in} - c_{out,air}\, T_{out}\right) + \left(w_{in}\, h_{g,in} - w_{out}\, h_{g,out}\right)\right] \tag{S4.14}$$

Using the molar mass of air and water, the humidity ratio can be expressed as a molar ratio x, which can be related to the ratio of vapor pressure p_{H2O} to total pressure p_F, as

per Dalton's law. Finally, the vapor pressure can be related to the relative humidity rh via the saturation pressure p_{sat}.

$$\dot{Q} = \dot{m}_{air}\left[\left(c_{in,air}\,T_{in} - c_{out,air}\,T_{out}\right) + \left(x_{in}\,h_{g,in} - x_{out}\,h_{g,out}\right)\frac{M_{H2O}}{M_{air}}\right] \tag{S4.15}$$

$$\dot{Q} = \dot{m}_{air}\left[\left(c_{in,air}\,T_{in} - c_{out,air}\,T_{out}\right) + \left(\frac{p_{H2O,in}}{p_{air,in}}\,h_{g,in} - \frac{p_{H2O,out}}{p_{air,out}}\,h_{g,out}\right)\frac{M_{H2O}}{M_{air}}\right] \tag{S4.16}$$

$$\dot{Q} = \dot{m}_{air}\left[\left(c_{in,air}\,T_{in} - c_{out,air}\,T_{out}\right) + \left(\frac{RH_{in}\,p_{sat,in}}{p_F - rh_{in}\,p_{sat,in}}\,h_{g,in} - \frac{RH_{out}\,p_{sat,out}}{p_F - rh_{out}\,p_{sat,out}}\,h_{g,out}\right)\frac{M_{H2O}}{M_{air}}\right] \tag{S4.17}$$

In cases where the total mass flow rate $\dot{m}_F$ is measured rather than the mass of dry air $\dot{m}_{air}$, the expression can be rewritten using the ratio $\frac{\dot{m}_{air}}{\dot{m}_F} = (1+\omega)^{-1}$.

$$\dot{Q} = \frac{\dot{m}_{F,in}}{1+\omega_{in}}\left[\left(c_{in,air}\,T_{in} - c_{out,air}\,T_{out}\right) + \left(\frac{RH_{in}\,p_{sat,in}}{p_F - RH_{in}\,p_{sat,in}}\,h_{g,in} - \frac{RH_{out}\,p_{sat,out}}{p_F - RH_{out}\,p_{sat,out}}\,h_{g,out}\right)\frac{M_{H2O}}{M_{air}}\right] \tag{S4.18}$$

Or rather, for simplicity, it can also be assumed that the mass flow rate of dry air $\dot{m}_{air}$ is approximately equal to the total mass flow rate $\dot{m}_F$. In this case we obtain the

following expression which can be solved using experimental data from our experimental test bench.

$$\dot{Q} = \dot{m}_F \left[\left(c_{in,air}\, T_{in} - c_{out,air}\, T_{out} \right) + \left(\frac{RH_{in}\, p_{sat,in}}{p_F - RH_{in}\, p_{sat,in}}\, h_{g,in} - \frac{RH_{out}\, p_{sat,out}}{p_F - RH_{out}\, p_{sat,out}}\, h_{g,out} \right) \frac{M_{H2O}}{M_{air}} \right] \quad \text{S4.19}$$

From equation (S4.19) we can conclude that the cooling load of the system $\dot{Q}$ can be experimentally evaluated from the measurements of air flow rate $\dot{m}_{air}$, and the inlet and outlet temperatures and humidities, T and w. Thermophysical properties for air and water, including specific heat cp and specific enthalpy h, can be readily obtained from standard references such as the NIST database.

Alternatively, the cooling load of the system $\Delta\dot{E}$ can also be expressed in terms of the rate of vapor transfer $\Delta\dot{m}$. To show this, consider again equation (S4.14) where the specific enthalpy of saturated vapor at a given temperature is written in terms of the specific enthalpy of saturated vapor at a reference temperature and the specific heat at a given temperature, $h_{g@T} = h_{g@0°C} + cp\, T$.

$$\dot{Q} = \dot{m}_{air} c_{air} (T_{in} - T_{out}) + \dot{m}_{in,H2O}\, h_{g,in} - \dot{m}_{out,H2O}\, h_{g,out} \quad \text{S4.20}$$

$$\dot{Q} = \dot{m}_{air} c_{air} (T_{in} - T_{out}) + \dot{m}_{in,H2O}\, h_{g,in} - (\dot{m}_{in,H2O} - \Delta\dot{m})\, h_{g,out} \quad \text{S4.21}$$

$$\dot{Q} = \dot{m}_{air} c_{air} (T_{in} - T_{out}) + \dot{m}_{in,H2O} (h_{g,in} - h_{g,out}) + \Delta\dot{m}\, h_{g,out} \quad \text{S4.22}$$

$$\dot{Q} = \dot{m}_{air} c_{air} (T_{in} - T_{out}) + \dot{m}_{in,H2O} \left[\left(h_{g@0°C} + c_{H2O} T_{in} \right) - \left(h_{g@0°C} + c_{H2O} T_{out} \right) \right] + \Delta\dot{m}\, h_{g,out} \quad \text{S4.23}$$

$$\dot{Q} = \dot{m}_{air} c_{air} (T_{in} - T_{out}) + \dot{m}_{in,H2O} c_{H2O} (T_{in} - T_{out}) + \Delta\dot{m}\, h_{g,out} \quad \text{S4.24}$$

$$\dot{Q} = \dot{m}_{air} c_{air} (T_{in} - T_{out}) + \dot{m}_{air}\, w_{in} c_{H2O} (T_{in} - T_{out}) + \Delta\dot{m}\, h_{g,out} \quad \text{S4.25}$$

Finally neglecting the term for specific heat of water vapor, which is small, the change in energy can be approximated by eq. (S4.26).

$$\dot{Q} = \dot{m}_{air} \left[c_{air} (T_{in} - T_{out}) + \left(w_{in}\, h_{g,in} - w_{out}\, h_{g,out} \right) \right] \quad \text{S4.26}$$

By further analysis, it is also possible to distinguish between the two mechanisms by which energy is transferred from the warm air to the cool desiccant, namely by heat transfer $\dot{Q}_{gain}$ and by the enthalpy of mass transfer $\dot{H}$.

$$\dot{Q} = \dot{Q}_{gain} + \dot{H} \quad \text{S4.27}$$

$$\dot{Q} = \dot{Q}_{gain} + \int h\, d\Delta\dot{m} \quad \text{S4.28}$$

4.6.5 Supplementary Note 4.5: Sample Experimental Data, Analysis and Uncertainty

Dehumidification and specific energy performance were evaluated experimentally on a laboratory test bench at Oakland University by taking a mass and energy balance at the membrane inlets and outlets. Figure S4.3 shows a sample of the raw data collected and Table S4.1 provides an outline of how raw data is analyzed, including how experimental uncertainty propagates throughout the analysis.

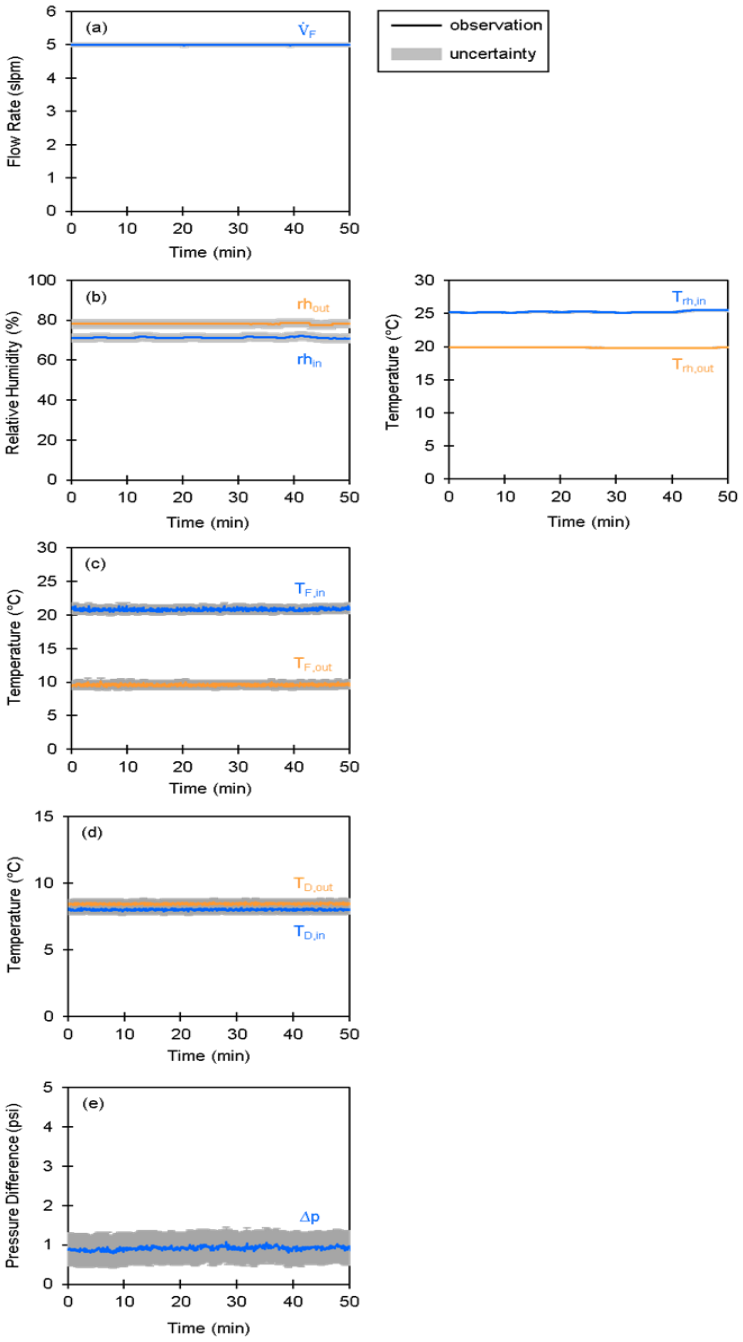

Figure S4.3 Raw test data for a sample dehumidification test. (a) Air feed flow rate as measured by mass flow controller (GH-32907-69, Masterflex, Radnor, PA). (b) Air feed temperature and humidity at the inlet and outlet measured by temperature and humidity sensors (AM2315 i2C, Aosong, Guangzhou, China). (c) Temperature of air at the inlet and exit of membrane port is measured by Resistive temperature detector (MT-6340-30, TWTADE, Suzhou, China) (d) Liquid desiccant temperature at the inlet and outlet as measured by temperature transmitter (800-32/140-11880256, Noshok, Berea, OH). (e) Pressure difference between air feed and liquid desiccant as measured by pressure transducer (GC557F0142CD, Ashcroft, Stratford, CT).

Table S4.1 Analysis of raw data and propagation of uncertainty

Parameter	Value	Measurement or Analysis
Liquid desiccant preparation		
Desiccant water mass $m_{D,w}$	980.4 ± 0.1 g	Balance (AX8201, Ohaus, Parsippany, NJ), full scale ± uncertainty = 8000 ± 0.1 g
Desiccant salt mass $m_{D,s}$	1.3 ± 0.1 g	Balance (AX8201, Ohaus, Parsippany, NJ), full scale ± uncertainty = 8000 ± 0.1 g
Sensor data at steady state (average over 50 minutes)		
Air feed flow rate $\dot{V}_F$	4.99 ± 0.05 slpm	Mass flow controller (GH-32907-69, Masterflex, Radnor, PA), full scale ± uncertainty = 5 slpm ± (0.8 % reading + 0.2 % full scale)
Air feed temperature at inlet $T_{F,in}$	20.82 ± 0.5 °C	Resistance Temperature Detectors (MT-6340-30, TWTADE, Suzhou, China), full scale ± uncertainty = 200 °C ± 0.3 %
Air feed humidity at inlet rh_{in} @ $T_{rh,in}$	71.2 ± 2 %rh @ 25.2 ± 0.1 °C	Capacitive humidity sensor (AM2315, Aosong, China), full scale ± uncertainty = 100 ± 2 %rh
Air feed temperature at outlet $T_{F,out}$	9.60 ± 0.5 °C	Resistance Temperature Detectors (MT-6340-30, TWTADE, Suzhou, China), full scale ± uncertainty = 200 °C ± 0.3 % full scale
Air feed humidity at outlet rh_{out}@ $T_{rh,out}$	78.1 ± 2 %rh @ 19.81 ± 0.1 °C	Capacitive humidity sensor (AM2315, Aosong, China), full scale ± uncertainty = 100 ± 2 %rh
Differential pressure Δp	0.91 ± 0.38 psia	Pressure transducer (GC557F0142CD, Ashcroft, Stratford, CT), full scale ± uncertainty = 75 ± 0.38 psi
Liquid desiccant flow rate $\dot{V}_D$	2.08 ± 0.19 lpm	Flowmeter (8051K107, McMaster-Carr, Elmhurst, IL), full scale ± uncertainty = 1.6 ± 0.05 gpm
Liquid desiccant temperature at inlet $T_{D,in}$	8.02 ± 0.3 °C	Thermal resistance sensor, (800-32/140-1188, Noshok, Berea, OH), full scale ± uncertainty = 60 ± 0.3 °C
Liquid desiccant temperature at outlet $T_{D,out}$	8.45 ± 0.3 °C	Thermal resistance sensor, (800-32/140-1188, Noshok, Berea, OH), full scale ± uncertainty = 60 ± 0.3 °C
Liquid desiccant pressure p_D	18.9 ± 0.38 psia	Pressure transducer (GC557F0142CD, Ashcroft, Stratford, CT), full scale ± uncertainty = 75 ± 0.38 psi
Mass balance analysis		
Air feed mass flow rate $\dot{m}_F$	366.6 g/h ± 1 %	$\dot{m}_F = \frac{p_F \dot{V}_F}{R T_F} M_{air}$, $\frac{\delta \dot{m}_F}{\dot{m}_F} = \sqrt{\left(\frac{\delta \dot{V}_F}{\dot{V}_F}\right)^2}$ where R =8.314 J.K^{-1}mol^{-1}, $p_F = 101$ kPa, and T_F =273 K
Water vapor content at the inlet $x_{H2O,in}$	0.0173 mol/mol ± 3.50 %	$x_{H2O,in} = rh_{in} \frac{p_{sat,in}}{p_F - rh_{in}\, p_{sat,in}}$, where $p_{sat,in} = 10^{A-\left(\frac{B}{C+T_{rh,in}}\right)}$, A, B and C are constants of Antoine equation.

Table S4.1—continued

Parameter	Value	Measurement or Analysis
Water vapor content at the outlet $x_{H2O,out}$	0.014 mol_{H2O}/mol ± 3.3 %	$x_{H2O,out} = rh_{out} \frac{p_{sat,out}}{p_F - rh_{out}\, p_{sat,out}}$, where $p_{sat,out} = 10^{A-\left(\frac{B}{C+T_{rh,out}}\right)}$, $\frac{\delta x_{H2O,out}}{x_{H2O,out}} = \sqrt{\left(\frac{\delta rh_{out}}{rh_{out}}\right)^2 + \left(\frac{\delta p_F}{p_F}\right)^2 + \left(B \ln(10) \frac{\delta T_{rh,out}}{(C+T_{rh,out})^2}\right)^2}$
Water vapor mass flow rate at the inlet $\dot{m}_{F,H2O,in}$	4.05 g/h ± 3.7 %	$\dot{m}_{F,H2O,in} = \dot{m}_F \left(\frac{x_{H2O,in}}{1-x_{H2O,in}}\right) \frac{M_{H2O}}{M_{air}}$, $\frac{\delta \dot{m}_{F,H2O,in}}{\dot{m}_{F,H2O,in}} = \sqrt{\left(\frac{\delta \dot{m}_F}{\dot{m}_F}\right)^2 + \left(\frac{\delta x_{H2O,in}}{x_{H2O,in}(1-x_{H2O,in})}\right)^2}$
Water vapor mass flow rate at the outlet $\dot{m}_{F,H2O,out}$	3.23 g/h ± 3.6 %	$\dot{m}_{F,H2O,out} = \dot{m}_F \left(\frac{x_{H2O,out}}{1-x_{H2O,out}}\right) \frac{M_{H2O}}{M_{air}}$, $\frac{\delta \dot{m}_{F,H2O,out}}{\dot{m}_{F,H2O,out}} = \sqrt{\left(\frac{\delta \dot{m}_F}{\dot{m}_F}\right)^2 + \left(\frac{\delta x_{H2O,out}}{x_{H2O,out}(1-x_{H2O,out})}\right)^2}$
Water vapor flux J	0.82 $g/m^2/h$ ± 22.0 %	$J = \frac{\dot{m}_{F,H2O,in} - \dot{m}_{F,H2O,out}}{a}$, where $a = 1\ m^2$, $\frac{\delta J}{J} = \sqrt{\left(\frac{\delta \dot{m}_{F,H2O,in}}{\dot{m}_{F,H2O,in}}\right)^2 + \left(\frac{\delta \dot{m}_{F,H2O,out}}{\dot{m}_{F,H2O,out}}\right)^2}$
Energy balance analysis		
Heat flux $\dot{q}$	1.16 W/m^2 ± 6.2 %	$\dot{q} = \frac{\dot{m}_F\, c\, T_{F,in} - \dot{m}_F\, c\, T_{F,out}}{a}$, where c = specific heat, $\delta \dot{q} = \sqrt{\left(\frac{c\, T_{F,in} - c\, T_{F,out}}{a} \delta \dot{m}_F\right)^2 + \left(\frac{\dot{m}_F\, c}{a} \delta T_{F,in}\right)^2 + \left(\left(-\frac{\dot{m}_F\, c}{a}\right) \delta T_{F,out}\right)^2}$
Energy flux from mass transfer $J\, h_g$	0.57 W/m^2 ± 22.0 %	$J\, h_g$, where h_g = enthalpy of water vapor, $\frac{\delta J\, h_g}{J\, h_g} = \frac{\delta J}{J}$
Energy flux $\Delta \dot{E}$	1.73 W/m^2 ± 8 %	$\Delta \dot{E} = \dot{q} + J\, h_g$, $\frac{\delta \Delta \dot{E}}{\Delta \dot{E}} = \sqrt{\left(\frac{\delta \dot{q}}{\dot{q}}\right)^2 + \left(\frac{\delta J\, h_g}{J\, h_g}\right)^2}$
Specific energy e	2.11 Wh/g ± 22.8 %	$e = \frac{\dot{q}}{J}$, $\frac{\delta e}{e} = \sqrt{\left(\frac{\delta \Delta \dot{E}}{\Delta \dot{E}}\right)^2 + \left(\frac{\delta J}{J}\right)^2}$
Specific work w	0.41 Wh/g ± 22.9 %	$w = \frac{e}{cop}$, where cop = 5, $\frac{\delta w}{w} = \frac{\delta e}{e}$

4.6.6 Supplementary Note 4.6: Fertilizer Precipitation Observed in High Concentration Blends

Figure S4.4 shows precipitation in the fertilizer desiccant solution at higher concentrations for the multi-ion solution case. At lower concentrations the solution was clear and stable, but as the concentration increased, the solution turned turbid and cloudy due to solid precipitates. For future testing with fertilizer blends and commercial fertilizers, the precipitates can be avoided by maintaining pH level between 6-8. To maintain the pH level, a buffer solution can be added to resist any changes due to ionic interactions. It is also recommended to periodically flush the system with deionized water to prevent any maintenance issues like corrosion and scaling.

Figure S4.4 Precipitated fertilizer desiccant during experimental testing at higher concentrations for multi-ion blends. The clear solution transitions into a cloudy state, marked by the precipitation of solids within the liquid.

CHAPTER FIVE

PROTOTYPE AND DEMONSTRATION OF A FERTILIZER-BASED LIQUID DESICCANT SYSTEM FOR CONTROLLED PLANT ENVIRONMENTS

5.1 Introduction

As mentioned earlier in previous chapters, one of the key conditions in the indoor plant environment is humidity regulation. Due to plant evapotranspiration, moisture is continuously released into the indoor environment and if left uncontrolled, humidity can reach very high levels. For example, Figure 5.1 shows an uncontrolled plant chamber in our laboratory, with condensation on the surfaces of the chamber clearly visible. Such high humidity can cause fungal disease, degrade crop health, reduce absorption of solar radiation, hinder plant transpiration and nutrient uptake, and ultimately compromise productivity [93,94]. Figure 5.1 shows the same laboratory plant chamber when humidity is properly controlled. For many common plant crops, the vapor pressure should be kept between 0.8 and 1.2 kPa below the dew point [108]. This is known as the vapor pressure deficit, and is one of the key parameters that regulates evapotranspiration.

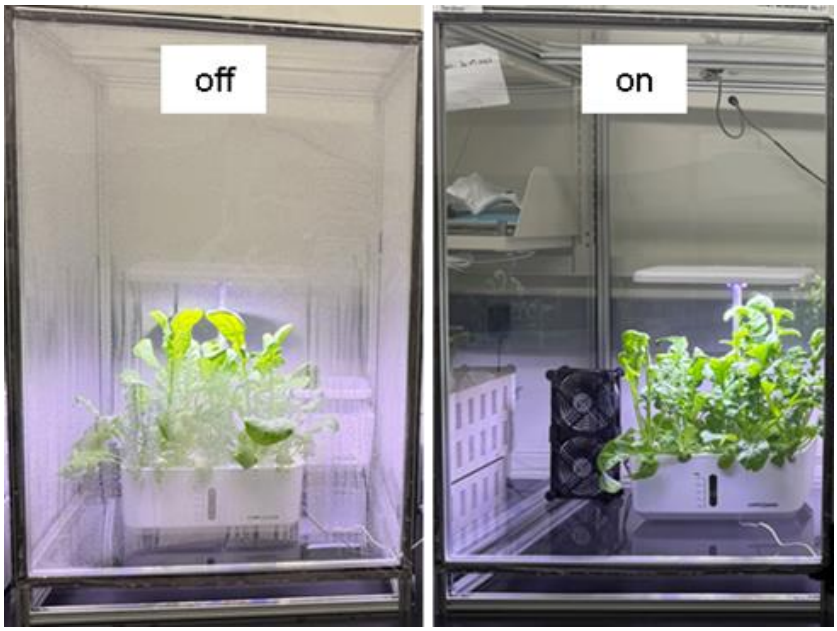

Figure 5.1 Humidity control is an important part of creating an ideal plant environment. The image on the left shows a small plant chamber in our laboratory, operating without any humidity control, and high humidity can clearly be seen with condensation of the clear enclosure. The image on the right shows the same system with proper dehumidification.

In earlier chapters, various humidity control methods such as heat pumps, mechanical refrigeration, and solid desiccants are discussed, supported by the existing literature [25,109-111]. Among these, liquid and solid desiccants have gained considerable popularity [112-114]. However, they typically use high energy due to the need for regeneration and subsequent cooling. These systems can be cost-effective when a low-grade heat source is available. To enhance dehumidification performance, the contact area between air and desiccant is often increased using delivery methods like spray towers, falling films, packed beds, or as demonstrated in this study though vapor permeable membrane [123,124]. As previously discussed, and illustrated in Figure 5.2, our study in recent years has advanced a novel approach by using fertilizer solutions as liquid desiccants to dehumidify controlled plant environments [30,47].

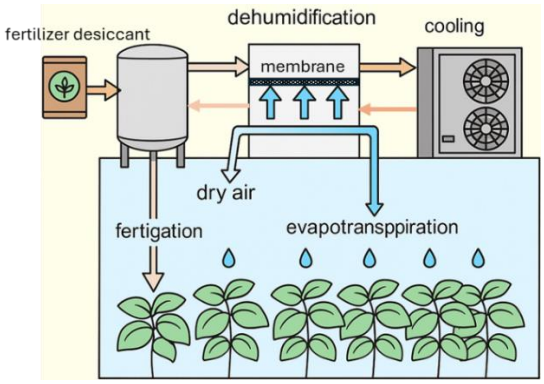

Figure 5.2 In the proposed dehumidification system, concentrated fertilizer solution is used in place of traditional liquid desiccants. Water vapor is transferred from the humid plant environment to the liquid desiccant, driven by the vapor pressure difference between the two. Liquid desiccant is cooled to ensure consistent dehumidification performance as the batch of fertilizer is diluted. After sufficient time, fertilizer solution can be delivered to the plants, as intended, to provide nutrients for plant growth.

In summary then, each of these technologies mentioned comes with its own advantages and disadvantages. Table 5.1 provides a summary of how these various technologies have been considered for application to controlled plant environments. Studies by De Halleux and Gauthier [115] and Rousse et al. [116] found that ventilation with heat recovery offers moderate humidity control and improved energy efficiency, though its performance may be limited under high humidity conditions. Heat pump systems studied by Chasseriaux et al. [117] and Gilli et al. [118], showed high dehumidification efficiency, with performance influenced by ambient conditions and design considerations. Sultan et al. [119, 120] demonstrated that solid desiccants are effective across multiple crops—including tomato, cucumber, lettuce, and soybean, while consuming relatively low energy. Liquid desiccant technologies were explored in greater depth, with Ali et al. [66] presenting theoretical potential, and Bettahalli et al. [45] offering both the theoretical and experimental validation. Ganguly and Ghosh [121] showed that liquid desiccants effectively controlled humidity for cucumber and lettuce,

balancing moisture removal and energy input. Lefers et al. [44,70] confirmed the operational stability of such systems and proposed methods for efficient regeneration. Finally, Lynchos and Davies [122] validated liquid desiccant use for lettuce cultivation through experiments and simulations, demonstrating reliable humidity control and energy savings.

Table 5.1 Studies conducted on dehumidification of indoor farming using different moisture removal technologies

Investigators	Dehumidification technology	Study method	Crop
De Halleux and Gauthier [115]	Ventilation with heat recovery	Simulation	Tomato
Rousse et al. [116]	Ventilation with heat recovery	Experimental	Tomato, cucumber
Chasseriaux et al. [117]	Heat pump	Theoretical	Tomato
Gilli et al. [118]	Heat pump	Experimental	Cucumber
Sultan et al. [119,120]	Solid desiccant	Experimental	Tomato, cucumber, lettuce, soybean
Ali et al. [66]	Liquid desiccant	Theoretical	n/a
Bettahalli et. al [45]	Liquid desiccant	Experimental and theoretical	n/a
Ganguly and Gosh [121]	Liquid desiccant	Experimental and theoretical	Cucumber and lettuce
Lefers et al. [44,70]	Liquid desiccant	Experimental	n/a
Lynchos and Davies [122]	Liquid desiccant	Experimental and simulation	Lettuce

So far, in previous work from our lab on this subject, they have successfully validated the concept showing dehumidification with a variety of common fertilizer solution [30], and we have evaluated the thermodynamic limits, process' energy efficiency and controlled experimental study, showing that it compares very well with other dehumidification technologies and standards [47]. However, to this date, fertilizer-based liquid desiccants have not actually been applied to a controlled plant environment. The scope of this study is therefore to demonstrate the operation of a fertilizer-based liquid desiccant dehumidification system when it is integrated with a real plant chamber. This

chapter begins by describing the plant chamber that has been developed in our laboratory. The plant chamber includes a commercial hydroponic grow system that is used for cultivation of arugula throughout the study. Then, the dehumidification apparatus is described, which includes a series of hollow fiber membrane modules across which water vapor is transferred from the humid air to the concentrated fertilizer. A simple illustration of the prototype is provided in Figure 5.3. Test conditions and methods of analysis are described. Finally, results are included, showing dehumidification for a number of test trials with plant crops at different stages, kept at different humidity levels. Ultimately, the contribution of this work to scientific literature is the first demonstration of fertilizer solution being used to control humidity of a real plant growth chamber. This successful demonstration represents an important step forward in enabling energy efficient dehumidification for controlled plant environments.

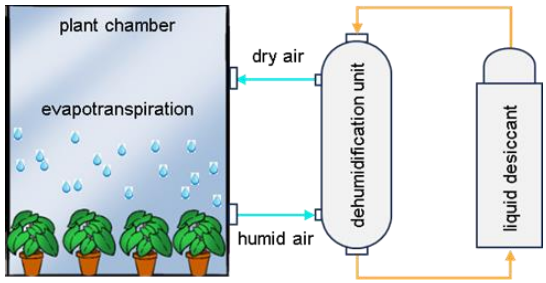

Figure 5.3 Closed plant environment and dehumidification unit used to demonstrate dehumidification with fertilizer-based liquid desiccants.

5.2 Materials and Methods

5.2.1 Hydroponic Plant Chamber

A laboratory scale plant chamber was designed and fabricated at Oakland University as shown in Figure 5.4(a). The chamber is made of anodized 2020 aluminum extrusion rails for framing (IXGNIJ, Dongguan, China) with transparent plexiglass for glazing

(Duco Plus, Warminster, PA) and has overall dimensions of 24×24×34 inches. In the chamber is placed a commercial hydroponic grow system (Ahopegarden, Guangzhou, China). The hydroponic system has a 3-L capacity for hydroponic solution that is aerated and mixed by a small internal pump, as well as 10 pods that can accommodate conical sponge inserts that are used to promote germination and root development. The pods are shown in Figure 5.4(b). The hydroponic system includes a full spectrum LED grow light that is maintained at 14 inches above the base. Air from the plant chamber is circulated towards an external dehumidification unit before being returned to the chamber, where temperature and humidity are monitored by a sensor (AM2315, Aosong Electronics, Guangzhou, China). A 12 V, 1.2 W fan (ELUTENG, ShenZhen Engesen Electronics, Shenzhen, China) is operated continuously in the plant chamber to ensure that the microclimate is evenly mixed.

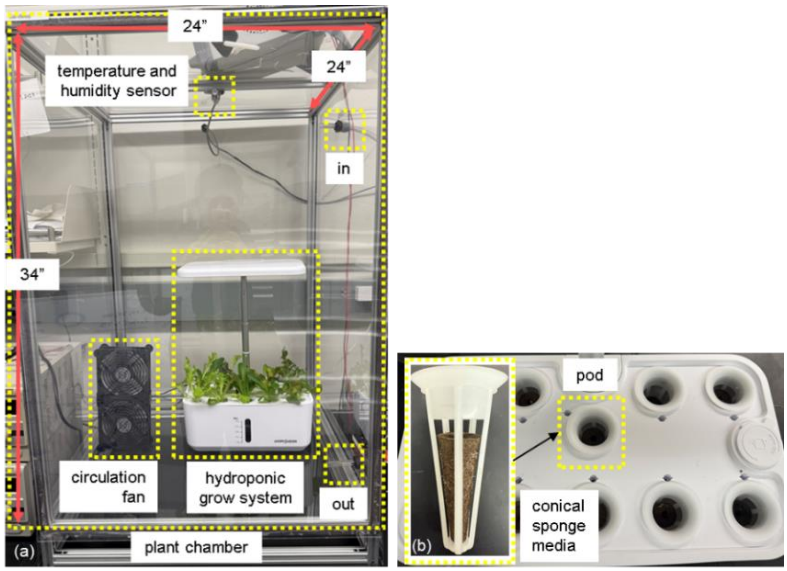

Figure 5.4 (a) Custom plant chamber with hydroponic grow system. The unit measures 24 × 24 × 34 inches and is equipped with a fan for air circulation, temperature and humidity sensors, and ports for circulating air to an external dehumidification unit. (b) The hydroponic system has a volume capacity of 3 L and can accommodate up to 10 plants grown in conical sponge media that is submerged in the hydroponic solution.

5.2.2 Liquid Desiccant Dehumidification

Air is drawn from the plant chamber and directed towards an external dehumidification unit using a 12 V diaphragm air pump (SEAFLO 21 Series, Xiamen, China). Air flow rate is regulated using a mass flow controller (GFC17, Aalborg, Orangeburg, NY). The temperature and humidity of air are measured at the inlet (when air is removed from the plant chamber) and at the outlet (prior to returning air to the plant chamber) using capacitive sensors (AM2315, Aosong Electronics, Guangzhou, China). Inlet and outlet pressures are also measured with a pressure transducer (GC557F0142CD, Ashcroft, Stratford, CT). Since dehumidification performance is sensitive to pressure, a pressure regulator is installed at the air outlet to ensure that both air and desiccant are at equal applied pressure in the dehumidification unit.

The external dehumidification unit is shown in Figure 5.5 and additional renderings are included in Supplementary Note 5.1. As shown, the system features two hollow fiber membrane modules (PDMSXA-1.0, PermSelect, Ann Arbor, MI) that are placed in parallel to increase contact area and dehumidification capacity. Each module includes five ports, enabling a counterflow configuration where warm, humid air flows through the lumens and cold fertilizer desiccant solution circulates through the shell side. Additional membrane specifications are provided in Section 5.3.3. A positive displacement diaphragm pump (SFDP1-030-045-33, Seaflo, Xiamen, China) is used to draw liquid desiccant from a 3 L reservoir and circulate it through the membrane modules. The flow rate is monitored using a mass flow meter (8051K107, McMaster-Carr, Elmhurst, IL) and controlled by adjusting the DC voltage supply to the pump. To dampen any flow pulsations and reduce vibration, an inline accumulator tank (SFAT-

075-125-01, Seaflo, Xiamen, China) is included. Liquid desiccant is cooled before entering the membrane modules using a stacked plate heat exchanger (35115K62, McMaster-Carr, Elmhurst, IL) that receives chilled water from a thermostatically controlled bath (TC550-SD, Brookfield, Middleboro, MA). Desiccant temperatures at the membrane inlets and outlets are tracked using inline thermal resistance sensors (800-32/140-1188, Noshok, Berea, OH) housed within protective thermowells (75-025-316SS, Noshok, Berea, OH). Desiccant pressure at the membrane inlet is also monitored with a pressure transducer (GC557F0142CD, Ashcroft, Stratford, CT). All desiccant lines are insulated with foam tubing to minimize heat gain from the ambient environment.

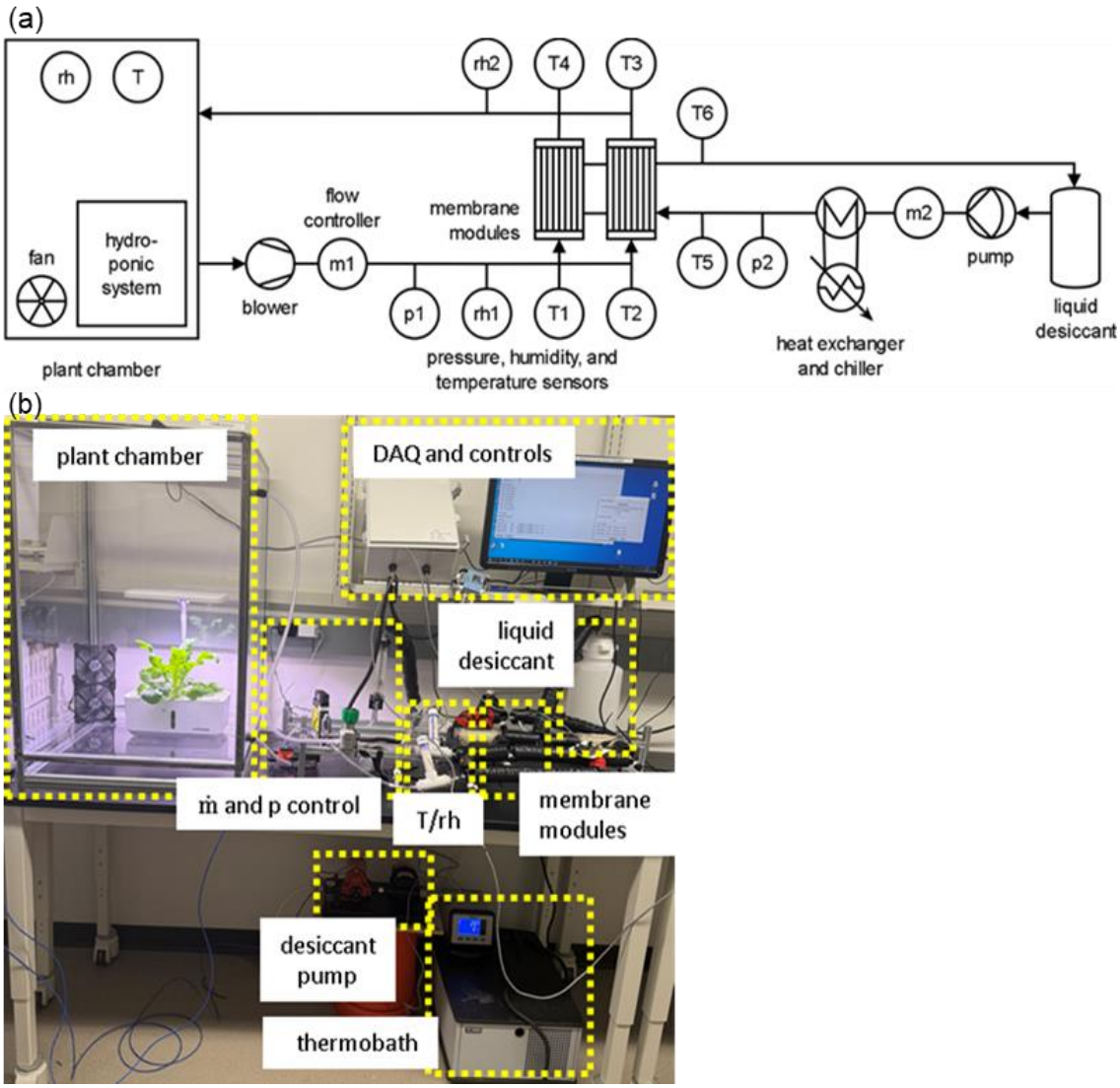

Figure 5.5 (a) Schematic and (b) picture of the laboratory-scale liquid desiccant dehumidification system. In this study, concentrated fertilizer solution is used as the liquid desiccant. Air is circulated from the plant chamber to the dehumidification unit in order to control humidity. Instrument numbers are listed in Table 5.2 with key specifications.

Table 5.2 provides a summary of all sensors and instrumentation included in the plant chamber and desiccant dehumidification system, with their key specifications including full scale and uncertainty. Instrument numbers correspond to locations indicated on Figure 5.5.

Table 5.2 Sensor and instrumentation specifications

Instrument	Manufacturer	Model number	Full scale ± Uncertainty	Instrument number
Liquid desiccant				
Mass flow meter	McMaster-Carr	8051K107	1.6 ± 0.05 GPM	m2
Thermal resistance sensor	Noshok	800-32/140-1188	60 ± 0.3 °C	T5, T6
Pressure transducer	Ashcroft	GC557F0142CD	75 ± 0.38 psi	p2
Air feed				
Mass flow controller	Aalborg	GFC17	5 ± 0.05 SLPM	m1
Resistive temperature detector	TWTADE	MT-6340-30	200 ± 0.5 °C	T1, T2, T3, T4
Capacitive humidity and temperature sensor	Aosong Electronics	AM2315	100 ± 2 %	rh1, rh2
Pressure transducer	Ashcroft	GC557F0142CD	75 ± 0.38 psi	p1

5.2.3 Membrane Module

For this study, two commercial membrane modules placed in parallel, were selected as the core component of the dehumidification process. Each module includes 12,600 dense hollow fiber membranes made from dense polydimethylsiloxane, providing a total surface area of 2 m^2 across which water vapor is driven by the vapor pressure difference between humid air and concentrated desiccant. It should be noted that other methods of bringing air and liquid desiccant into contact could also be used in this place (e.g. spray, falling film, packed bed). Air is circulated through the membrane hollow fibers, while the liquid desiccant is circulated around these fibers on the shell side of the module in a counter flow arrangement. Figure 5.6 shows an image of the membrane fibers captured with a scanning electron microscope (JSM 6510, Jeol, Peabody, MA). Key membrane specifications are listed in Table 5.3.

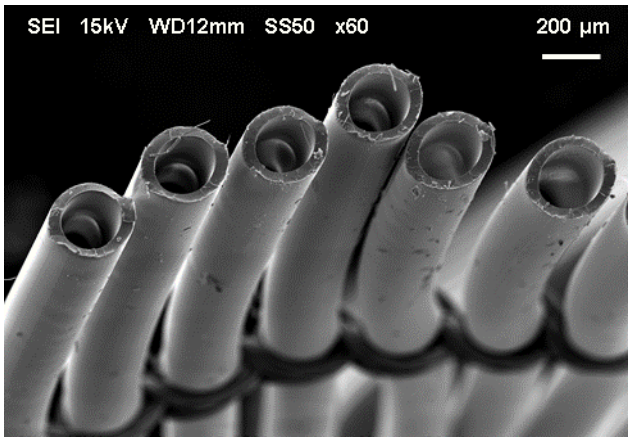

Figure 5.6 SEM image of membrane hollow fibers at 60× magnification.

Table 5.3 Membrane specifications

Material	Polydimethylsiloxane
Module type	Hollow fiber
Membrane area	1 m^2
Fiber length	0.14 m
Fiber diameter (outer)	300×10^{-6} m
Fiber thickness	55×10^{-6} m
Number of fibers	12,600
Flow orientation	Counter flow

5.2.4 Data Analysis

Performance of the dehumidification system is evaluated in terms of several key metrics. First, the relative humidity RH and temperature T of the plant chamber are directly observed. As a reference, the associated vapor pressure p_{H2O} can be easily calculated and compared to the saturation pressure p_{sat}, which can be obtained from the empirical Magnus-Tetens equation shown in equation (5.2) (where p_{sat} is in Pa and T is in ^{o}C) [125]. For convenience, the difference between these two can also be expressed as the vapor pressure deficit VPD.

$$p_{H2O} = RH\, p_{sat} \tag{5.1}$$

$$p_{sat} = 613.87 \exp\left(\frac{17.50\ T}{241.2 + T}\right) \tag{5.2}$$

$$\mathrm{VPD} = \mathrm{p_{sat}} - \mathrm{p_{H2O}} = \mathrm{p_{sat}}\,(1 - \mathrm{RH}) \tag{5.3}$$

Second, the rate of dehumidification $\dot{\mathrm{m}}_{\mathrm{dehumidification}}$ achieved by the fertilizer desiccant system is experimentally evaluated. This is done by taking a mass balance of the humid air at the dehumidification unit's inlet and outlet. Supplementary Note 5.2 provides a detailed derivation of how equation (5.4) can be obtained from the difference between inlet and outlet water vapor and then related to pressure and humidity sensors that are mounted on the bench. As a measure of the membrane performance (or as an indication of how effectively the membrane area is utilized), the rate of dehumidification can also be normalized over the membrane surface area A to obtain vapor flux J.

$$\dot{\mathrm{m}}_{\mathrm{dehumidification}} = \dot{\mathrm{m}}_{\mathrm{F}}\left(\left(\frac{\mathrm{RH}\ \mathrm{p_{sat}}}{\mathrm{p} - \mathrm{RH}\ \mathrm{p_{sat}}}\right)_{\mathrm{in}} - \left(\frac{\mathrm{RH}\ \mathrm{p_{sat}}}{\mathrm{p} - \mathrm{RH}\ \mathrm{p_{sat}}}\right)_{\mathrm{out}}\right)\frac{\mathrm{M_{H2O}}}{\mathrm{M_{air}}} \tag{5.4}$$

$$\mathrm{J} = \dot{\mathrm{m}}_{\mathrm{dehumidification}}/\mathrm{a} \tag{5.5}$$

Where $\dot{\mathrm{m}}_{\mathrm{F}}$ is the circulation rate of air, p is the air pressure, and M is the molar mass.

For reference, the dehumidification rate can also be compared to the plant evapotranspiration rate $\dot{\mathrm{m}}_{\mathrm{evapotranspiration}}$. This can be calculated from the change in water vapor content that is observed over some discrete time interval $\Delta\mathrm{t} = \mathrm{t_2} - \mathrm{t_1}$ in the plant chamber, and by accounting for water vapor that is removed by dehumidification. From equation (5.6) it follows that when there is no change in humidity in the plant chamber $\dot{\mathrm{m}}_{\mathrm{evapotranspiration}} = \dot{\mathrm{m}}_{\mathrm{dehumidification}}$.

$$\dot{\mathrm{m}}_{\mathrm{evapotranspiration}} = \frac{\Delta\mathrm{m}}{\Delta\mathrm{t}} + \dot{\mathrm{m}}_{\mathrm{dehumidification}} \tag{5.6a}$$

$$\dot{m}_{evapotranspiration}$$

$$= \frac{\rho_{air}\, V}{t_2 - t_1}\left(\left(\frac{RH\, p_{sat}}{p - RH\, p_{sat}}\right)_2 - \left(\frac{RH\, p_{sat}}{p - RH\, p_{sat}}\right)_1\right)\frac{M_{H2O}}{M_{air}} \qquad 5.6b$$

$$+ \dot{m}_{dehumidification}$$

Where ρ is density of air inside the plant chamber and V is the volume of the plant chamber.

Supplementary Note 5.1 provides sample calculations to illustrate dehumidification analysis from equations (5.1)-(5.5) with the associated propagation of experimental uncertainty.

5.2.5 Test Conditions

Three sets of tests were completed to evaluate the proposed fertilizer-based liquid desiccant dehumidification system under a range of conditions. Table 5.4 provides a summary of all test conditions.

Table 5.4 Test conditions for the fertilizer-based desiccant dehumidification system

	Round 1 no dehumidification	Round 2 short tests	Round 3 extended tests
Hydroponic System			
Plant crop	arugula (*Eruca sativa)*	arugula (*Eruca sativa)*	arugula (*Eruca sativa)*
Photoperiod	16 h	16 h	16 h
Nutrient solution	1.5 ml/day	1.5 ml/day	1.5 mL/day
Plant stage	day 21	day 21	days 1-36
Dehumidification System			
Humidity setpoint	n/a	60, 70, 80 % rh	60 % rh
Air circulation rate	n/a	1.5-2 sl/min	1.5-2 sl/min
Air pressure	n/a	1 atm	1 atm
Desiccant circulation rate	n/a	2 l/min	2 l/min
Desiccant pressure	n/a	1.2 atm	1.2 atm
Desiccant temperature	n/a	2-7 °C	3-5 °C
Fertilizer desiccant	n/a	$Ca(NO_3)_2{\cdot}4H_2O$	$Ca(NO_3)_2{\cdot}4H_2O$
Desiccant concentration	n/a	1,000 g/l	25 g/l

In the first set of tests, all hydroponic pods were seeded with arugula (*Eruca sativa*, Johnny's Selected Seeds, Winslow, ME) which was grown to maturity (~ 36 days). Plants were provided a commercial two-part nutrient blend (Ahopegarden, Guangzhou, China) with composition specified in Table 5.5. Plants were grown with a 16-hour photoperiod with daily light integral (DLI) value of 13 mol/m^2/day. Once plants reached maturity, conditions of the plant chamber (including temperature, relative humidity, vapor pressure deficit, and evapotranspiration rates) were observed in the absence of any dehumidification control. The objective of this testing was to characterize the passive response of the plant chamber and evaluate the maximum dehumidification load.

Table 5.5 Nutrient composition of commercial fertilizer blend supplied to plants

Solution A	(%)
N	8.5
Soluble P_2O_5	7.5
K_2O	29.5
Mg	2.5
EDTA-Fe	0.3
EDTA-Mn	0.06
EDTA-Cu	0.005
EDTA-Zn	0.01
Solution B	
Total N	11
CaO	25

In the second round of tests, the fertilizer dehumidification system was switched on to confirm its capacity for reducing indoor humidity to target levels of 60, 70, and 80 %. These humidity targets were achieved by regulating the liquid desiccant temperature and manually operating the dehumidification system's duty cycle. Throughout this round of tests, super concentrated calcium nitrate tetrahydrate $Ca(NO_3)2{\cdot}4H_2O$ (99 % purity, Fisher Scientific, Hampton, NH) at 1,000 g/l was used as liquid desiccant and circulated at a rate of 2 lpm and pressure of 18 psia. Of note, for the purpose of these experiments,

the hydroponic plant system continued to be provided with the two-part nutrient blend, rather than the concentrated nitrogen fertilizer, as intended. This was done due to concerns about membrane fouling and fertilizer precipitation, which must be further investigated before fertilizer desiccant can be fully integrated with the plant nutrient supply.

Finally, in the third round of testing, the dehumidification system was operated throughout all stages of the plant development, from germination to maturity, in order to observe dehumidification performance. Due to limited capacity of the dehumidification system, only two of the hydroponic pods were seeded with arugula (Eruca sativa, Johnny's Selected Seeds, Winslow, ME). Plants were grown under similar conditions reported above. Calcium nitrate tetrahydrate $Ca(NO_3)2{\cdot}4H_2O$ (99 % purity, Fisher Scientific, Hampton, NH) was again used as the fertilizer-based desiccant, but was limited to a concentration of 25 g/l. This concentration was selected to be more representative of the diluted fertilizer that can be expected in real applications, given that such plants only require about ~15 g/plant to complete their growth cycle.

5.3 Results

5.3.1 Response of the Plant System Without Dehumidification

The first round of testing was done to characterize the response of the plant system in the absence of any dehumidification. Figure 5.7 showed the resulting plant environment over a sample period of 96 hours (4 days) when hydroponic arugula is growing. At this stage, the plants were fully-mature with a dense, well-developed leafy canopy, as shown in the image.

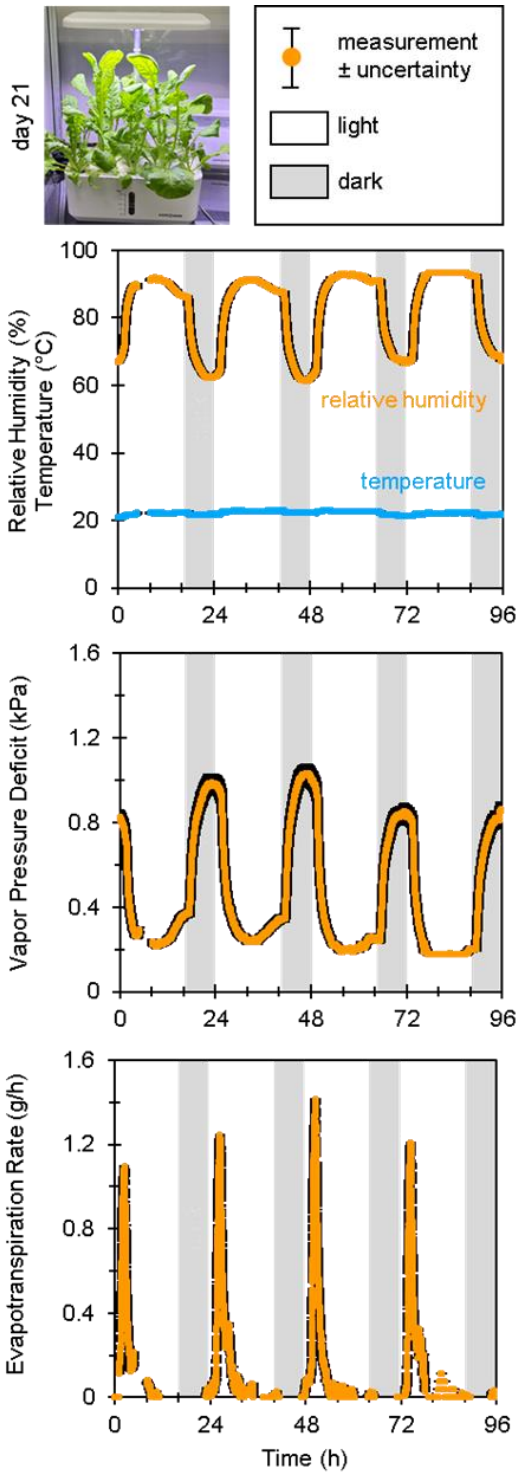

Figure 5.7 Temperature (a), humidity (a), vapor pressure deficit (b) and evapotranspiration rate (c) inside the mini greenhouse chamber for a period of 96 hours with fully grown arugula at its mature stage (day 21 after germination). Relative humidity and vapor pressure showed clear diurnal fluctuations driven by plant evapotranspiration. No dehumidification system was used during this period.

The daily cycle was clearly driven by the photoperiod which includes a 16-hour light period and an 8-hour dark period, as marked on the figure. As shown, temperature increased from 21.4 ± 0.2 °C at the start of the day to a peak of 23.3 ± 0.2 °C, and humidity likewise from 62 ± 2 % to near saturation at its peak. Such a cyclical, daily response was expected and is characteristic of plant systems. During light periods, stomata opened, increasing transpiration, and releasing moisture into the environment. Conversely, stomata closed during dark periods, reducing transpiration, and a drop in humidity was observed as some humidity is taken up by the plant and some condenses.

Figure 5.7 also showed the vapor pressure deficit in the plant environment and the resulting rate of evapotranspiration that it causes. Evapotranspiration peaked at the start of each day, when the vapor pressure deficit was at its highest and when lighting is first switched on. The maximum rate of evapotranspiration was useful to note as it provided a measure of the dehumidification capacity that is needed for the liquid desiccant system, which was important for sizing. The maximum rate of evapotranspiration observed during these tests was 1.39 ± 0.08 g/h, which occurred when the vapor pressure deficit is 1.0 ± 0.6 kPa. For reference, a vapor pressure deficit between 0.8 and 1.2 kPa was generally considered ideal for vegetative plant growth [126]. Also, for comparison, the evapotranspiration rate can be expressed on a per plant unit, which gives 0.139 ± 0.008 g/h/plant for the previously mentioned maximum. Or it can be expressed per unit of grow space, which gave 48.1 ± 2.8 g/h/m^2. These values compared reasonably well with evapotranspiration rates reported in the literature, which range from 0.1 to 0.8 g/h/plant for fully-developed arugula [127].

5.3.2 Dehumidifying the Plant Chamber with Fertilizer-Based Desiccant

In the second round of testing, the dehumidification system was switched on to verify the capacity of the fertilizer-based liquid desiccant to manage humidity at a range of setpoints, including 60, 70, and 80 % relative humidity. These tests were conducted with the hydroponic system at full capacity, including 10 fully-developed arugula plants (day), and under light conditions. Calcium nitrate solution near its solubility limit was selected as the fertilizer desiccant.

Figure 5.8 showed the results, and confirms successful dehumidification of the plant system. The fertilizer-based liquid desiccant was able to effectively maintain constant humidity within 2.3 % of each of the setpoints. After successfully maintaining humidity for a period of approximately 60 minutes, the dehumidification system was then switched off to observe the response of the system for an additional period. As shown, humidity steadily increased, nearing saturation after about 60 minutes.

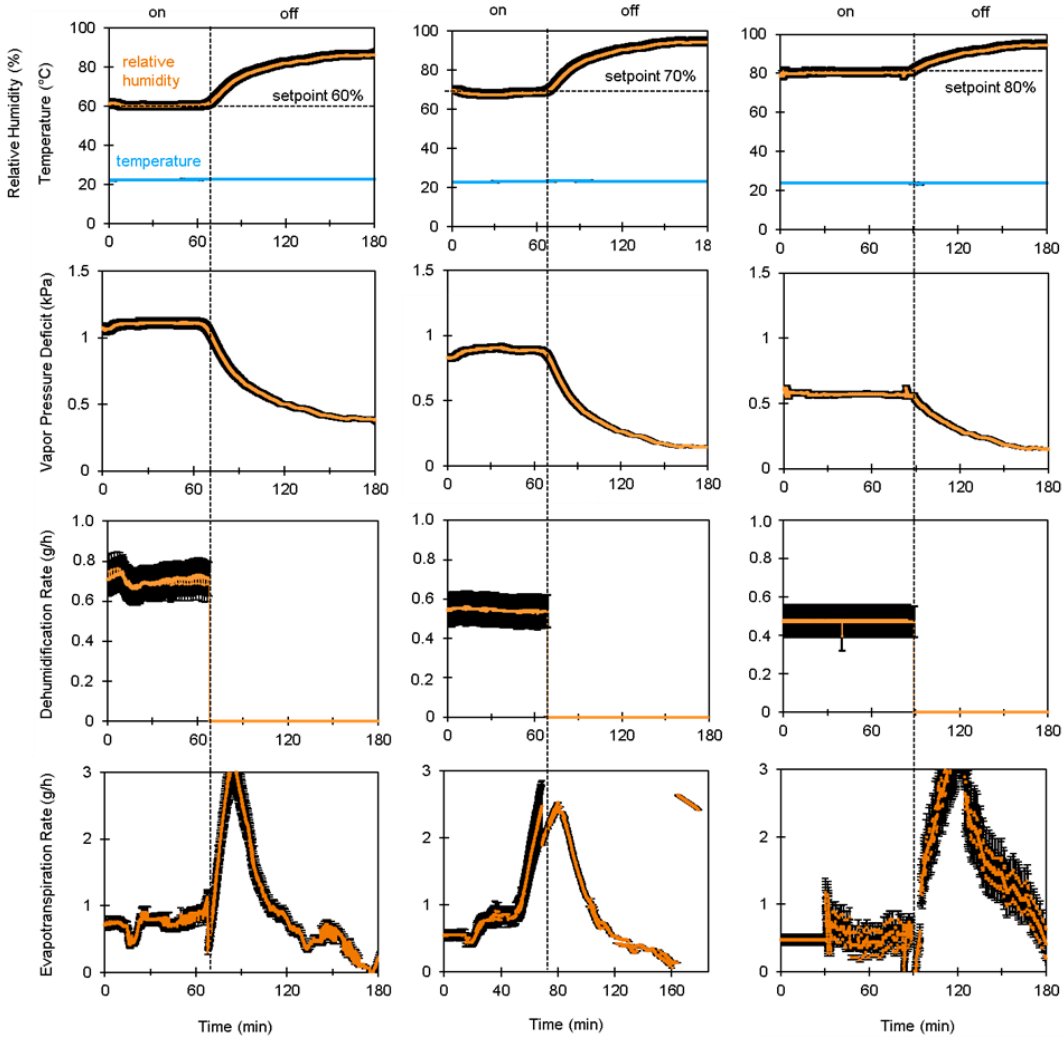

Figure 5.8 Humidity, temperature, and vapor pressure deficit of the plant chamber with fully mature arugula. Humidity was initially controlled by the proposed liquid desiccant system and the dehumidification rate is observed. At ~ 60 minutes, the dehumidification system was turned off and the response of the plant chamber was observed, including the evapotranspiration rate. Complete test conditions were provided in Table 5.4. Supporting data was provided in Supplementary Note 5.3.

During operation, the dehumidification rate ranged from 0.46 to 0.70 ± 0.08 g/h, with the higher values required for the drier environment. For reference, the evapotranspiration rate was also shown. During the period when the dehumidification system was on and humidity was held constant, we would expect the evapotranspiration rate to be nearly equal to the dehumidification rate. This was mostly true, except that the

plot for evapotranspiration was noisy, as it was very sensitive to small but sudden changes in the humidity sensor output. But when the dehumidification system was switched off, evapotranspiration initially spiked and then began to settle towards zero as humidity began rising, the vapor pressure deficit began dropping, and as the environment approached saturation.

For reference, the dehumidification rate can also be normalized per unit of membrane surface area, which gave a range of 0.23 to 0.45 ± 0.04 g/m^2/h. These values of membrane performance were somewhat low. For example, in our previous work related to fertilizer-based liquid desiccants, we achieved vapor flux as high as 2.1 ± 0.2 g/m^2/h during laboratory testing [44]. The reason for this low flux was that in this study, vapor flux was increased only so much as was needed to achieve the desired humidity target (this is done by controlling the liquid desiccant temperature). It was likely that flux could be further increased if desired.

A final note, the dehumidification system did not currently have automated control, for this reason, achieving the desired set point was a matter of monitoring the humidity levels in real-time and then manually adjusting liquid desiccant temperatures in response. Proper controls can obviously be integrated in future work.

5.3.3 Maintaining Stable Humidity Throughout the Complete Growth Cycle

In the next round of testing, performance was evaluated over an extended period including the complete growth cycle from germination to maturity, which is approximately 36 days for hydroponic arugula. For this testing, two arugula plants were grown under conditions previously described. Calcium nitrate fertilizer was again used as liquid desiccant, but this time was prepared at lower concentrations of 25 g/l, which

was closer to the fertilizer concentrations that were expected when solution was fully integrated with closed-loop plant fertigation.

Figure 5.9 showed that the fertilizer desiccant system was able to successfully maintain constant humidity at the set point of 60 % rh throughout the duration of the plant's development in the chamber. Snapshots of the plants throughout the complete growth cycle were provided for reference. As shown, at the earliest stages, humidity remained relatively low and it was unnecessary to turn on the dehumidification system. Only on day 15 when plants had 5 fully formed leaves, the humidity rose above the setpoint, signaling the need for active humidity control. From this date onward, the dehumidification system was operated, initially removing 2.5 ± 0.1 g/day from day 14 to 21, and then at a much higher rate as plants further developed and evapotranspiration increased. By day 35, the dehumidification rate had reached 12.4 ± 0.6 g/day. Across this range of conditions, relative humidity remained approximately stable at the 60 % setpoint.

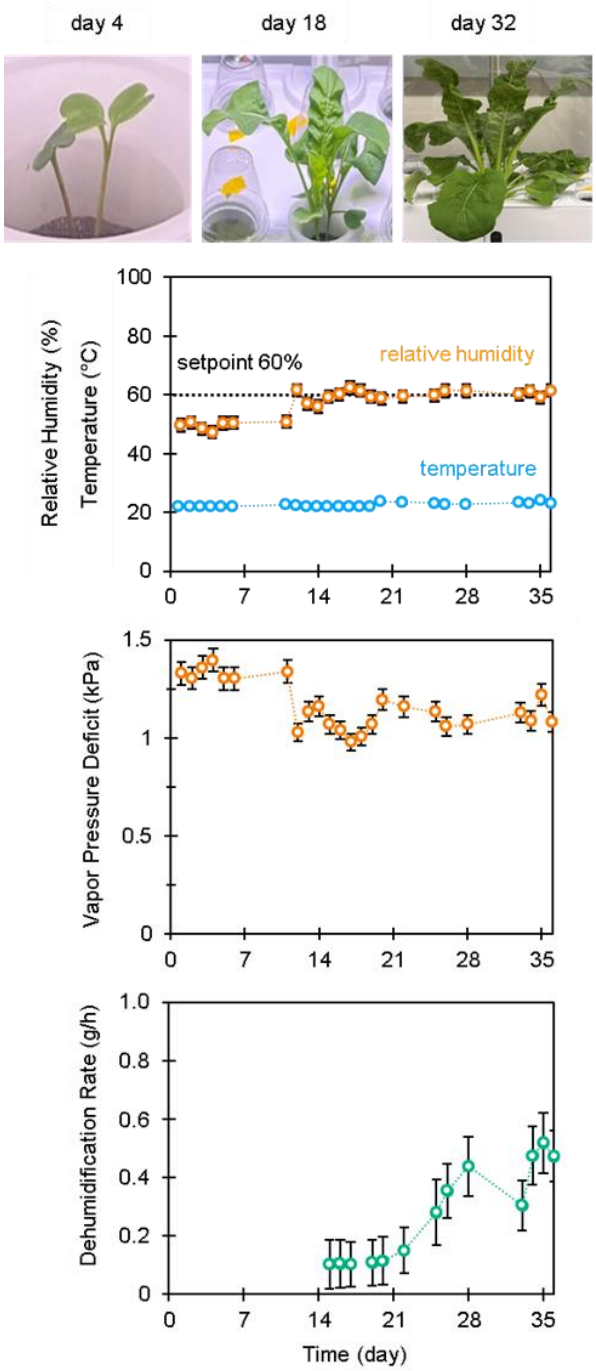

Figure 5.9 Humidity, temperature, and vapor pressure deficit of the plant chamber throughout the life cycle of arugula, from germination to maturity. On day 15 humidity exceeds the 60 % rh setpoint, and the dehumidification system was activated. Dehumidification rates increased steadily to keep up with the increasing evapotranspiration rates from more mature plants. For complete test conditions see Table 5.4. Supporting data was provided in Supplementary Note 5.4. The growth progression photos of arugula were provided in Supplementary Note 5.5.

5.4 Conclusions

This study was the first demonstration that fertilizer-based solution can be used to effectively control the humidity of a real and dynamic controlled plant environment. The plant environment consisted of a small 0.32 m^3 laboratory plant chamber, equipped with a commercial hydroponic grow system that was used to cultivate arugula. A custom liquid desiccant dehumidification apparatus with membrane contactors was built and together with calcium nitrate solution as the fertilizer. With this setup, the possibility of using fertilizer to control humidity was studied.

In the first series of tests, it was shown that in the absence of any dehumidification, humidity of the plant environment exceeded 90 % relative humidity, and condensation on many of the surfaces of the chamber was noticeable. This was done with the hydroponic system filled to capacity with mature arugula plants, and under these conditions evapotranspiration loads reached up to 1.4 ± 0.08 g/h. In a second series of tests, the fertilizer-based dehumidification system was able to successfully control humidity of the plant environment at desired setpoints of 60, 70, and 80 % relative humidity. By controlling the temperature of the liquid desiccant, the dehumidification rates were able to keep up with the evapotranspiration loads and thereby keep humidity stable. In this case the dehumidification rate as high as 0.76 ± 0.08 g/h was reached. In the final series of tests, the fertilizer-based dehumidification system was able to successfully maintain 60 % relative humidity throughout all stages of the plant growth cycle, from germination to maturity, (i.e., ~ 36 days). Significantly, the total amount of calcium nitrate required by the arugula was sufficient to manage humidity throughout the entire growth cycle, demonstrating the system's dual functionality without additional fertilizer input.

A number of areas for improvement and future study have also been identified throughout the study. First, control of the liquid desiccant operating conditions, including temperature, pressure, and flow rate should be automated. This was accomplished manually in this study, but this is obviously impractical for commercial systems. Automation should also enable the implementation of more sophisticated control strategies. For example, in our previous work we have shown that energy efficiency is closely tied to operating conditions. Our focus here was simply to track the evapotranspiration load in order to maintain stable humidity, but operating an on/off duty cycle at some preferred desiccant temperature would be more energy efficient. Second, the desiccant system should be better insulated so that unintended heat gain from the environment is avoided, improving efficiency. Third, improvements to the prototype design should be considered to enable scale up, simplify maintenance, and reduce costs. Integrating the fertilizer liquid desiccant with the plant fertigation system is also needed in future work.

In summary, this represented the first time that fertilizer-based solutions had been demonstrated to effectively control the humidity of a real and dynamic controlled plant environment. These results confirmed the viability of fertilizer-based desiccant systems as a practical solution for integrated humidity control in indoor farming. With further development this approach holds strong potential as a sustainable and scalable alternative for managing humidity in controlled plant environments. Also one recommendation is that by controlling the rate of evapotranspiration, the fertilizer dehumidification capacity could be matched to handle full humidity load, and this could be new aspect of future research as well.

5.5 Supplementary Information

5.5.1 Supplementary Note 5.1: CAD Model of the Fertilizer-Based Dehumidification System

Figure S1 shows a stylistic rendering of the plant chamber and liquid desiccant dehumidification system drawn in Autodesk Fusion 360 (Inventor 2024, Autodesk, San Francisco, CA).

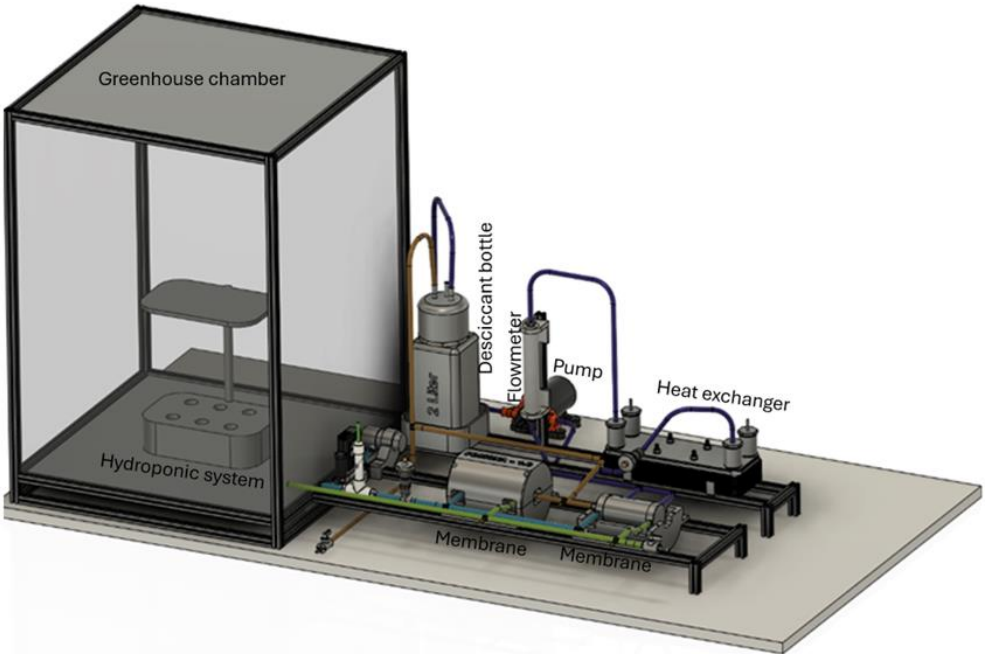

Figure S5.1. Schematic representation of the laboratory plant chamber and liquid desiccant system used to demonstrate fertilizer-based dehumidification.

5.5.2 Supplementary Note 5.2: Mass Balance of the Dehumidification Process

The rate of dehumidification $\dot{m}_{\mathrm{dehumidification}}$ can be evaluated by considering the mass balance of moist air as it enters and leaves the dehumidification unit.

$$\dot{m}_{\mathrm{dehumidification}} = \dot{m}_{\mathrm{H2O,in}} - \dot{m}_{\mathrm{H2O,out}} \quad \text{S5.1}$$

Then we can then relate the mass flow rate of water to the mass flow rate of dry air $\dot{m}_{\mathrm{air}}$ via the humidity mass ratio ω. For a perfectly selective membrane, such as we assume here, the mass of air $\dot{m}_{\mathrm{air}}$at the inlet and outlet are equal.

$$\dot{m}_{dehumidification} = \dot{m}_{air}(\omega_{in} - \omega_{out}) \quad \text{S5.2}$$

Using the molar mass of air and water, the humidity ratio can be expressed as a molar ratio x, which can be related to the ratio of vapor pressure p_{H2O} to total feed pressure p, as per Dalton's law. Finally, the vapor pressure can be related to the relative humidity rh via the saturation pressure p_{sat}.

$$\dot{m}_{dehumidification} = \dot{m}_{air}(x_{in} - x_{out})\frac{M_{H2O}}{M_{air}} \quad \text{S5.3}$$

$$\dot{m}_{dehumidification} = \dot{m}_{air}\left(\frac{p_{H2O,in}}{p_{air,in}} - \frac{p_{H2O,out}}{p_{air,out}}\right)\frac{M_{H2O}}{M_{air}} \quad \text{S5.4}$$

$$\dot{m}_{dehumidification} = \dot{m}_{air}\left(\frac{RH_{in}\, p_{sat,in}}{p - RH_{in}\, p_{sat,in}} - \frac{RH_{out}\, p_{sat,out}}{p - RH_{out}\, p_{sat,out}}\right)\frac{M_{H2O}}{M_{air}} \quad \text{S5.5}$$

In cases where the total mass flow rate $\dot{m}$ is measured rather than the mass of dry air $\dot{m}_{air}$, the expression can be rewritten using the ratio $\frac{\dot{m}_{air}}{\dot{m}} = (1 + \omega)^{-1}$.

$$\dot{m}_{dehumidification} = \frac{\dot{m}_{in}}{1 + \omega_{in}}\left(\frac{RH_{in}\, p_{sat,in}}{p - RH_{in}\, p_{sat,in}} - \frac{RH_{out}\, p_{sat,out}}{p - RH_{out}\, p_{sat,out}}\right)\frac{M_{H2O}}{M_{air}} \quad \text{S5.6}$$

Or rather, for simplicity, it can also be assumed that the mass flow rate of dry air $\dot{m}_{air}$ is approximately equal to the total mass flow rate $\dot{m}$. In this case we obtain the following expression which can be solved using experimental data from our experimental test bench.

$$\dot{m}_{dehumidification} = \dot{m}_{F}\left(\frac{rh_{in}\, p_{sat,in}}{p - RH_{in}\, p_{sat,in}} - \frac{rh_{out}\, p_{sat,out}}{p - RH_{out}\, p_{sat,out}}\right)\frac{M_{H2O}}{M_{air}} \quad \text{S5.7}$$

5.5.3 Supplementary Note 5.3: Supporting Data for Figure 5.8 Showing Dehumidification with Fertilizer-Based Liquid Desiccant Over Short Period

In the second round of testing, the dehumidification system was switched on to verify the capacity of the fertilizer-based liquid desiccant to manage humidity at a range of

setpoints, including 60, 70, and 80 % relative humidity. Figure 5.8 in the Results section shows the most pertinent results but Figure S5.2 is included below to provide additional supporting data. As shown, data from a total of 7 sensors is recorded and used in the analysis. Table S5.1 details how raw data is analyzed to obtain results for vapor pressure deficit, dehumidification rate, and evapotranspiration rate. Table S5.1 also provides a detailed description of how experimental uncertainty from sensors propagates throughout the analysis.

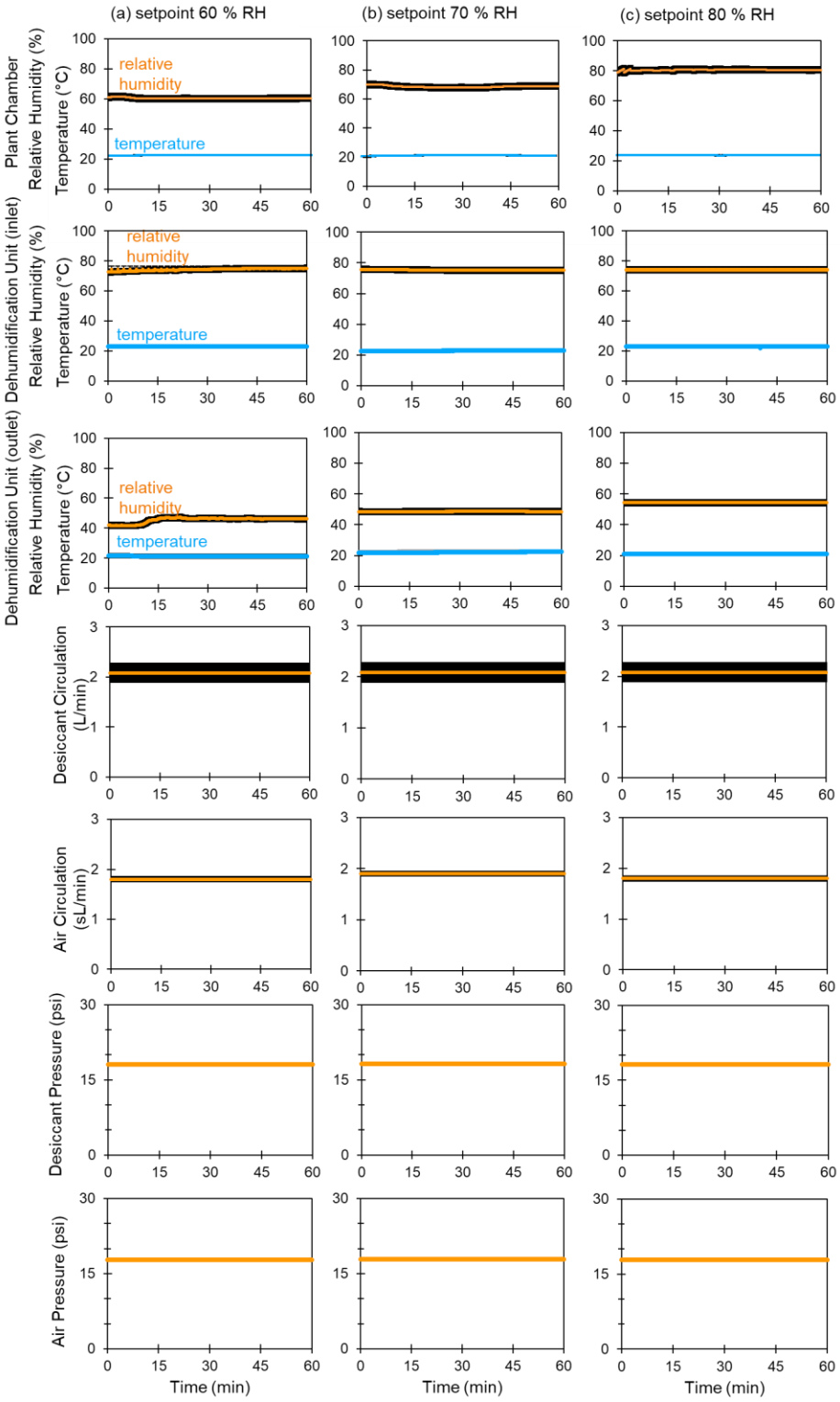

Figure S5.2 Raw test data from round 2 of testing where relative humidity is controlled at several setpoints including (a) 60 %, (b) 70 %, and (c) 80 %. Data is collected from temperature and humidity sensors (AM2315 i2C, Aosong, Guangzhou, China), mass flow controllers, and pressure transducers.

Table S5.1 Analysis of raw data (sampled at t = 180 s from humidity control) and propagation of uncertainty.

Parameter	Value	Measurement or Analysis
Liquid desiccant preparation		
Desiccant water mass $m_{D,w}$	1962.8 ± 0.1 g	Balance (AX8201, Ohaus, Parsippany, NJ), full scale ± uncertainty = 8000 ± 0.1 g
Desiccant salt mass $m_{D,s}$	36.33 ± 0.1 g	Balance (AX8201, Ohaus, Parsippany, NJ), full scale ± uncertainty = 8000 ± 0.1 g
Desiccant concentration c_D	0.02 ± 0.3 %	$c_D = \frac{m_{D,s}}{m_{D,w}}$, $\frac{\delta c_D}{c_D} = \sqrt{\left(\frac{\delta m_{D,s}}{m_{D,s}}\right)^2 + \left(\frac{\delta m_{D,w}}{m_{D,w}}\right)^2}$
Sensor data at continuous operation after stable greenhouse conditions		
Air feed flow rate $\dot{V}_F$	1.8 ± 0.05 sL/min	Mass flow controller (GH-32907-69, Masterflex, Radnor, PA), full scale ± uncertainty = 5 SLPM ± (0.8 % reading + 0.2 % full scale)
Air feed humidity at inlet rh_{in} @ $T_{rh,in}$	74.1 ± 2 %rh @ 23 ± 0.1 °C	Capacitive humidity sensor (AM2315, Aosong, China), full scale ± uncertainty = 100 ± 2 %rh
Air feed humidity at outlet rh_{out}@ $T_{rh,out}$	54.4 ± 2 %rh @ 20.9 ± 0.1 °C	Capacitive humidity sensor (AM2315, Aosong, China), full scale ± uncertainty = 100 ± 2 %rh
Humidity at greenhouse rh_g@ $T_{rh,g}$	78.9 ± 2 %rh @ 23.7 ± 0.1 °C	Capacitive humidity sensor (AM2315, Aosong, China), full scale ± uncertainty = 100 ± 2 %rh
Pressure at membrane inlet P_F (air side)	17.8 psi ± 0.25 %	Pressure transducer (GC557F0142CD, Ashcroft, Stratford, CT), full scale ± uncertainty = 75 psi ± 0.38 psi
Liquid desiccant flow rate $\dot{V}_D$	2.08 ± 0.19 sL/min	Flowmeter (8051K107, McMaster-Carr, Elmhurst, IL), full scale ± uncertainty = 6 ± 0.2 SLPM
Liquid desiccant pressure P_D	18.2 psi ± 0.25 %	Pressure transducer (GC557F0142CD, Ashcroft, Stratford, CT), full scale ± uncertainty = 75 psi ± 0.38 psi
Mass balance analysis		
Air feed mass flow rate $\dot{m}_F$	132.24 g/h ± 2.38 %	$\dot{m}_F = \rho \dot{V}_F$, where ρ =1.22 g/l, $\frac{\delta \dot{m}_F}{\dot{m}_F} = \sqrt{\left(\frac{\delta \dot{V}_F}{\dot{V}_F}\right)^2}$
Water vapor content at the inlet $x_{H2O,in}$	0.016 mol/mol ± 2.78 %	$x_{H2O,in} = rh_{in} \frac{p_{sat,in}}{p_{F-rh_{in}p_{sat,in}}}$, where $p_{sat,in} = 10^{A-\left(\frac{B}{C+T_{rh,in}}\right)}$, $\frac{\delta x_{H2O,in}}{x_{H2O,in}} = \sqrt{\left(\frac{\delta rh_{in}}{rh_{in}}\right)^2 + \left(\frac{\delta p_F}{p_F}\right)^2 + \left(B \ln(10) \frac{\delta T_{rh,in}}{(C+T_{F,in})^2}\right)^2}$
Water vapor content at the outlet $x_{H2O,out}$	0.010 mol_{H2O}/mol ± 3.74 %	$x_{H2O,out} = rh_{out} \frac{p_{sat,out}}{p_{F-rh_{out}p_{sat,out}}}$, where $p_{sat,out} = 10^{A-\left(\frac{B}{C+T_{rh,out}}\right)}$, where A, B and constants given from the Antoine equations.

Table S5.1—continued.

Parameter	Value	Measurement or Analysis
Water vapor mass flow rate at the inlet $\dot{m}_{F,H2O,in}$	1.33 g/h ± 4.84 %	$\dot{m}_{F,H2O,in} = \dot{m}_F \left(\frac{x_{H2O,in}}{1-x_{H2O,in}}\right)\frac{M_{H2O}}{M_{air}}$, $\frac{\delta\dot{m}_{F,H2O,in}}{\dot{m}_{F,H2O,in}} = \sqrt{\left(\frac{\delta\dot{m}_F}{\dot{m}_F}\right)^2 + \left(\frac{\delta x_{H2O,in}}{x_{H2O,in}(1-x_{H2O,in})}\right)^2}$
Water vapor mass flow rate at the outlet $\dot{m}_{F,H2O,out}$	0.85 g/h ± 5.45 %	$\dot{m}_{F,H2O,out} = \dot{m}_F \left(\frac{x_{H2O,out}}{1-x_{H2O,out}}\right)\frac{M_{H2O}}{M_{air}}$, $\frac{\delta\dot{m}_{F,H2O,out}}{\dot{m}_{F,H2O,out}} = \sqrt{\left(\frac{\delta\dot{m}_F}{\dot{m}_F}\right)^2 + \left(\frac{\delta x_{H2O,out}}{x_{H2O,out}(1-x_{H2O,out})}\right)^2}$
Water vapor flux J	0.23 g/m²/h ± 16.6 %	$J = \frac{\dot{m}_{F,H2O,in}-\dot{m}_{F,H2O,out}}{A}$, where A = 2 m², $\frac{\delta J}{J} = \sqrt{\left(\frac{\delta\dot{m}_{F,H2O,in}}{\dot{m}_{F,H2O,in}}\right)^2 + \left(\frac{\delta\dot{m}_{F,H2O,out}}{\dot{m}_{F,H2O,out}}\right)^2}$

5.5.4 Supplementary Note 5.4: Supporting Data for Figure 5.9 Showing Dehumidification with Fertilizer-Based Liquid Desiccants Over Extended Periods

In the final round of testing, performance of the dehumidification system was evaluated over an extended period including the complete growth cycle from germination to maturity, which is approximately 36 days for hydroponic arugula. Figure 5.9 in the Results section shows the most pertinent results but Figure S5.3 provides additional supporting data. Figure S5.3 (a) shows the raw data obtained from testing on sample day 35. Figure S5.3 (b) shows the average sensor data for all dates on which the dehumidification system was operated. Figure S5.3 (c) includes a selection of photos taken throughout the plant development.

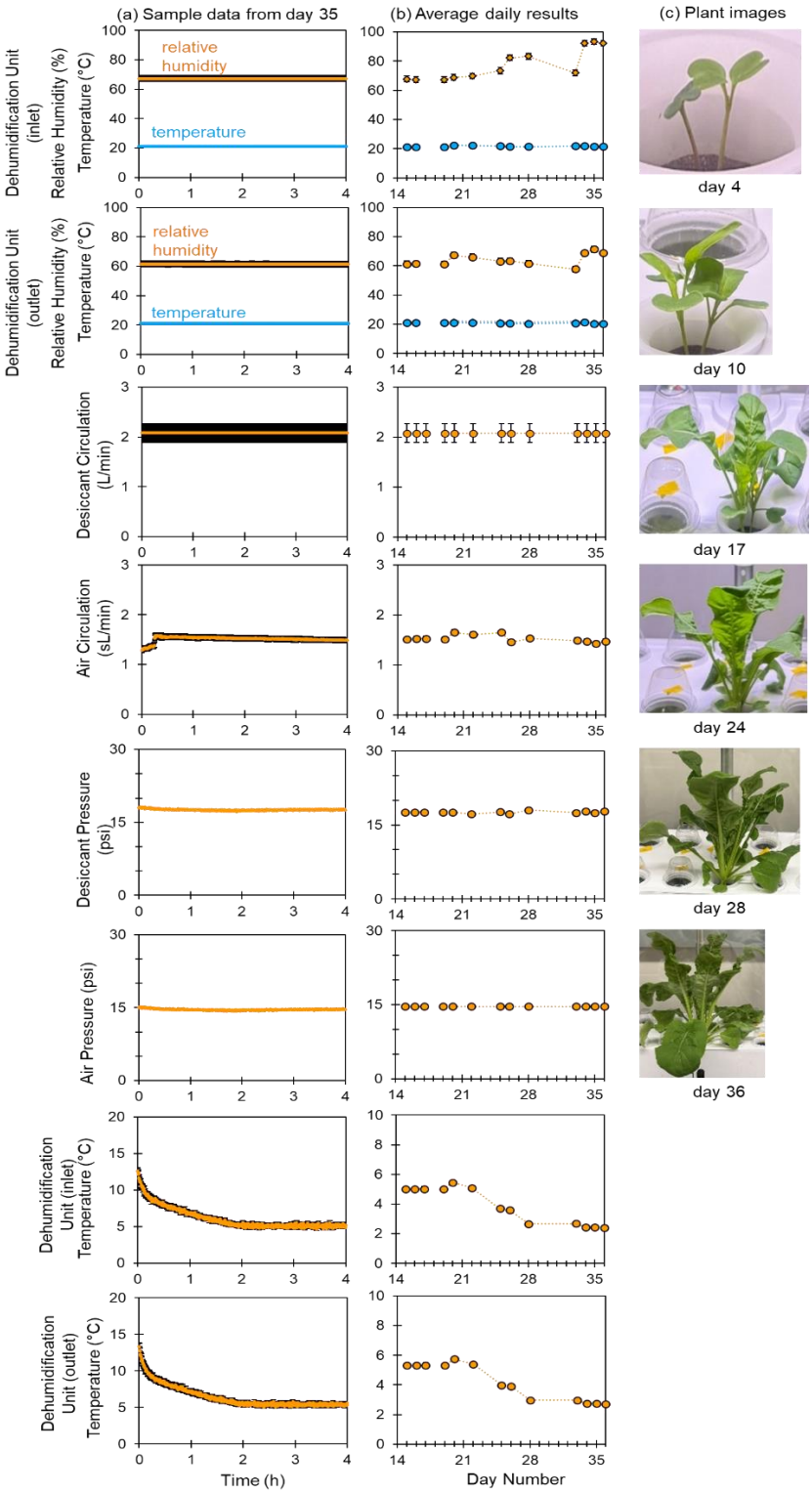

Figure S5.3 Raw test data from round 3 of testing where relative humidity is controlled at 60 % at different times throughout the complete plant growth cycle. (a) Real-time data from sample day 35. (b) Average results obtained on a given date. (c) Sample images collected throughout the plant growth period.

CHAPTER SIX

CONCLUSIONS

6.1 Contributions

This dissertation explores the feasibility of a new fertilizer-based desiccant for humidity regulation in the controlled plant environments. Since there is a growing need for more energy-efficient ways to manage humidity, fertilizer-based desiccants are a promising and scalable alternative by simultaneously enabling humidity control and fertigation.

6.1.1 Energy Savings of Fertilizer-Based Liquid Desiccants: A Thermodynamic Study

Chapter Two makes a noteworthy contribution by establishing the thermodynamic limits and maximum energy savings achievable by using fertilizer-based liquid desiccants for humidity control in indoor farming which were unknown until now. In contrast to traditional liquid desiccants that require thermal regeneration, often consuming energy well above the thermodynamic minimum, fertilizer-based liquid desiccants avoid the regeneration step due to simultaneous integration of dehumidification and fertigation process. By thermodynamic analysis and crop-specific study, this chapter shows that when dehumidification capacity of fertilizer input needed for plants is aligned with the dehumidification load, energy savings are maximum. The results show that crops like basil and lettuce can achieve high energy savings, making this method not only feasible but also highly effective for certain crop types. Also, the generalized analysis shown in the chapter offers a practical design tool, helping crop growers to identify energy savings

and optimize systems taking into account dehumidification load, final fertilizer concentration, and fertilizer requirements.

6.1.2 Specific Energy Analysis of Dehumidification Based on Transport Modeling

Chapter Three advances the understanding of fertilizer-based liquid desiccant systems by calculating the specific energy of dehumidification using a transport model. While the earlier chapter assumed no heat gain to establish the thermodynamic limits and ideal energy savings, this chapter provides more realistic evaluation by simulating heat flux for heat gain with respect to vapor flux. The results show that using a membrane assisted fertilizer-based liquid desiccant dehumidification system can achieve specific work values as low as 0.24 Wh/g. This value compares favorably with both industry standards. This study also pinpoints the importance of desiccant temperature control to maintain optimal performance as fertilizer concentration changes because heat gain is proportional to the desiccant temperature. So, this temperature directly influences the specific energy and work. Another important analysis in this chapter is the influence of variables such as membrane type, air and desiccant circulation rates on energy required for dehumidification. All these variables are useful for optimizing the design and operation of membrane-based fertilizer desiccant systems so that the system runs efficiently.

6.1.3 Energy Efficiency of Fertilizer-Based Liquid Desiccant System: An Experimental Analysis

Chapter Four experimentally evaluates the energy efficiency of fertilizer-based liquid desiccant through comprehensive tests conducted by varying desiccant temperatures, concentrations, and fertilizer types. Prior studies established the applicability of concentrated fertilizer solutions for dehumidification and indicated its prospects for

greenhouse dehumidification, but no detailed experimental evidence had been conducted until now. By developing a controlled boundary condition in lab-scale bench, this chapter quantifies the specific work required for dehumidification and using a concentrated fertilizer solution, this value could be as low as 0.29 kWh/kg. This specific work value is not very far off from what was obtained from the transport modeling and also compares favorably with current state-of-the art technologies and regulatory benchmark standards. The systematic study with multi-ion fertilizer blends, desiccant temperature and concentration shows that there is a tradeoff between vapor flux and energy flux. The energy flux is directly influenced by desiccant temperature. Thus, again highlighting the need for dynamic control of desiccant temperature for low specific energy. This chapter bridges the gap between thermodynamic analysis and transport modeling and paves a path for further research in real-time plant environment as shown in Chapter Five.

6.1.4 Prototype Demonstration of a Fertilizer-Based Desiccant Dehumidification for Controlled plant Environments

Chapter Five is the outcome of all the contributions laid out in previous chapters. It demonstrates and shows for the first time the practical application of fertilizer-based liquid desiccants for humidity control in real, and active plant chamber. This work validates the concept under real-time conditions using a plant chamber equipped with hydroponic system, where arugula was cultivated. By integrating the dehumidification system with a plant chamber, the humidity was maintained at different setpoints (60-80 %) in the presence of real-time crop evapotranspiration. The study also showed that amount of fertilizer required for crop fertigation was sufficient to meet dehumidification demand across the full plant life cycle. The major contribution of this chapter is that it

brides the gap between theoretical, controlled experimental study and real-time operation. This study lays the foundation for future studies like scalability and technoeconomic study to assess the feasibility and profitability of fertilizer-based liquid desiccant dehumidification in controlled plant environments.

6.2 Future Work

6.2.1 Impact of Buffer Solution Addition on Dehumidification Capacity of Fertilizer Desiccants

In this dissertation, I have presented thermodynamic analysis, transport modeling for specific energy analysis, experimental analysis and prototype demonstration of a fertilizer-based desiccant dehumidification system. There are some analyses not taken into account in these studies. In the experimental study, for multi-solute fertilizer at high concentrations, there were issues with precipitation that affect the equipment used in the dehumidification system. However, precipitations can be avoided by adding a buffer solution. The impact on dehumidification capacity of fertilizer solution after buffer addition is unknown. Therefore, the future work could be the experimental investigation of dehumidification capacity of multi-solute fertilizer solutions after buffer addition.

6.2.2 Automated Temperature Controls to Optimize Specific Energy for Dehumidification

I have shown that desiccant temperatures highly influence the specific energy consumption of the fertilizer-based liquid desiccant dehumidification system because of trade-off between heat flux and water vapor flux. In the prototype system, energy analysis is absent. So, another future work could be adding automated temperature controls to optimize the specific energy consumption of the real-time system. It is simply automating the system such that system operates with minimum energy consumption. For

this adaptive feedback control system has to be developed and then needs to be added to the prototype system.

6.2.3 Technoeconomic Analysis

Technoeconomic assessment of the fertilizer-based liquid desiccant dehumidification system could also be done in future to measure the possibility and cost-effectiveness before it is scaled up and commercially adopted as a sustainable solution for dehumidification inside the controlled plant environments. This analysis will also help optimize the system design for lower capital cost and energy costs. We can also incorporate lifecycle cost analysis of fertilizer desiccant systems and compare it with traditional systems to show its potential edge over them.

6.3 Outlook

This dissertation is important for indoor farming, dehumidification and liquid desiccant technology. For indoor farming, it suggests a practical solution that minimizes energy use while supporting crops by integrating moisture removal process and fertigation in one single process. This helps sustainability in controlled plant environments. For dehumidification, the work in this dissertation introduces a low-energy method that bypasses thermal regeneration, which is needed for traditional liquid desiccants. For liquid desiccant technology, this research expands the field by showing that fertilizers can indeed grab moisture from humid air environment. The proof for this is shown from thermodynamic analysis, transport modeling, experimental study, and real-time application with real plants growing in plant chamber. Overall, this study lays the basis for energy efficient, sustainable and dual-application (dehumidification and fertigation) systems that can be scaled up for commercial indoor farming industry.

REFERENCES

[1] F&D, Finance & Development, vol. 61, no. 4, pp. 2-78, Dec. 2024. [Online]. Available: https://www.imf.org/en/Publications/fandd/issues/2020/03/infographic-global-population-trends-picture

[2] M. van Dijk, T. Morley, M. L. Rau, and Y. Saghai, “A meta-analysis of projected global food demand and population at risk of hunger for the period 2010–2050,” *Nature Food*, vol. 2, pp. 494–501, Jul. 2021, doi: 10.1038/s43016-021-00322-9.

[3] S. Feng, X. Gu, S. Luo, R. Liu, A. Gulakhmadov, L. J. Slater, J. Li, X. Zhang, and D. Kong, "Greenhouse gas emissions drive global dryland expansion but not spatial patterns of change in aridification," J. Climate, vol. 35, no. 20, pp. 6501–6517, Oct. 2022, doi: 10.1175/JCLI-D-22-0103.1.

[4] S. Feng and Q. Fu, "Expansion of global drylands under a warming climate," Atmos. Chem. Phys., vol. 13, pp. 10081–10094, Oct. 2013, doi: 10.5194/acp-13-10081-2013.

[5] K. F. Davis, S. Downs, and J. A. Gephart, "Towards food supply chain resilience to environmental shocks," Nature Food, vol. 2, pp. 54–65, 2021, doi: 10.1038/s43016-020-00196-3.

[6] R. D. Tchonkouang, H. Onyeaka, and H. Nkouatchou, "Assessing the vulnerability of food supply chains to climate change-induced disruptions," Sci. Total Environ., vol. 920, Art. no. 171047, Apr. 2024, doi: 10.1016/j.scitotenv.2024.171047.

[7] A. Dsouza, L. Newman, T. Graham, and E. D. G. Fraser, "Exploring the landscape of controlled environment agriculture research: A systematic scoping review of trends and topics," Agric. Syst., vol. 209, Art. no. 103673, Jun. 2023, doi: 10.1016/j.agsy.2023.103673.

[8] A. L. Garcia, M. A. C. Griffith, G. P. Buss, X. Yang, J. L. Griffis, S. Bauer, and A. K. Singh, "Controlled environment agriculture and its ability to mitigate food insecurity," Agric. Sci., vol. 14, no. 2, Feb. 2023, doi: 10.4236/as.2023.142019.

[9] C. Vatistas, D. D. Avgoustaki, and T. Bartzanas, "A systematic literature review on controlled-environment agriculture: How vertical farms and greenhouses can influence the sustainability and footprint of urban microclimate with local food production," Atmosphere, vol. 13, no. 8, Art. no. 1258, Aug. 2022, doi: 10.3390/atmos13081258.

[10] J. R. Schramski, C. B. Woodson, and J. H. Brown, "Energy use and the sustainability of intensifying food production," Nature Sustainability, vol. 3, pp. 257–259, Apr. 2020, doi: 10.1038/s41893-020-0496-6.

[11] C. Stanghellini, "Horticultural production in greenhouses: Efficient use of water," Acta Hortic., vol. 1034, pp. 25-42, 2014, doi: 10.17660/ActaHortic.2014.1034.1.

[12] P. Padmanabhan, A. Cheema, and G. Paliyath, "Solanaceous fruits including tomato, eggplant, and peppers," in Encyclopedia of Food and Health, 1st ed., vol. 5, Academic Press, 2016, pp. 24–32, doi: 10.1016/B978-0-12-384947-2.00696-6.

[13] M. Blois, "Growing more food with less chemicals," C&EN, vol. 101, no. 15, pp. 28–33, May 8, 2023.

[14] M. D'Ostuni, L. Zaffi, E. Appolloni, and F. Orsini, "Understanding the complexities of Building-Integrated Agriculture: Can food shape the future built environment?" Futures, vol. 144, Art. no. 103061, Dec. 2022, doi: 10.1016/j.futures.2022.103061.

[15] S. Thomaier et al., "Farming in and on urban buildings: Present practice and specific novelties of Zero-Acreage Farming (ZFarming)," Renew. Agric. Food Syst., vol. 30, Special Issue 1, pp. 43–54, Apr. 2014, doi: 10.1017/S1742170514000143.

[16]"Deep Space Food Challenge," Deep Space Food Challenge. https://www.deepspacefoodchallenge.org/ (accessed Jul. 10, 2024).

[17] A. C. Wartenberg et al., "Cannabis and the environment: What science tells us and what we still need to know," Environ. Sci. Technol. Lett., vol. 8, no. 2, pp. 52-68, Jan. 2021, doi: 10.1021/acs.estlett.0c00845.

[18] M. Shahbandeh, "Global market value of indoor farming 2022-2032," Statista, Apr. 17, 2023. [Online]. Available: https://www.statista.com/topics/4467/indoor-farming/#topicOverview.

[19] "U.S. Indoor Farming Market Size, Share & Trends Analysis Report By Facility Type (Greenhouses, Vertical Farms), By Component (Hardware, Software), By Growing Mechanism, By Crop Category, And Segment Forecasts, 2024 - 2030," Grand View Research, 2024.

[20] C. Gómez et al., "Controlled environment food production for urban agriculture," HortScience, vol. 54, no. 9, pp. 1448–1458, Sep. 2019, doi: 10.21273/HORTSCI14073-19.

[21] O. Jolliet, "Modelling of water uptake, transpiration and humidity in greenhouses, and of their effects on crops," Acta Hortic., vol. 328, pp. 69–78, 1993, doi: 10.17660/ActaHortic.1993.328.4.

[22] S. Y. Chia and M. W. Lim, "A critical review on the influence of humidity for plant growth forecasting," IOP Conf. Ser.: Mater. Sci. Eng., vol. 1257, Art. no. 012001, 2022, doi: 10.1088/1757-899X/1257/1/012001.

[23] L. Yao et al., "High air humidity dampens salicylic acid pathway and NPR1 function to promote plant disease," EMBO J., vol. 42, no. 21, Art. no. e113499, Nov. 2023, doi: 10.15252/embj.2023113499.

[24] M. Soussi, M. T. Chaibi, M. Buchholz, and Z. Saghrouni, "Comprehensive review on climate control and cooling systems in greenhouses under hot and arid conditions," Agronomy, vol. 12, no. 3, Art. no. 626, Mar. 2022, doi: 10.3390/agronomy12030626.

[25] M. Amani, S. Foroushani, M. Sultan, and M. Bahrami, "Comprehensive review on dehumidification strategies for agricultural greenhouse applications," Appl. Therm. Eng., vol. 181, Art. no. 115979, Nov. 2020, doi: 10.1016/j.applthermaleng.2020.115979.

[26] M. Xie, E. Chen, G. Huang, T. Jia, and Y. Dai, "Recent advancements in deep dehumidification technology: A review," Renewable and Sustainable Energy Reviews, vol. 211, Art. no. 115321, Apr. 2025, doi: 10.1016/j.rser.2024.115321.

[27] A. Costantino, L. Comba, G. Sicardi, M. Bariani, and E. Fabrizio, “Energy performance and climate control in mechanically ventilated greenhouses: A dynamic modelling-based assessment and investigation,” Appl. Energy, vol. 288, Art. no. 116583, Apr. 2021, doi: 10.1016/j.apenergy.2021.116583.

[28] B. Khoshnevisan, H. M. Shariati, S. Rafiee, and H. Mousazadeh, “Comparison of energy consumption and GHG emissions of open field and greenhouse strawberry production,” Renew. Sustain. Energy Rev., vol. 29, pp. 316–324, Jan. 2014, doi: 10.1016/j.rser.2013.08.098.

[29] D.S. de Villiers, H.C. Wien, J.E. Reid, and L.D. Albright, “Energy use and yields in tomato production: Field, high tunnel and greenhouse compared for the northern tier of the USA (Upstate New York),” Acta Hortic., vol. 893, pp. –, 2011, doi: 10.17660/ActaHortic.2011.893.34.

[30] S. Moussaddy, S. Pushparajah, and J. Maisonneuve, “Fertilizer-based liquid desiccants: A novel concept for energy efficient dehumidification and water vapor recycling in indoor plant environments,” Applied Thermal Engineering, vol. 219, no. Part B, p. 119529, Jan. 2023, doi: 10.1016/j.applthermaleng.2022.119529.

[31] T. Venegas, M. Qu, L. Wang, X. Liu, K. Gluesenkamp and Z. Gao, "Review of liquid desiccant air dehumidification systems coupled with heat pump: System configurations, component design, and performance," Energy and Buildings, vol. 279, p. 112655, Jan. 2023. doi: 10.1016/j.enbuild.2022.112655.

[32] Y. Bai et al., "Effect of mechanical ventilation on indoor environment and condensation in high-humidity industrial buildings during winter: field investigation and numerical study," Building and Environment, p. 113133, Jun. 2025. doi: 10.1016/j.buildenv.2025.113133.

[33] I. Attar, N. Naili, N. Khalifa, M. Hazami, M. Lazaar, and A. Farhat, "Experimental study of an air conditioning system to control a greenhouse microclimate," Energy Conversion and Management, vol. 79, pp. 543–553, Mar. 2014. [Online]. Available: https://doi.org/10.1016/j.enconman.2013.12.023

[34] P. Wolkoff, "Indoor air humidity revisited: Impact on acute symptoms, work productivity, and risk of influenza and COVID-19 infection," Int. J. Hyg. Environ. Health, vol. 256, 114313, Mar. 2024. [Online]. Available: https://doi.org/10.1016/j.ijheh.2023.114313.

[35] D. T. Bui, M. K. Ja, J. M. Gordon, K. C. Ng, and K. J. Chua, "A thermodynamic perspective to study energy performance of vacuum-based membrane dehumidification," Energy, vol. 132, pp. 106–115, Aug. 2017, doi: 10.1016/j.energy.2017.05.075.

[36] L. Zou, F. Yu, Y. Li, and J. Yu, “Experimental performance evaluation and refrigerant charge optimization of a dehumidifier with 5mm diameter finned tube evaporator,” Appl. Therm. Eng., vol. 278, no. Part A, p. 127233, Nov. 2025, doi: 10.1016/j.applthermaleng.2025.127233.

[37] Q. Zhang, R. Tu, and M. Liu, “Performance analyses and optimization studies of desiccant wheel assisted atmospheric water harvesting system under global ambient conditions,” Energy, vol. 283, p. 128477, Nov. 2023, doi: 10.1016/j.energy.2023.128477.

[38] Y. J. Dai, R. Z. Wang, H. F. Zhang, and J. D. Yu, "Use of liquid desiccant cooling to improve the performance of vapor compression air conditioning," Applied Thermal Engineering, vol. 21, no. 12, pp. 1185–1202, Aug. 2001. doi: 10.1016/S1359-4311(01)00002-3

[39] Y. J. Dai, R. Z. Wang, H. F. Zhang, and J. D. Yu, "Use of liquid desiccant cooling to improve the performance of vapor compression air conditioning," Applied Thermal Engineering, vol. 21, no. 12, pp. 1185–1202, Aug. 2001. doi: 10.1016/S1359-4311(01)00002-3

[40] X. Chen, S. Riffat, H. Bai, X. Zheng, and D. Reay, "Recent progress in liquid desiccant dehumidification and air-conditioning: A review," Energy and Built Environment, vol. 1, no. 1, pp. 106–130, Jan. 2020. doi: 10.1016/j.enbenv.2019.09.001

[41] S. Liu and J.-W. Jeong, "Energy performance comparison between two liquid desiccant and evaporative cooling-assisted air conditioning systems," Energies, vol. 13, no. 3, p. 522, Jan. 2020. doi: 10.3390/en13030522

[42] J. Woods, "2021 BTO Peer Review – NREL: Supporting development and analysis of a liquid desiccant regeneration technology," U.S. Department of Energy, 2021. [Online]. Available: https://www.energy.gov/sites/default/files/2021-10/bto-peer-2021-supporting-dev-analysis-liquid-desiccant.pdf

[43] A. E. Tourab, A. M. Blanco-Marigorta, A. M. Elharidi, and M. J. Suárez-López, "A novel configuration of hybrid reverse osmosis, humidification–dehumidification, and solar photovoltaic systems: Modeling and exergy analysis," Journal of Marine Science and Engineering, vol. 12, no. 1, p. 19, Dec. 2023. doi: 10.3390/jmse12010019

[44] R. M. Lefers, N. M. S. Bettahalli, N. V. Fedoroff, N. Ghaffour, P. A. Davies, S. P. Nunes, and T. O. Leiknes, "Hollow fibre membrane-based liquid desiccant humidity control for controlled environment agriculture," Biosyst. Eng., vol. 183, pp. 47–57, Jul. 2019, doi: 10.1016/j.biosystemseng.2019.04.010.

[45] N. M. S. Bettahalli, R. Lefers, N. Fedoroff, T. O. Leiknes, and S. P. Nunes, "Triple-bore hollow fiber membrane contactor for liquid desiccant based air dehumidification," J. Membr. Sci., vol. 514, pp. 135–142, Sep. 2016, doi: 10.1016/j.memsci.2016.04.059.

[46] U.S. Environmental Protection Agency, “Dehumidifiers Key Efficiency Criteria,” ENERGY STAR, Oct. 31, 2019. [Online]. Available: https://www.energystar.gov/products/dehumidifiers/key_efficiency_criteria. [Accessed: Jun. 17, 2024].

[47] S. Moussaddy, S. Aryal, and J. Maisonneuve, "Specific energy analysis of using fertilizer-based liquid desiccants to dehumidify indoor plant environments," Applied Thermal Engineering, vol. 238, p. 121849, Feb. 2024. doi: 10.1016/j.applthermaleng.2023.121849.

[48] C. de la Calle-Arroyo, J. López-Fidalgo, and L. J. Rodríguez-Aragón, "Optimal designs for Antoine Equation," Chemometrics and Intelligent Laboratory Systems, vol. 214, p. 104334, Jul. 2021. doi: 10.1016/j.chemolab.2021.104334.

[49] H. C. Duong, A. J. Ansari, L. D. Nghiem, H. T. Cao, T. D. Vu, and T. P. Nguyen, "Membrane processes for the regeneration of liquid desiccant solution for air conditioning," Current Pollution Reports, vol. 5, pp. 308–318, Jul. 2019.

[50] F. A. Al-Sulaiman, P. Gandhidasan, and S. M. Zubair, "Liquid desiccant based two-stage evaporative cooling system using reverse osmosis (RO) process for regeneration," Applied Thermal Engineering, vol. 27, no. 14–15, pp. 2449–2454, Oct. 2007. doi: 10.1016/j.applthermaleng.2007.02.010

[51] H. C. Duong, A. J. Ansari, H. T. Cao, N. C. Nguyen, K.-U. Do, and L. D. Nghiem, "Membrane distillation regeneration of liquid desiccant solution for air-conditioning: Insights into polarisation effects and mass transfer," Environmental Technology & Innovation, vol. 19, p. 100941, Aug. 2020. doi: 10.1016/j.eti.2020.100941

[52] V. K. Gorai, S. K. Singh, and D. B. Jani, "A comprehensive review on solid desiccant-assisted novel dehumidification and its advanced regeneration methods," Journal of Thermal Analysis and Calorimetry, vol. 2024, no. 17, pp. 8979–9000, 2024. doi: 10.1007/s10973-024-13479-9

[53] W.-J. Jeon, M.-G. Ham, J.-G. Lee, H. Ji, and Y.-D. Kim, "Performance evaluation of regeneration of high-concentration liquid desiccant using direct contact membrane distillation," Separation and Purification Technology, vol. 330, Part C, p. 125537, Feb. 2024. doi: 10.1016/j.seppur.2023.125537

[54] A. Giampieri, Z. Ma, J. Ling-Chin, H. Bao, A. J. Smallbone, and A. P. Roskilly, "Liquid desiccant dehumidification and regeneration process: Advancing correlations for moisture and enthalpy effectiveness," Applied Energy, vol. 314, p. 118962, May 2022. doi: 10.1016/j.apenergy.2022.118962

[55] A. A. Pesaran, A Review of Desiccant Dehumidification Technology, Golden, CO: National Renewable Energy Laboratory, 1993. Presented at the EPRI's Electric Dehumidification Conference, New Orleans, LA, USA, Jun. 2–3, 1993. NREL/TP-472-7010.

[56] P. Pourmovahed and J. Maisonneuve, "Thermodynamic limits of using fertilizer osmosis to produce mechanical work via pressure retarded osmosis," Journal of Membrane Science, vol. 629, p. 119268, Jul. 2021. doi: 10.1016/j.memsci.2021.119268

[57] Haifa Group, Haifa Group. https://www.haifa-group.com/, 2024 accessed September 30.

[58] J. V. Morgan and A. Tan, "Greenhouse lettuce production at high densities in hydroponics," Acta Horticulturae, no. 133, pp. 4, 1983. doi: 10.17660/ActaHortic.1983.133.4

[59] H. Farhangi, V. Mozafari, H. R. Roosta, H. Shirani, and M. Farhangi, "Optimizing growth conditions in vertical farming: enhancing lettuce and basil cultivation through the application of the Taguchi method," Scientific Reports, vol. 13, Article no. 6717, Apr. 2023. doi: 10.1038/s41598-023-33730-2

[60] T. Qian, J. A. Dieleman, A. Elings, A. De Gelder, L. F. M. Marcelis, and O. Van Kooten, "Comparison of climate and production in closed, semi-closed and open greenhouses," Acta Horticulturae, no. 893, pp. 201–208, 2011. doi: 10.17660/ActaHortic.2011.893.24

[61] L. D. Albright and M. L. Behle, "An air-liquid-air heat exchanger for greenhouse humidity control," Transactions of the ASAE, vol. 27, no. 5, pp. 1524–1530, 1984. doi: 10.13031/2013.32998

[62] N. Katsoulas, A. Sapounas, F. De Zwart, J. A. Dieleman, and C. Stanghellini, "Reducing ventilation requirements in semi-closed greenhouses increases water use efficiency," Scientific Reports, Apr. 2023. [Online]. Available: https://ideas.repec.org/p/ags/saea23/333123.html

[63] G. A. Longo and A. Gasparella, "Experimental and theoretical analysis of heat and mass transfer in a packed column dehumidifier/regenerator with liquid desiccant," International Journal of Heat and Mass Transfer, vol. 48, no. 25–26, pp. 5240–5254, Dec. 2005. doi: 10.1016/j.ijheatmasstransfer.2005.07.011

[64] A. Lowenstein, "Review of liquid desiccant technology for HVAC applications," HVAC&R Research, vol. 14, no. 6, pp. 729–752, Nov. 2008.

[65] X. Niu, F. Xiao, and Z. Ma, "Investigation on capacity matching in liquid desiccant and heat pump hybrid air-conditioning systems," International Journal of Refrigeration, vol. 34, no. 8, pp. 1989–1998, Dec. 2011. doi: 10.1016/j.ijrefrig.2011.08.004

[66] A. Ali, K. Ishaque, A. Lashin, and N. Al Arifi, "Modeling of a liquid desiccant dehumidification system for close type greenhouse cultivation," Energy, vol. 118, pp. 578–589, Jan. 2017. doi: 10.1016/j.energy.2016.10.069

[67] X. Liu, M. Qu, X. Liu, and L. Wang, "Membrane-based liquid desiccant air dehumidification: A comprehensive review on materials, components, systems and performances," Renew. Sustain. Energy Rev., vol. 110, pp. 444–466, Aug. 2019. doi: 10.1016/j.rser.2019.04.018

[68] J.L. Niu and L.Z. Zhang, "Membrane-based Enthalpy Exchanger: material considerations and clarification of moisture resistance," J. Membr. Sci., vol. 189, no. 2, pp. 179–191, Aug. 2001. doi: 10.1016/S0376-7388(00)00680-3

[69] R. S. Das and S. Jain, "Performance characteristics of cross-flow membrane contactors for liquid desiccant systems," Applied Energy, vol. 141, pp. 1–11, Mar. 2015. doi: 10.1016/j.apenergy.2014.12.014

[70] R. Lefers, N. M. S. Bettahalli, S. P. Nunes, N. Fedoroff, P. A. Davies, and T. O. Leiknes, "Liquid desiccant dehumidification and regeneration process to meet cooling and freshwater needs of desert greenhouses," Desalination and Water Treatment, vol. 57, no. 48–49, pp. 23430–23442, Oct. 2016, doi: 10.1080/19443994.2016.1173383.

[71] N. Zhang, S.-Y. Yin, and M. Li, "Model-based optimization for a heat pump driven and hollow fiber membrane hybrid two-stage liquid desiccant air dehumidification system," Applied Energy, vol. 228, pp. 12–20, Oct. 2018, doi: 10.1016/j.apenergy.2018.06.058.

[72] C. Tang, K. Vafai, C. Gu, K. N. Gloria, and M. D. R. Karim, "Experimental investigation of dehumidification performance of a vapor compression refrigeration system," Int. Commun. Heat Mass Transf., vol. 137, 106282, Oct. 2022, doi: 10.1016/j.icheatmasstransfer.2022.106282.

[73] K.-S. Yang, J.-S. Wang, S.-K. Wu, C.-Y. Tseng, and J.-C. Shyu, "Performance Evaluation of a Desiccant Dehumidifier with a Heat Recovery Unit," Energies, vol. 10, no. 12, p. 2006, 2017, doi: 10.3390/en10122006.

[74] Energy Solutions and Cultivate Energy and Optimization, Codes and Standards Enhancement (CASE) Initiative 2022 California Energy Code, Mar. 2022.

[75] J. Lee and R. Karnik, "Desalination of water by vapor-phase transport through hydrophobic nanopores," Journal of Applied Physics, vol. 108, no. 4, p. 044315, Aug. 2010, doi: 10.1063/1.3419751.

[76] J. Lee, A. P. Straub, and M. Elimelech, "Vapor-gap membranes for highly selective osmotically driven desalination," Journal of Membrane Science, vol. 555, pp. 407–417, Jun. 2018, doi: 10.1016/j.memsci.2018.03.059.

[77] G. He, Y. Mi, P. L. Yue, and G. Chen, "Theoretical study on concentration polarization in gas separation membrane processes," J. Membr. Sci., vol. 153, no. 2, pp. 243–258, Feb. 1999, doi: 10.1016/S0376-7388(98)00257-9.

[78] S. Moussaddy, G. Yuan, and J. Maisonneuve, "A new concept for generating mechanical work from gas permeation," J. Membr. Sci., vol. 614, 118489, Nov. 2020, doi: 10.1016/j.memsci.2020.118489.

[79] S. Moussaddy and J. Maisonneuve, "Energy from carbon dioxide: Experimental and theoretical analysis of power generation from membrane-based sweep gas permeation," J. Membr. Sci., vol. 644, 120053, Feb. 2022, doi: 10.1016/j.memsci.2021.120053.

[80] V. Karanikola, A. F. Corral, H. Jiang, A. E. Sáez, W. P. Ela, and R. G. Arnold, “Sweeping gas membrane distillation: Numerical simulation of mass and heat transfer in a hollow fiber membrane module,” J. Membr. Sci., vol. 479, pp. 205–216, Jul. 2015, doi: 10.1016/j.memsci.2015.02.010.

[81] S. W. L. Alan, M. R. Islam, and K. J. Chua, “A theoretical model on internally cooled liquid desiccant dehumidification and cooling processes,” Energy Procedia, vol. 142, pp. 1009–1014, Dec. 2017, doi: 10.1016/j.egypro.2017.12.347.

[82] W. Roetzel, X. Luo, and D. Chen, Design and Operation of Heat Exchangers and Their Networks, 1st ed., Academic Press, Sep. 24, 2019. ISBN: 9780128178942.

[83] P. Pourmovahed, M. Lefsrud, and J. Maisonneuve, "Thermodynamic limits of using fertilizer to produce clean fertigation solution from wastewater via forward osmosis," J. Membr. Sci., vol. 647, 120168, Apr. 2022, doi: 10.1016/j.memsci.2021.120168.

[84] S. Gumruk, M. K. Aktas, and F. Kasap, “Experimental investigation of spray dehumidification process in moist air,” Int. Commun. Heat Mass Transfer, vol. 97, pp. 163–171, Oct. 2018, doi: 10.1016/j.icheatmasstransfer.2018.07.011.

[85] N. Kapilan, A. M. Isloor, and S. Karinka, “A comprehensive review on evaporative cooling systems,” Results Eng., vol. 18, 101059, Jun. 2023, doi: 10.1016/j.rineng.2023.101059.

[86] Z.-X. Li and L.-Z. Zhang, “Flow maldistribution and performance deteriorations in a counter flow hollow fiber membrane module for air humidification/dehumidification,” Int. J. Heat Mass Transf., vol. 74, pp. 421–430, Jul. 2014, doi: 10.1016/j.ijheatmasstransfer.2014.03.047.

[87] F. H. Akhtar, M. Kumar, and K.-V. Peinemann, “Pebax® 1657/Graphene oxide composite membranes for improved water vapor separation,” J. Membr. Sci., vol. 525, pp. 187–194, Mar. 2017, doi: 10.1016/j.memsci.2016.10.045.

[88] E. E. Matula and J. A. Nabity, “Characterization of simultaneous heat, oxygen, and carbon dioxide transfer across a nonporous polydimethylsiloxane (PDMS) hollow fiber membrane,” Chem. Eng. J. Adv., vol. 6, 100106, May 2021, doi: 10.1016/j.ceja.2021.100106.

[89] P. G. Ingole et al., “Water vapor separation from flue gas using MOF incorporated thin film nanocomposite hollow fiber membranes,” Chem. Eng. J., vol. 334, pp. 2450–2458, Feb. 2018, doi: 10.1016/j.cej.2017.11.123.

[90] S. J. Metz, W. J. C. van de Ven, J. Potreck, M. H. V. Mulder, and M. Wessling, "Transport of water vapor and inert gas mixtures through highly selective and highly permeable polymer membranes," J. Membr. Sci., vol. 251, no. 1–2, pp. 29–41, Apr. 2005, doi: 10.1016/j.memsci.2004.08.036.

[91] S.-M. Huang, M. Yang, and X. Yang, "Performance analysis of a quasi-counter flow parallel-plate membrane contactor used for liquid desiccant air dehumidification," Appl. Therm. Eng., vol. 63, no. 1, pp. 323–332, Feb. 2014, doi: 10.1016/j.applthermaleng.2013.11.027.

[92] X. Liu, J. Warner, M. Qu, X. Liu, H. Opadrishta, A preliminary experimental study on the performance of a membrane-based air dehumidifier using ionic liquid, in: International Refrigeration and Air Conditioning Conference, Purdue University, West Lafayette, IN, vol. 2081 pp. 1-10, 2018.

[93] T. W. Tibbitts, "Humidity and Plants," BioScience, vol. 29, no. 6, pp. 358–363, Jun. 1979, doi: 10.2307/1307692.

[94] E. A. Lysenko, M. A. Kozuleva, A. A. Klaus, N. L. Pshybytko, and V. V. Kusnetsov, "Lower air humidity reduced both the plant growth and activities of photosystems I and II under prolonged heat stress," Plant Physiol. Biochem., vol. 194, pp. 246–262, Jan. 2023, doi: 10.1016/j.plaphy.2022.11.016.

[95] J. B. Campen, G. P. A. Bot, and H. F. de Zwart, "Dehumidification of Greenhouses at Northern Latitudes," Biosyst. Eng., vol. 86, no. 4, pp. 487–493, Dec. 2003, doi: 10.1016/j.biosystemseng.2003.08.008.

[96] P. Pourmovahed, M. Lefsrud, and J. Maisonneuve, "Thermodynamic limits of using fertilizer to produce clean fertigation solution from wastewater via forward osmosis," J. Membr. Sci., vol. 647, 120168, Apr. 2022, doi: 10.1016/j.memsci.2021.120168.

[97] F. Volpin, R.R. Gonzales, S. Lim, N. Pathak, S. Phuntsho, and H.K. Shon, "GreenPRO: A novel fertiliser-driven osmotic power generation process for fertigation," Desalination, vol. 447, pp. 158–166, Dec. 2018, doi: 10.1016/j.desal.2018.09.013.

[98] S. Phuntsho, H.K. Shon, S. Hong, S. Lee, and S. Vigneswaran, "A novel low energy fertilizer driven forward osmosis desalination for direct fertigation: Evaluating the performance of fertilizer draw solutions," Journal of Membrane Science, vol. 375, issues 1–2, pp. 172–181, Jun. 2011, doi: 10.1016/j.memsci.2011.03.038.

[99] M. Bhowmik, B.K. Naik, P. Muthukumar, and R. Anandalakshmi, "Performance assessment and optimization of liquid desiccant dehumidifier system using intelligent models and integration with solar dryer," Journal of Building Engineering, vol. 64, 105577, Apr. 2023, doi: 10.1016/j.jobe.2022.105577.

[100] H. Bai, J. Zhu, X. Chen, J. Chu, Y. Cui, and Y. Yan, "Steady-state performance evaluation and energy assessment of a complete membrane-based liquid desiccant dehumidification system," Applied Energy, vol. 258, 114082, Jan. 2020, doi: 10.1016/j.apenergy.2019.114082.

[101] T. Elmer, M. Worall, S. Wu, and S. Riffat, "Experimental evaluation of a liquid desiccant air conditioning system for tri-generation/waste-heat-driven applications," International Journal of Low-Carbon Technologies, vol. 12, no. 2, pp. 110–125, Jun. 2017, doi: 10.1093/ijlct/ctw012.

[102] W. Su, Z. Lu, X. She, J. Zhou, F. Wang, B. Sun, and X. Zhang, "Liquid desiccant regeneration for advanced air conditioning: A comprehensive review on desiccant materials, regenerators, systems and improvement technologies," Applied Energy, vol. 308, 15 Feb. 2022, 118394, doi: 10.1016/j.apenergy.2021.118394.

[103] N. Datta, Z. Zhuang, and W. Qin, "Experimental study of a liquid desiccant regeneration system: performance analysis for high feed concentrations," Clean Technologies and Environmental Policy, vol. 22, pp. 1255–1267, Jun. 2020, doi: 10.1007/s10098-020-01886-9.

[104] E. Lemmon, NIST Thermophysical Properties of Air and Air Component Mixtures: AIRPROPS, World Wide Web-Internet and Web Information Systems, NIST 72, 2003.

[105] P. R. Bevington, Data Reduction and Error Analysis for the Physical Sciences, Boston: McGraw-Hill, 2003.

[106] S. J. Kline and F. A. McClintock, "Describing Uncertainties in Single-Sample Experiments," Mechanical Engineering, vol. 75, no. 1, pp. 3–8, 1953.

[107] M. S. Odabas, H. Simsek, C. W. Lee, and I. Iseri, "Multilayer Perceptron Neural Network Approach to Estimate Chlorophyll Concentration Index of Lettuce (Lactuca sativa L.)," Communications in Soil Science and Plant Analysis, vol. 48, no. 2, pp. 162–169, 2017. DOI: 10.1080/00103624.2016.1253726.

[108] N. Lu, T. Nukaya, T. Kamimura, D. Zhang, I. Kurimoto, M. Takagaki, T. Maruo, T. Kozai, and W. Yamori, "Control of vapor pressure deficit (VPD) in greenhouse enhanced tomato growth and productivity during the winter season," Scientia Horticulturae, vol. 197, pp. 17–23, Dec. 2015, doi: 10.1016/j.scienta.2015.11.001.

[109] C. Kittas and T. Bartzanas, "Greenhouse microclimate and dehumidification effectiveness under different ventilator configurations," Building and Environment, vol. 42, no. 10, pp. 3774–3784, Oct. 2007, doi: 10.1016/j.buildenv.2006.06.020.

[110] C. Zeng, S. Liu, and A. Shukla, “A review on the air-to-air heat and mass exchanger technologies for building applications,” Renewable and Sustainable Energy Reviews, vol. 75, pp. 753–774, Aug. 2017, doi: 10.1016/j.rser.2016.11.052.

[111] J.-H. Cheng and C.-L. Zhang, “Capacity evaluation of mechanical dehumidification systems: A theoretical framework,” Energy Conversion and Management, vol. 295, 117610, Nov. 2023, doi: 10.1016/j.enconman.2023.117610.

[112] B. K. Naik, M. Joshi, P. Muthukumar, M. Sultan, T. Miyazaki, R. R. Shamshiri, and H. Ashraf, “Investigating Solid and Liquid Desiccant Dehumidification Options for Room Air-Conditioning and Drying Applications,” Sustainability, vol. 12, no. 24, p. 10582, Dec. 2020, doi: 10.3390/su122410582.

[113] F. G. Fahad, S. T. Al-Humairi, A. T. Al-Ezzi, H. Sh. Majdi, A. J. Sultan, T. M. Alhuza ymi, and T. M. Aljuwaya, “Advancements in Liquid Desiccant Technologies: A Comprehensive Review of Materials, Systems, and Applications,” Sustainability, vol. 15, no. 18, p. 14021, Sep. 2023, doi: 10.3390/su151814021.

[114] J. Luo and H. Yang, “A state-of-the-art review on the liquid properties regarding energy and environmental performance in liquid desiccant air-conditioning systems,” Applied Energy, vol. 325, 119853, Nov. 2022, doi: 10.1016/j.apenergy.2022.119853.

[115] D. de Halleux and L. Gauthier, “Energy Consumption Due to Dehumidification of Greenhouses under Northern Latitudes,” Journal of Agricultural Engineering Research, vol. 69, no. 1, pp. 35–42, Jan. 1998, doi: 10.1006/jaer.1997.0221.

[116] D. R. Rousse, D. Y. Martin, R. Thériault, F. Léveillée, and R. Boily, “Heat recovery in greenhouses: a practical solution,” Applied Thermal Engineering, vol. 20, no. 8, pp. 687–706, Jun. 2000, doi: 10.1016/S1359-4311(99)00048-4.

[117] G. Chasseriaux, A. Travers, and M. Ternoy, "Heat pumps for reducing humidity in plastics greenhouses," Plasticulture, vol. 1987, no. 73, pp. 29–40, Oct. 1987.

[118] C. Gilli, F. Kempkes, P. Munoz, J. I. Montero, F. Giuffrida, F. J. Baptista, A. Stepowska, and C. Stanghellini, “Potential of different energy saving strategies in heated greenhouse,” Acta Horticulturae, vol. 1164, pp. 467–474, 2017, doi: 10.17660/ActaHortic.2017.1164.61.

[119] M. Sultan, T. Miyazaki, B. B. Saha, and S. Koyama, “Steady-state investigation of water vapor adsorption for thermally driven adsorption based greenhouse air-conditioning system,” Renewable Energy, vol. 86, pp. 785–795, Feb. 2016, doi: 10.1016/j.renene.2015.09.015.

[120] M. Sultan, T. Miyazaki, B. B. Saha, S. Koyama, and V. S. Maisotsenko, “Steady-state Analysis on Thermally Driven Adsorption Air-conditioning System for Agricultural Greenhouses,” Procedia Engineering, vol. 118, pp. 185–192, 2015, doi: 10.1016/j.proeng.2015.08.417.

[121] D. Ghosh and A. Ganguly, “Performance analysis of a partially closed solar regenerated desiccant assisted cooling system for greenhouse lettuce cultivation,” Solar Energy, vol. 158, pp. 644–653, Dec. 2017, doi: 10.1016/j.solener.2017.10.030.

[122] G. Lychnos and P. A. Davies, “Modelling and experimental verification of a solar-powered liquid desiccant cooling system for greenhouse food production in hot climates,” Energy, vol. 40, no. 1, pp. 116–130, Apr. 2012, doi: 10.1016/j.energy.2012.02.021.

[123] M. Sadasivam and A. R. Balakrishnan, “Analysis of thermal effects in packed bed liquid desiccant dehumidifiers,” Chemical Engineering and Processing: Process Intensification, vol. 30, no. 2, pp. 79–85, Sep. 1991, doi: 10.1016/0255-2701(91)80014-G.

[124] A. Gurubalan and C. J. Simonson, “A comprehensive review of dehumidifiers and regenerators for liquid desiccant air conditioning system,” Energy Conversion and Management, vol. 240, 15 July 2021, 114234, doi: 10.1016/j.enconman.2021.114234.

[125] X. Junzeng, W. Qi, P. Shizhang, and Y. Yanmei, “Error of Saturation Vapor Pressure Calculated by Different Formulas and Its Effect on Calculation of Reference Evapotranspiration in High Latitude Cold Region,” Procedia Engineering, vol. 28, 2012, pp. 43–48, doi: 10.1016/j.proeng.2012.01.680.

[126] D. Cutress, "The importance of vapor pressure deficits (VPD) in agricultural plant growth," Farming Connect - Business Wales, Dec. 6, 2021.

[127] D. P. de Oliveira Mangarotti, R. Rezende, R. Saath, T. L. Hachmann, C. S. Lozano, and A. C. A. Gonçalves, “Water requirements and crop coefficients of arugula grown in a protected environment,” IDESIA (Chile), vol. 37, no. 2, pp. 75–79, Jun. 2019.